Journal of Materials Chemistry A

ROYAL SOCIETY OF CHEMISTRY

REVIEW

View Article Online
View Journal | View Issue

Cite this: J. Mater. Chem. A, 2025, 13, 11050

Synergistic effects of polymer integration on the properties, stability, and applications of MXenes

Sunil Kumar, †*[a] Syed Muhammad Zain Mehdi,†[ab] Manish Taunk,[c] Sanjeev Kumar,[c] Amit Aherwar,[d] Sudhanshu Singh[e] and Tej Singh[f]

MXenes are known for their exceptionally high electrical conductivity, mechanical resilience, and versatile surface chemistry. However, these tend to oxidize under ambient conditions, posing a major hurdle to their performance in various applications. In contrast, polymers are mostly stable under ambient conditions, making them ideal materials to combine with MXenes to create MXene–polymer nanocomposites with enhanced stability against oxidation, while also improving MXene functionality. This synergy can also enhance the mechanical strength, thermal stability, surface properties, and other characteristics of MXenes, improving the overall performance of MXenes. This review focuses on the role of polymers in improving the properties of MXenes and mitigating their oxidation under various conditions. Polymers serve as protective barriers and improve interfacial interactions, maintaining various properties of MXenes for longer periods. This review also highlights MXene–polymer nanocomposite fabrication techniques, like solution blending, layer-by-layer assembly, *in situ* polymerization, electrospinning, *etc.*, for their effective integration. The review also explores MXene–polymer nanocomposite applications in different areas, including energy storage devices, electronics, sensors, filtration membranes, biomedical applications, *etc.* Finally, the review also outlines various challenges and opportunities in synthesizing MXene–polymer nanocomposites for diverse applications, emphasizing the potential of MXene–polymer synergy to open new opportunities in future hybrid materials.

Received 14th November 2024
Accepted 26th February 2025

DOI: 10.1039/d4ta08094g

rsc.li/materials-a

[a]Department of Nanotechnology and Advanced Materials Engineering and HMC, Sejong University, Seoul 05006, South Korea. E-mail: skumar@sejong.ac.kr
[b]School of Chemical, Biological and Battery Engineering, Gachon University, 1342 Seongnam-daero, Sujeong-gu, Seongnam-si, Gyeonggi-do 13120, Republic of Korea
[c]Department of Physics, Chandigarh University, Gharuan, Mohali-140413, India
[d]Department of Mechanical Engineering, Madhav Institute of Technology and Science (Deemed University), Gwalior 474005, India
[e]Department of Computer Science and Engineering, Parul University, Vadodara, Gujarat, 391760, India
[f]Faculty of Informatics, ELTE Eötvös Loránd University, Budapest 1117, Hungary
† Equal 1st authors/equal contribution.

Sunil Kumar

Sunil Kumar received his BS and MS degrees in Physics from Panjab University, Chandigarh, India, in 2003 and 2008, respectively. He completed his PhD at Thapar University, Patiala, India, in 2016. In 2017, he joined Sejong University as a postdoctoral fellow. Since 2022, he has been working as an Assistant Professor at Sejong University, South Korea, in the Department of Nanotechnology and Materials Engineering. His current research interests include MXene-based smart windows, flexible transparent electrodes, and energy storage devices.

Syed Muhammad Zain Mehdi

Syed Muhammad Zain Mehdi received his BS degree in Metallurgy and Materials Engineering from the University of the Punjab, Pakistan, in 2017. He completed his MS-PhD in Nanotechnology at Sejong University, South Korea, in February 2024. Following this, in March 2024, he joined Sejong University as a Postdoctoral Fellow in the Department of Nanotechnology and Materials Engineering. His research interests include doped-carbon nanotube properties in field emission and the utilization of MXenes in energy storage and electrocatalysis.

1. Introduction

Nanocomposites have been identified as a promising way to meet the growing global demands in various sectors, including the energy sector. The combination of nanoparticles, nanofillers, and a polymer matrix material leads to improved properties like strength, conductivity, catalytic activity, *etc.* in these materials.[1] The potential of nanocomposites lies in their ability to revolutionize energy storage, conversion, and transportation technologies, which can offer more efficient and sustainable solutions for the future.[2] Polymers are the most popular for nanocomposite synthesis due to their versatility, easy processing, and ability to incorporate various nanofillers.[3] Different materials can be used as fillers for the synthesis of polymer-based nanocomposites.[4] In this perspective, 2D MXenes are now recognized as promising candidates.[5] MXenes originate from MAX phases, which are compounds of transition metals and are obtained through an etching process using HF or LiF/HCl acids.[6] Following the etching process, the A component is

Manish Taunk

Manish Taunk received his BS and MS degrees in Physics from Himachal Pradesh University, Shimla, India, in 2004 and 2008, respectively. He completed his PhD at the National Institute of Technology, Himachal Pradesh, India, in 2012. He has worked as an Assistant Professor at various universities. Currently, he is working as an Associate Professor at Chandigarh University, Mohali, India, in the Department of Physics. His current research interests include MXene-based nanocomposites, conducting polymers, and their applications.

Sanjeev Kumar

Sanjeev Kumar earned his BS and MS degrees in Physics from GNDU, Amritsar, India, in 2005 and 2007, respectively. He completed his PhD at Thapar University, Patiala, India, in 2012. He served as an Assistant Professor at Sri Guru Granth Sahib World University for 10 years. Currently, he is an Associate Professor in the Department of Physics at Chandigarh University, Mohali, India. His research focuses on TiO_2 and ZnO-based nanocomposites and their applications in photocatalysis.

Amit Aherwar

Amit Aherwar obtained his BE degree in Mechanical Engineering in 2006 and MTech in Production Engineering from Madhav Institute of Technology and Science (MITS) Gwalior, India, in 2010. He completed his Doctor of Philosophy (PhD) at the Malaviya National Institute of Technology (MNIT) Jaipur, India, in 2017. Currently, he is an Assistant Professor at MITS Gwalior. His research focuses on biomaterials, tribology, composite materials, and metal casting, with an emphasis on advancing material properties and manufacturing processes.

Sudhanshu Singh

Sudhanshu Singh obtained his BS degree in Electronics & Communication from Uttar Pradesh Technical University, Lucknow, India, in 2006, followed by an MS degree in Nanotechnology from the National Institute of Technology Kurukshetra, Haryana, India, in 2008. He completed his PhD at Amity University Rajasthan, Jaipur, India, in 2021. With over a decade of experience as an Assistant Professor at Amity University Rajasthan, he is currently serving as an Associate Professor at Parul University, Gujarat, India. His research interests include the development of polymers and nanocomposites for wastewater treatment, photocatalysis, and the tribological properties of fiber-reinforced phenolic composites.

Tej Singh

Tej Singh earned his BS and MS degrees from Panjab University, Chandigarh, India, in 2003 and 2008, respectively, and a PhD degree from the National Institute of Technology, Hamirpur, India, in 2013. He has gained experience at various academic institutions. Currently, Tej Singh is serving as an Associate Professor at the Faculty of Informatics, Eötvös Loránd University, Hungary. His areas of interest and expertise include polymer composites, tribology, nanoparticle synthesis, optimization methods, waste and natural renewable materials utilization for potential applications, and heat transfer.

removed from the MAX phases, and the resulting MXenes are thoroughly washed with DI water. MXenes possess surface terminal groups such as –OH, –O, –Cl, or –F, and are commonly denoted as $M_{n+1}X_nT_x$, where M denotes a transition metal, X typically denotes a carbon/nitrogen/carbonitride, and T_x represents surface functionalities as terminal groups.[7]

MXenes have remarkable features such as high electrical conductivity,[8,9] hydrophilicity,[10] electrochemical characteristics,[11,12] adjustable band gap,[13,14] and substantial surface area.[15] These characteristics make MXenes versatile materials with applications in fields such as energy storage,[8,11,15–18] fuel cells,[19,20] photodetectors,[14,21] sensors,[22] conductive ink,[23] 3D printing,[24–26] smart windows,[27] electromagnetic interference (EMI),[28,29] *etc.* $Ti_3C_2T_x$ MXene stands out as the most widely recognized member of the MXene family. High electrical conductivity, a tailored surface, thermal stability, mechanical strength, *etc.* make it the most favored member of the MXene family. In addition to $Ti_3C_2T_x$, the MXene family includes other potential members, such as Ti_2CT_x,[30] V_2CT_x,[18,31,32] Nb_2CT_x,[33] *etc.* These MXenes, each possessing unique characteristics, offer a wide range of properties useful in diverse potential applications.[34] MXenes, including Ti_2C, V_2C, Nb_2C, Mo_2TiC_2, and $Mo_2Ti_2C_3$, showcase distinctive characteristics distinguishing them from the widely studied Ti_3C_2. For example, Ti_2C has thinner layers, offering a slightly larger bandgap and rapid ion transport, making it suitable for photothermal therapy,[35] energy storage applications,[36] electrocatalysis for water splitting,[37] *etc.* V_2C demonstrates superior redox properties due to the variable oxidation states of vanadium, improving its performance in pseudocapacitors and catalytic reactions.[38] Similarly, Nb_2C is known for its superior electrochemical durability in aqueous and organic electrolytes, making it highly suitable for robust energy storage[39,40] and photocatalytic applications.[41] Additionally, Nb_2C MXene demonstrates good electrical conductivity and improved wettability, attributed to its lower Fermi energy level relative to Ti_3C_2.[39] In the case of dual-transition metal MXenes $(M'_2M''C_2)$, structurally stable Mo_2TiC_2 combines the enhanced catalytic performance of Mo with the structural integrity of Ti, offering improved HER/OER performance[42] and N_2 reduction reaction activity.[43] Similarly, $Mo_2Ti_2C_3$, with its thicker multilayer structure, offers tunable conductivity and thermal stability, positioning it as a promising material for thermal management and electronics. $Mo_2Ti_2C_3$ MXene exhibits elevated photothermal conversion efficiency due to its substantial optical absorption across a wide spectral range and layered structure, which facilitates efficient heat transfer and energy dissipation.[44] Partially oxidized $Mo_2Ti_2C_3$ MXene has demonstrated significant potential for energy storage applications due to its enhanced electrochemical properties and structural stability.[45]

MXenes boast various remarkable properties; however, they are vulnerable to oxidative degradation when exposed to ambient conditions or during processing, which restricts their practical application.[46] Therefore, enhancing oxidation stability is crucial for their broader adoption in real-world uses. Various methods have been proposed to enhance the oxidation stability of MXenes. These methods include storing MXenes at low temperatures in an Ar atmosphere,[47] or in eutectic solvents,[48] using sodium L-ascorbate,[49] or integrating MXenes into polymer blends.[50,51] The use of polyanions for preservation has shown promising results in minimizing MXene oxidation, as this process usually begins at the edges of the material.[52] MXenes treated with antioxidants have demonstrated better stability under ambient conditions, allowing their use in energy storage applications for more than 80 days.[53] Among these approaches, MXene–polymer hybrids or nanocomposites stand out most favorably as they provide various functionalities to these hybrid materials. However, the techniques of passivation or blending may lead to decreased electrical conductivity compared to pure MXenes.

Polymers are recognized for their outstanding capability to be processed and shaped. Incorporating MXenes into polymers can enhance and customize their characteristics for particular uses. MXene–polymer nanocomposites can improve mechanical attributes, including flexibility, tensile strength, and toughness.[54,55] MXenes are prone to oxidation and deterioration under typical environmental conditions[56] but polymers can form a protective barrier around the MXene flakes, which increases their stability against oxidation.[50,51] Additionally, the polymers mixed with MXenes provide numerous possibilities for functionalization and alteration.[57] MXene–polymer nanocomposites have found applications in flexible electronics,[24,58–60] self-healing sensors,[61] 3D printing,[62–64] energy storage,[50,65] anti-corrosion,[66,67] fire retardants,[68] water purification/treatment,[69–71] solar cells,[72,73] and antibacterial applications.[74–76]

MXene–polymer nanocomposites can be prepared using methods, such as solution casting,[68,77] solution blending,[78] electrospinning,[79,80] *in situ* polymerization,[81,82] thin film coating or polymer lamination,[50] fiber formation,[83,84] *etc.* Some of the popular polymers that are hybridized with MXene include polyvinyl alcohol (PVA),[85] polydimethylsiloxane (PDMS),[86] poly(3,4-ethylenedioxythiophene) polystyrene sulfonate (PEDOT:PSS),[87,88] polyaniline (PANI),[89] polypyrrole (PPy),[90] *etc.* The polymers can serve as intercalants or spacers within MXene–polymer nanocomposites.[16,91]

Some earlier reviews on MXene–polymer composites are available; however, these primarily focus on synthesis and general applications,[92,93] or the role of MXenes as fillers,[94] and a few are outdated.[95] This article uniquely highlights the synergistic effects of MXene–polymer integration, showcasing enhancements in mechanical strength, conductivity, and thermal stability. By emphasizing these synergistic effects and the latest advancements, this review provides a comprehensive and up-to-date perspective on their advanced applications, filling the gaps left by previous studies.

2. Synthesis of MXenes

The synthesis of 2D MXenes was first achieved in 2011 by etching Ti_3AlC_2 using a highly concentrated acid. This top-down approach involves removing the "A" layer from the MAX phases. A strong acid like HF effectively breaks the M–A metallic bond, leading to the formation of layered MXene structures. The reaction mechanism of selective etching using HF is as follows:[96]

$$M_{n+1}AX_n + 3HF \rightarrow M_{n+1}X_n + AlF_3 + 1.5H_2$$

$$M_{n+1}X_n + 2H_2O \rightarrow M_{n+1}X_n(OH)_2 + H_2$$

$$M_{n+1}X_n + 2HF \rightarrow M_{n+1}X_nF_2 + H_2$$

During the HF etching process, Al (A layer) removal creates surface terminations, leading to the functionalization of the M layer. The chemical etching in an acidic medium inevitably results in defect sites in the synthesized MXene flakes. These defect sites play a key role in the oxidation of MXenes and reduce their self-life to a few days in an ambient environment, limiting their extensive use. Later, many synthesis routes were developed but selective etching methods using fluoride-containing agents in an acidic medium were widely used.[97] The reaction time, temperature, and acid concentration affect the quality and quantity of the resultant MXenes.

Despite the successful synthesis of MXenes using concentrated HF etching, environmental concerns and the need for a safer, simpler method have prompted the use of mild etching agents like HCl with various fluoride salts for large-scale production. The HCl and fluoride salt mixture forms *in situ* HF for etching the "A" layer in the MAX phases (Fig. 1a). The MXenes synthesized using HCl have high yields and fewer defects and resulted in higher electrical conductivity. However, the MAX phase's purity is also a crucial factor in deciding the resultant properties of MXenes.[98] Natu *et al.* reported a water-free synthesis method using polar solvents along with ammonium dihydrogen fluoride.[99] The etching process in this method is reported to be very slow but surprisingly the resultant MXene has only the –F group as the termination species.

One of the major issues associated with MXene synthesis is the use of hazardous chemicals, such as HF or *in situ*-produced HF from fluoride salts and strong acids, which pose significant ecological and health hazards. These chemicals can lead to hazardous waste, requiring meticulous management and disposal processes. To address these issues, researchers have been exploring environmentally friendly or less harmful methods for MXene synthesis. Recently, fluoride-free synthesis methods including the electrochemical method,[100] molten salts assisted etching,[101] the alkali etching method,[102] the chemical vapor deposition (CVD) synthesis approach,[103] *etc.*, have been developed to minimize hazardous byproducts. These methods not only mitigate safety and environmental concerns but also allow the alteration of the MXene structure and surface chemistry, making them promising approaches for scalable and eco-friendly MXene production.

The electrochemical etching method selectively removes the "A" layer from the MAX phase using non-acidic electrolytes, making it safer and more environmentally friendly than traditional acid-based methods. In a two-electrode system (Fig. 1b), the bulk MAX phase (like Ti_3AlC_2) serves as both the anode and counter electrode, with an electrolyte including ammonium chloride and tetramethylammonium hydroxide (TMAOH, pH > 9). The anode undergoes etching at room temperature, under a constant potential while the electrolyte is stirred. After a few hours, the electrolyte turns grey-white with a gelatinous precipitate, and black powders (stacked $Ti_3C_2T_x$) settle at the bottom.

The alkali etching method employs alkali solutions (like NaOH or KOH) to selectively remove the "A" layer from the MAX phase, resulting in the synthesis of layered MXenes (Fig. 1c). In this method, an alkaline solution is dissolved in argon-purged deionized water before adding the MAX phase powder. The mixture is transferred to an autoclave, sealed, and subjected to heating under an argon atmosphere for 12 hours. After the hydrothermal process, the resulting suspension is filtered, thoroughly rinsed, and dried under vacuum, producing MXene with minimal impurities and a high degree of purity. This method is considered safer and more straightforward than fluorine-based acidic etching but may yield lower amounts of MXene or require extended reaction times depending on the alkali concentration and reaction conditions.

These methods lead to MXene formation but exhibit low yield and are more time-consuming than fluoride-based synthesis approaches. Recently, a new approach called dry selective extraction has been proposed theoretically.[105] In this method, a glass ampoule filled with a known quantity of MAX phase is placed in a tube furnace at an elevated temperature (Fig. 1d). Iodine vapors are then passed through the ampoule containing the MAX phase at 350 °C, acting as an etchant to remove the A layer and leaving behind MXenes. It was reported that the reaction does not occur below 350 °C and temperatures above 400 °C result in over-etching.

Bottom-up synthesis methods allow precise control over material chemistry, thus enabling tailored customization of material design. These approaches include the CVD method[103] (Fig. 1e) and direct solid-state synthesis. In a recent article, Wang *et al.* reported Ti-based and Zr-based MXenes by combining Ti metal and graphite powder with the desired quantity of $TiCl_4$.[103] The sealed ampoules containing this mixture were placed in a furnace at 950 °C for 2 h to obtain MXenes. The process involved methane or N_2 gas reacting with $TiCl_4$ on the titanium surface, resulting in Cl-terminated Ti_2CCl_2 or Ti_2NCl_2 MXenes. The proposed method is shown to have the potential for bulk production.

Besides these, salt-template MXene synthesis was reported by Xiao *et al.* to synthesize molybdenum nitride.[106] In this method, a 2D template of MoO_3 is prepared and coated with NaCl by annealing in an Ar atmosphere. The NaCl-coated 2D MoO_3 mixture was heated to 650 °C in an NH_3 atmosphere to yield MoN MXene. Ding *et al.* introduced a chemical scissor-mediated method for precise structural editing of layered transition metal carbides to synthesize MXene.[107] This method uses chemical scissors to open non-van der Waals gaps in MAX phases, followed by atomic replacement *via* diffusion of metal ion intercalants into interlayer vacancies. The scissors are also used for termination removal.

3. MXene structure and surface chemistry

MXenes exhibit a surface-rich chemistry that endows them with unique properties and potential applications.[108] In MXene synthesis, when the "A" layer is selectively etched from the precursor MAX phase, interlayer spaces are generated between the MXene layers, where solvent molecules or functional groups

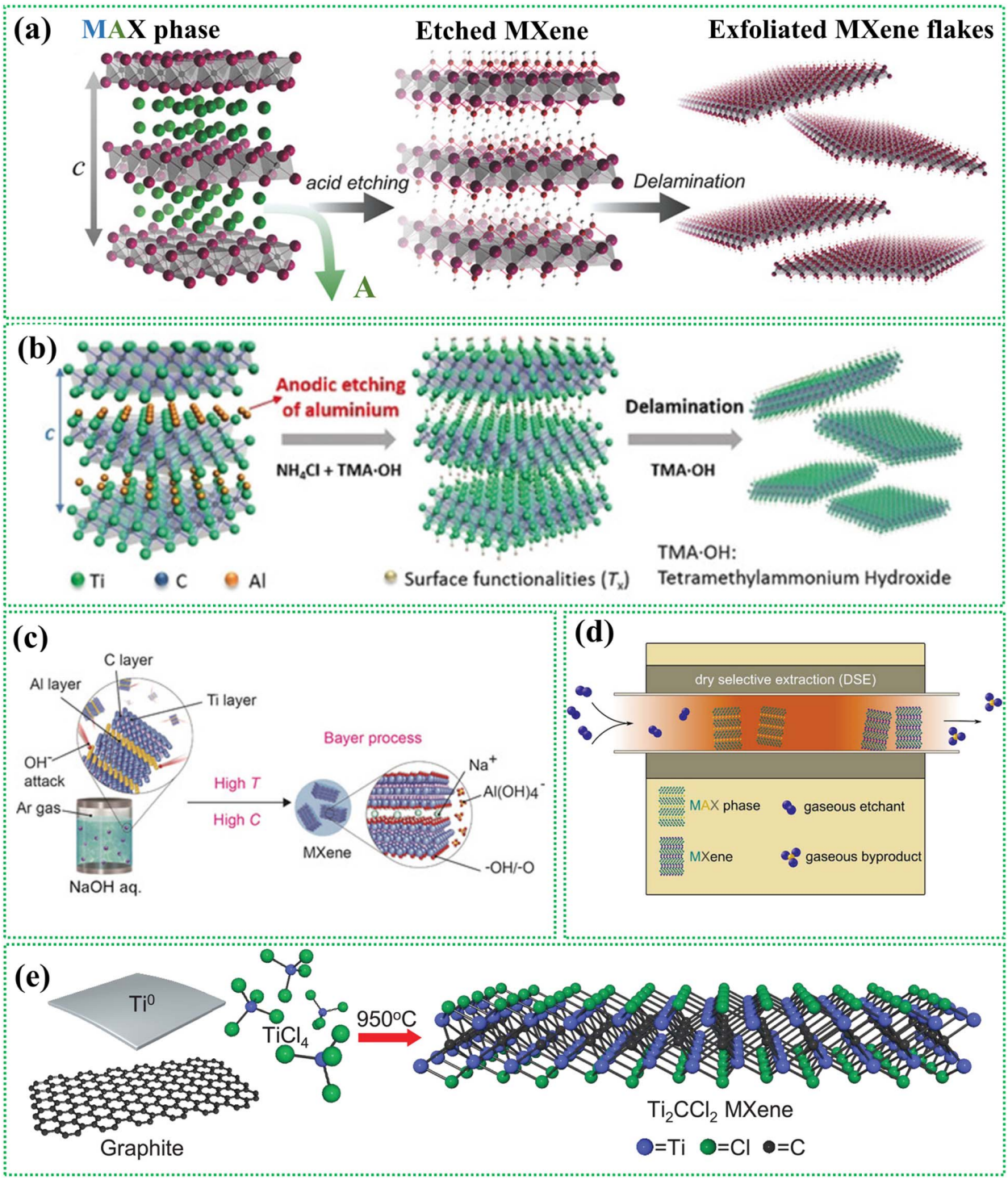

Fig. 1 MXene synthesis strategies. (a) MXene etching with fluorine-based etchants. Reproduced with permission from ref. 104. Copyrights 2016, Wiley. (b) Electrochemical etching method. Reproduced with permission from ref. 100. Copyrights 2018, Wiley. (c) Alkali-assisted etching method. Reproduced with permission from ref. 102. Copyrights 2018, Wiley. (d) Dry selection extraction approach. Reproduced with permission from ref. 105. (e) CVD method-based MXene synthesis using Ti, graphite, and $TiCl_4$. Reproduced with permission from ref. 103. Copyrights 2023, The American Association for the Advancement of Science.

are developed (Fig. 2a). These surface terminations on the MXene surface play an important role in defining the properties of MXenes.[109] The nature of the surface terminations can be altered during the synthesis of MXenes to tailor the surface chemistry of MXenes.[110] The layered structure of MXenes, combined with their tunable surface chemistry and properties, allows various applications in electronics, energy storage, catalysis, sensing, medicine, and more.[111,112]

MXenes typically possess surface terminations, such as –OH, –O, –Cl, or –F, resulting from the etching process used to synthesize

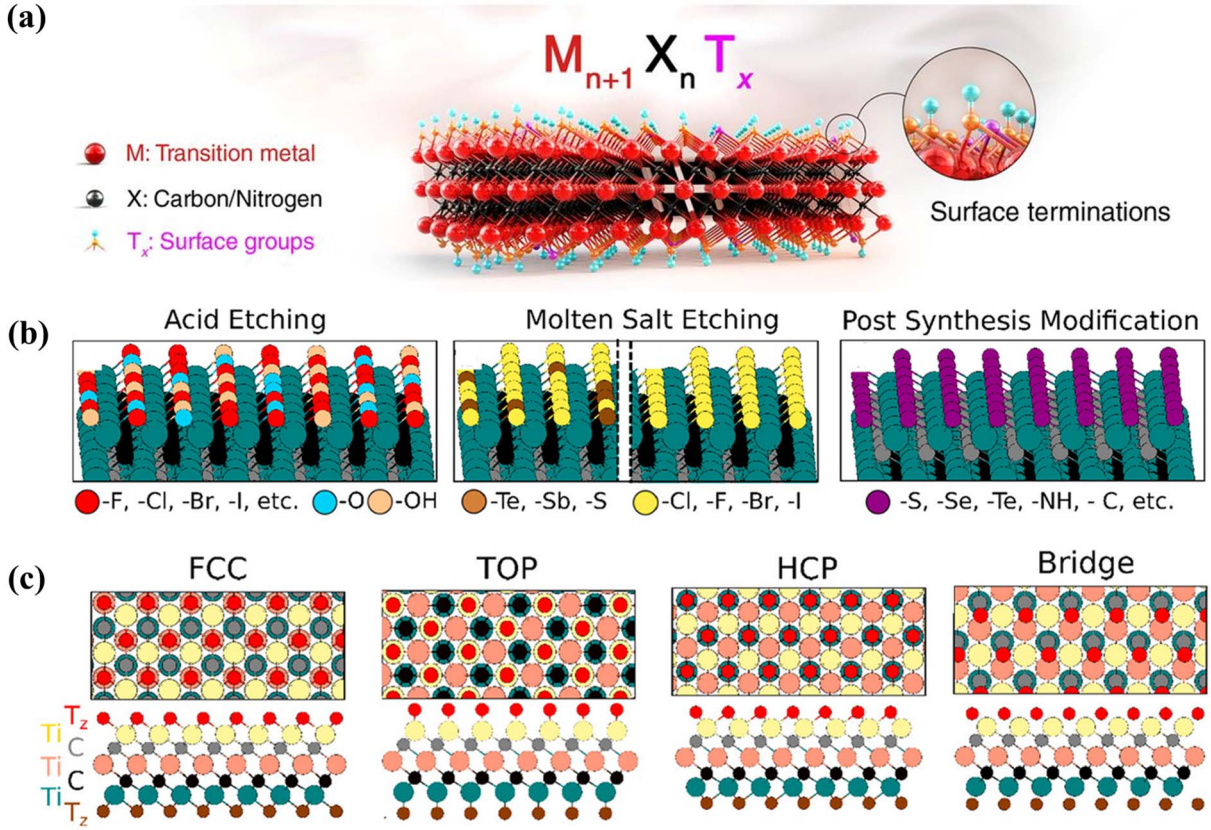

Fig. 2 MXene surface terminations. (a) A schematic representation of MXene structures, indicating the surface terminations of the outer metal layers. Reproduced with permission from ref. 111. Copyrights 2021, The American Association for the Advancement of Science. (b) MXene termination scenarios: (i) halogen and –O/–OH terminations from the acidic etching of MAX phases, (ii) surface terminations from molten salts, (iii) surface terminations *via* molten salts *via* altered treatment, and (iv) post-synthesis modification introducing uniform terminations. (c) Surface terminations: (i) FCC sites, (ii) "Top" positions on surface Ti, (iii) HCP sites, and (iv) bridge sites between Ti atoms. Reproduced with permission from ref. 116. Copyrights 2023, American Chemical Society.

them. During acidic etching, which mainly involves fluoride ions, MXenes typically exhibit –F and –O/–OH groups (Fig. 2b). F terminations can be modulated by adjusting acid concentrations, while their complete replacement with –O/–OH groups can be achieved through alkaline treatments using KOH, NaOH, or TBAOH.[113,114] Molten salt etching (like $ZnCl_2$) facilitates Lewis acid–base reactions between cations and the A layer, substituting it with Zn, followed by –Cl terminations.[115] Variation in the composition of molten salts during MAX phase etching facilitates the incorporation of halogen terminations, such as –Cl, –Br, and –I. In addition to these, a wide range of terminations, such as –S, –Se, –Te, –P, and –Sb, can be uniformly introduced onto MXene surfaces, enabling tailored surface functionalities for diverse applications (Fig. 2b). Heating MXenes under reactive gases further allows the formation of uniform –O and –C terminations. The molten salt method also produces –Cl or –Br terminated MXenes like $Ti_3C_2Cl_2$, Nb_2CBr_2, *etc.*, which can act as templates for post-synthesis modifications, yielding MXenes terminated with –S, –Se, –Te, –NH, –O, or bare/–H groups (Fig. 2b).

Theoretical investigations show that MXene surface terminations occupy distinct crystallographic sites.[117] For $Ti_3C_2T_x$ MXene, terminations above middle Ti atoms align with FCC sites, while those above surface Ti atoms adopt a "top" configuration, and those above C atoms occupy "HCP" sites. Terminations between Ti atoms form a "bridge" configuration (Fig. 2c). FCC sites are the most energetically favorable among these, with most terminations preferring these positions.

These terminations play a significant role in determining the surface chemistry, stability, and interactions of MXene with other materials.[118] The surface terminations of MXenes offer opportunities for functionalization.[119] The presence of water-loving polar surface terminations, particularly –OH groups, leads to a strong affinity for water molecules and promotes wetting of the MXene surface.[119] This hydrophilicity can be advantageous for applications such as water treatment and filtration.[120] The surface chemistry of MXenes influences their solubility and interactions with solvents. MXenes are generally not soluble in common organic solvents but are dispersible in water-based solutions due to their hydrophilic nature.[121] This solubility behavior enables their use in solution processing techniques and the fabrication of MXene-based films, coatings, and composites.

3.1 MXene oxidation and its factors

MXenes oxidize when exposed to ambient conditions or elevated temperatures, transforming into their corresponding

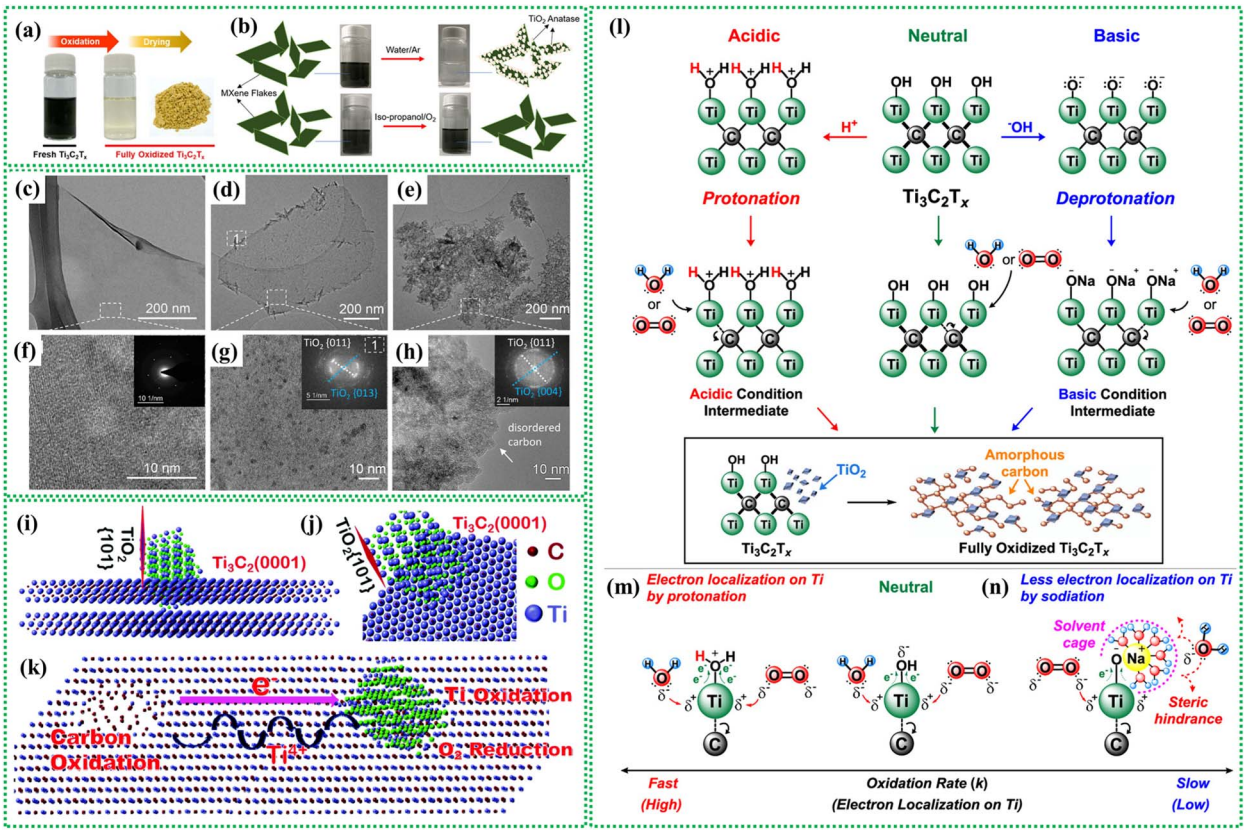

Fig. 3 (a) Digital images of $Ti_3C_2T_x$ suspensions before and after oxidation. Reproduced with permission from ref. 123. Copyrights 2021, American Chemical Society. (b) MXene dispersion impact in water and isopropanol. Reproduced with permission from ref. 134. Copyrights 2019, American Chemical Society. TEM images of (c) MXene flakes of fresh $Ti_3C_2T_x$ solution and solutions stored at room temperature in the air after (d) 7 days and (e) 30 days. (f–h) HRTEM images corresponding to panels (c–e), respectively. In figure (f), the inset shows the corresponding SAED pattern, while figures (g and h) display the respective FFT patterns. Reproduced with permission. Reproduced with permission from ref. 47. Copyright 2017, American Chemical Society. Defects in MXenes: (i and j) depiction of TiO_2 cluster bonding with Ti_3C_2, highlighting the TiO_2-(101) plane-oriented perpendicular to the MXene basal plane (0001). (k) Schematic illustrating Ti_3C_2 oxidation, showing carbon oxidation at the positive side and Ti-ion oxidation at the negative side of the internal electric field. Rapid electron transport to the convex area and slow Ti-ion diffusion create the internal electric field. Reproduced with permission from ref. 127. Copyright 2022, Royal Society of Chemistry. Effect of pH on MXene oxidation: (l) proposed mechanism for the oxidation reaction in $Ti_3C_2T_x$ mixtures under (m) acidic and (n) basic conditions. Reproduced with permission.[123] Copyright 2021, American Chemical Society.

oxides. For example, $Ti_3C_2T_x$ MXene evolves into $Ti_3C_2T_x/TiO_2$ and eventually forms carbon-supported TiO_2 nanoparticles.[122,123] It has been reported earlier that MXene oxidation starts at the edges of MXene flakes and advances toward interior basal planes.[124,125]

The oxidation can be observed through color changes; fresh $Ti_3C_2T_x$ MXene dispersed in water has a dark green color, which is converted to a translucent, cloudy hue as oxidation progresses with time (Fig. 3a). MXene oxidation is relatively faster in aqueous suspensions than in organic dispersions.[108,126] MXene hydrolysis is crucial in transforming MXenes into respective oxides in aqueous suspensions, a process that can be inhibited in organic solvents. For instance, no oxidation was observed in iso-propanol solutions of MXenes stored under an O_2 atmosphere for the same duration[126] (Fig. 3b). TEM analysis of freshly prepared MXenes shows clean surfaces and edges (Fig. 3c), with high-resolution TEM images revealing single-crystalline nanosheets (Fig. 3f).[47] The SAED pattern confirms a hexagonal atomic structure (Inset: Fig. 3f). After one week of exposure to air at room temperature, MXene edges display "branch-like" features and crystalline nanoparticles form on the basal planes of the flakes (Fig. 3d and g), identified as anatase in fast Fourier transform (FFT). After 30 days, MXenes completely decompose into anatase clumps and disordered carbon (Fig. 3e and h). The presence of dissolved oxygen and water leads to a reaction with the active edges of the flakes, resulting in TiO_2 formation. MXene oxidation is influenced by various factors. For example, the chemical etching process used to synthesize MXenes in strong acids creates surface defects in MXene flakes.[127,128] Under ambient conditions or in aqueous suspension, these defect-rich sites ease oxidative degradation, which in turn affects the properties of MXenes.[129] Environmental factors, such as exposure to air or immersion in water, further contribute to MXene degradation. The stability and reactivity of MXenes are significantly influenced by factors like the pH of the dispersion,[130,131] storage temperature,[131] MXene concentration,[132,133] flake size, *etc*[125,132].

During sonication-assisted delamination, maintaining a constant temperature and using Ar can prevent oxidation. Storing solutions in Ar-sealed vials or refrigeration reduces oxidation. Using mild etchants like tetraethylammonium hydroxide (TMAOH) avoids fluorine by-products, enhancing the stability of MXenes.[135] MXenes should be protected from UV exposure, as prolonged exposure leads to faster oxidation.[136] Synthesis methods determine surface terminations, with HF-etching resulting in more –F terminations compared to those synthesized with LiF–HCl.[137]

Etching MAX phases with alkali and molten salts prevents MXene oxidation and hydrolysis.[101,138] HF etching introduces defects, accelerating degradation to TiO_2. Relatively mild acids like HCl/LiF and fluorine-free etchants like TMAOH, NaOH, or KOH reduce the MXene defects.

Defects in MXenes also facilitate oxidation. Defects in MXenes, created during etching, drive oxidation and affect reactivity, structural changes, conductivity, and functional group formation.[128,139] Adjusting etchant concentration can control defects, which can also boost the resistance against oxidation as well as the performance in desired applications. In Ti_3C_2 MXene, Ti atoms form TiO_2 nanoparticles, while the remaining carbon atoms cluster to produce amorphous carbon, resulting in C@TiO_2 heterojunctions.[127] During oxidation at room temperature, the anatase TiO_2 (101) plane is oriented perpendicular to the Ti_3C_2 basal plane (Fig. 3i and j). The rotation of the TiO_2-(101) lattice plane during nucleation depletes Ti^{3+} in adjacent Ti_3C_2 crystals, creating Ti vacancies and excess carbon atoms. Ti vacancies are commonly found in the surface layer of MXenes prepared *via* exfoliation methods. Ti-vacancies in Ti_3C_2 MXenes create an internal electric field that drives electron flow, carbon cluster nucleation, and Ti-cation diffusion. This field enhances carbon oxidation, forming TiO_2 nanoparticles and amorphous carbon. Ti-vacancies also facilitate O_2 entry into the lattice, promoting TiO_2 nucleation and growth. Wrinkles and atomic steps act as nucleation sites for oxidation, with Ti-vacancies promoting carbon oxidation and TiO_2 formation (Fig. 3k).

Temperature and pH significantly influence MXene oxidation by affecting its reaction kinetics and pathways.[52,87] Higher pH slows oxidation at 20 °C, while increased temperature accelerates it.

The oxidation mechanism of aqueous $Ti_3C_2T_x$ MXene dispersions starts at –OH group sites, with pH significantly impacting reaction intermediates (Fig. 3l). Acidic conditions protonate surface hydroxyls, enhancing Ti atom electrophilicity and promoting nucleophilic addition reactions with H_2O or O_2. Under basic conditions, excess OH– deprotonates hydroxyls, forming sodiated intermediates and bulky solvent cages that hinder oxidation due to steric effects and reduced electrophilicity (Fig. 3m and n).

4. MXene–polymer hybrids for oxidation prevention

MXene–polymer nanocomposites are increasingly recognized for their ability to prevent MXene oxidation, as polymers serve as protective layers that shield MXenes from environmental degradation. Polymers can preserve MXenes for more than 180 days.[140] These nanocomposites can preserve MXenes not only at room temperature but also under higher temperatures and moist conditions.[141] This integration not only enhances the stability of MXenes but also improves their overall performance in various applications. Table 1 summarizes some MXene–polymer combinations investigated to enhance MXene stability over different periods.

4.1 Polystyrene/MXene for oxidation improvement

To address the issue of MXene oxidation, a 'particle manufacturing technique' (Fig. 4a) was employed to develop polystyrene/MXene (PS/MXene) composites with a 3D conductive network structure.[140] The material conductivity reached 3846.15 S m^{-1} when the filler content was merely 1.81 vol%. Due to the compact and ordered structure of the fabricated PS/MXene composite, it retains 53.4% of its initial conductivity after 180 days.

The fundamental procedure for exfoliating $Ti_3C_2T_x$ MXene and creating PS/MXene composites with a 3D ordered structure follows the "particle construction" approach.[153] First, this work used the conventional technique of manufacturing MXene

Table 1 MXene–polymer nanocomposites for MXene stability improvement

S. no.	MXene–polymer composition	MXene etchant	Preventive measure	Stability duration	Ref.
1	MXene/poly(tannic acid)	LiF/HCl	Oxygen-rich macromolecule	60 days	142
2	MXene/melamine	LiF/HCl	Nanocomposite	60 days	143
3	MXene/PVA–CA hydrogel	LiF/HCl	Nanocomposite	30 days	144
4	MXene/polymer	—	Nanocomposite	42 days	145
5	MXene/polyacrylamide	—	Nanocomposite	15 days	146
6	MXene/aramid nanofiber (ANF)	LiF/HCl	Nanocomposite	—	147
7	MXene/polystyrene	LiF/HCl	Nanocomposite	180 days	140
8	MXene/dopamine	LiF/HCl	Nanocomposite	13 hours at 170 °C	148
9	MXene/bentonite	LiF/HCl	Nanocomposite	2 hours at 600 °C	149
10	MXene/sodium alginate	LiF/HCl	Nanocomposite	30 days	150
11	MXene/PVA	LiF/HCl	Nanocomposite	50 days	151
12	MXene/PET	LiF/HCl	Nanocomposite	200 hours at 70 °C	141
13	MXene/polymer	LiF/HCl	Nanocomposite	180 days	152

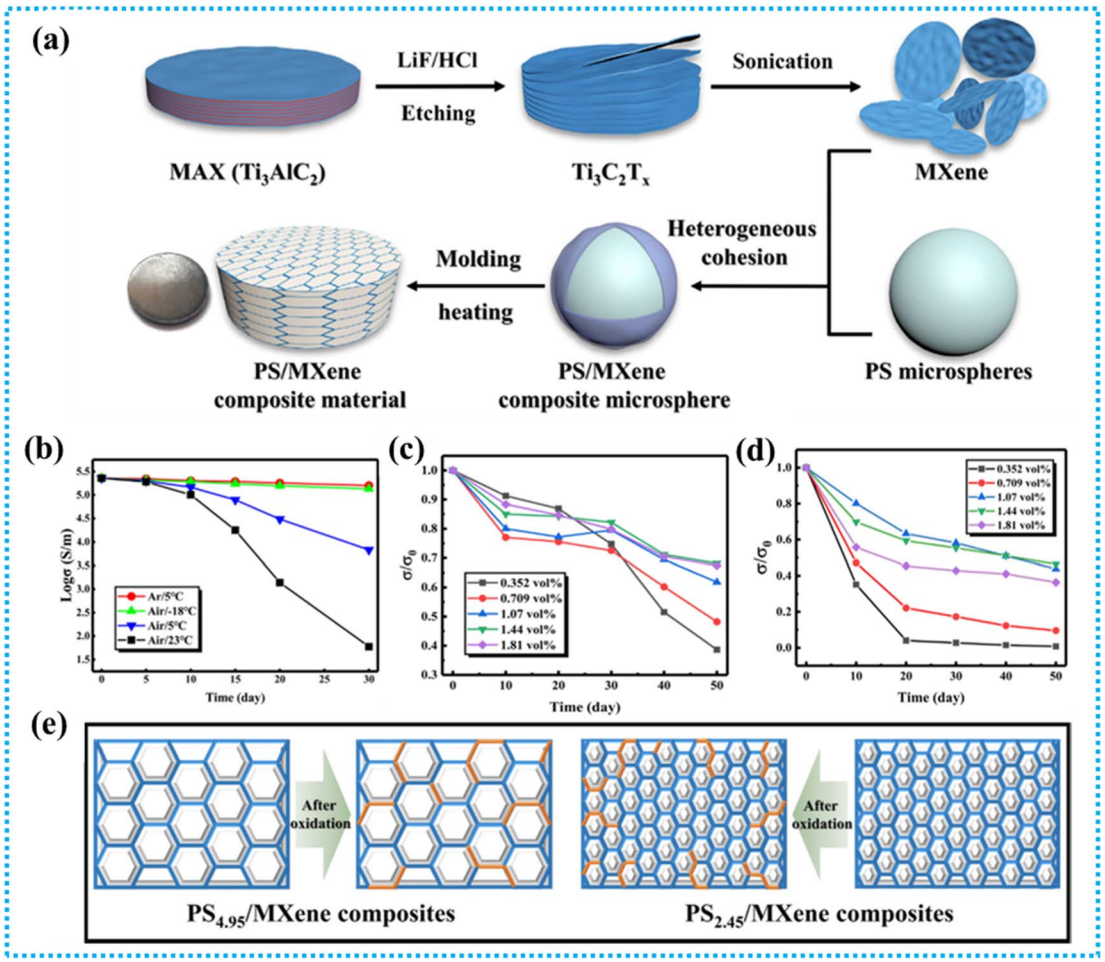

Fig. 4 (a) Schematic showing the exfoliation of $Ti_3C_2T_x$ MXene and fabrication of composites with a three-dimensional conductive network framework, (b) storage environment effects on MXene's intrinsic conductivity. (c and d) Impact of environmental factors on conductivity during composite material preparation, and (e) schematic of the oxidation mechanism in the MXene–polymer composite. Reproduced with permission from ref. 140. Copyright 2021, Elsevier Ltd.

because of its benefits, which include large lamellae, fewer flaws, and good electrical conductivity when created by LiF/HCl etching.[154] The electrical conductivity of freshly prepared MXene sheets was initially determined to be 2.28×10^5 S m^{-1}, as shown in Fig. 4b. This conductivity remained stable over 30 days in an argon atmosphere or at low temperatures. However, in the air at room temperature, MXene's conductivity dropped drastically, retaining only 0.026% of its initial value, highlighting its rapid oxidation and reduced practicality. The relationship between conductivity and storage time for PS/MXene composites is illustrated in Fig. 4c and d. Key findings include: (1) composites with higher MXene content maintain conductivity better over time compared to those with lower MXene content, showing slower degradation. (2) Larger particle composites exhibit greater conductivity loss than those with smaller particles, regardless of MXene concentration. Additionally, smaller PS microspheres create a denser conductive network, providing superior protection for MXene, as depicted in Fig. 4e. At larger microspheres, the conductive network is not well established, while smaller microspheres can form a much denser network that certainly offers superior MXene protection.

4.2 Polymer passivation

Polymer passivation is a technique used to improve the oxidation stability of MXenes, particularly against oxidation. By applying a polymer coating, such as polydopamine, the surface of MXenes is protected from environmental factors that can lead to degradation. This passivation method effectively reduces the oxidation rate and maintains the electrical properties of MXenes over time.[152] Under ambient conditions, pristine MXene begins to oxidize at room temperature. FE-SEM images of untreated MXene after 30 days (Fig. 5a) reveal powdery particles around the edges, indicating early oxidation. This process starts at edges and imperfections, progressing inward as shown in Fig. 5b, where oxidized TiO_2 (orange) replaces the MXene flakes (greenish). Prior reports have indicated that the smaller the MXene flake, the higher the oxidation rate.[155] Even in its dry state, MXene will eventually oxidize; nevertheless, the rate of oxidation is slower under ambient circumstances than in humid environments or DI water.[151] To prevent oxidation, an MXene film was coated with a 1% polymer solution in acetone. The polymer layer thickness was ~50 nm. Sheet resistance (R) was measured over 180 days to evaluate

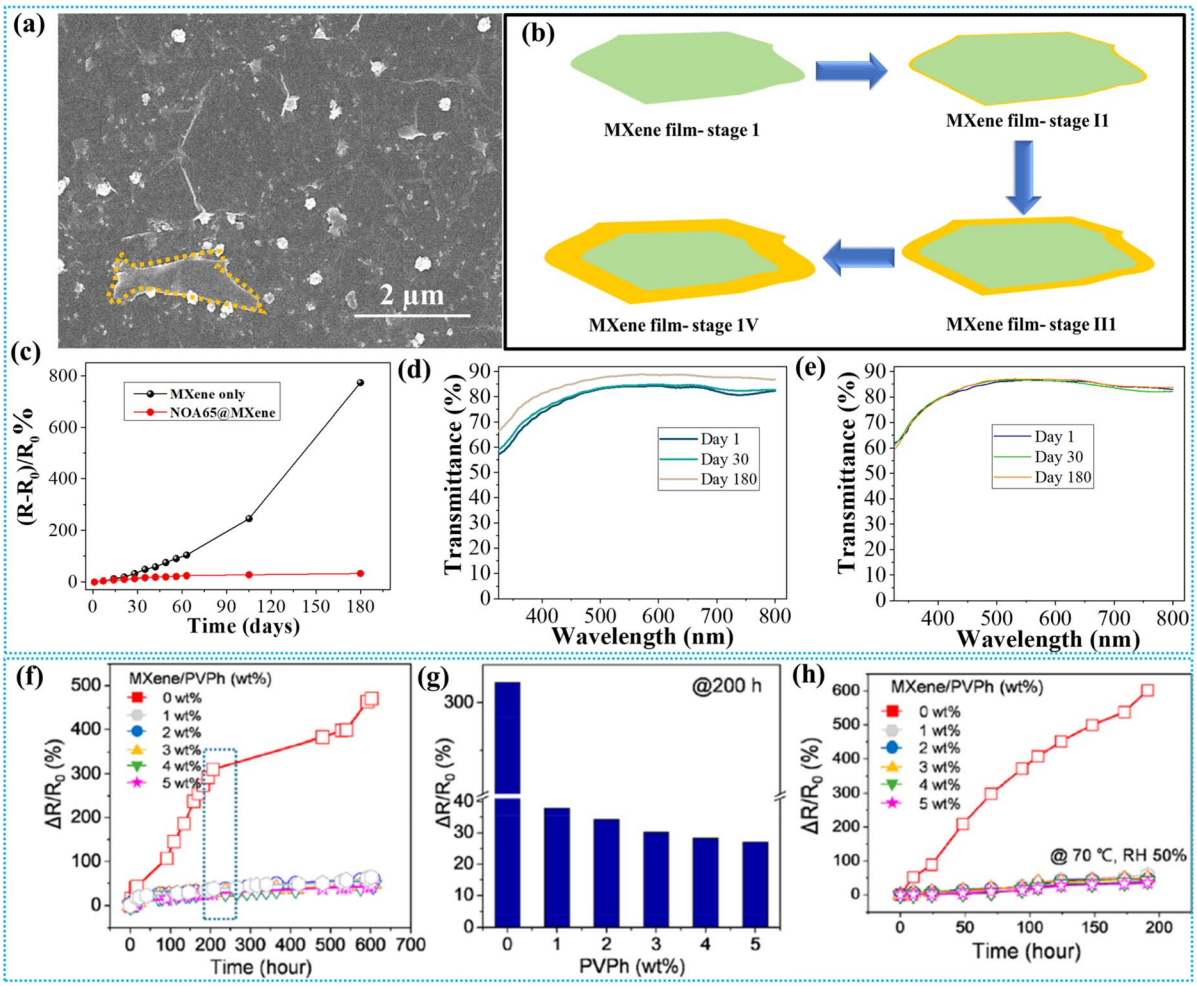

Fig. 5 MXene passivation by polymers. (a) FE-SEM image of an MXene sheet after 30 days of exposure to ambient conditions. The MXene flake that has been highlighted indicates the start of oxidation. (b) An illustration of the oxidation phases of MXene flakes. (c) The ratio of resistance change $(R - R_0/R_0)\%$ for treated and non-treated MXene films up to 180 days, where R_0 is the initial sheet resistance. UV-vis spectra of MXene films (d) non-treated and (e) treated at varying times. Reproduced with permission from ref. 152. Copyright 2022, Elsevier Ltd. (f) PL-MXene electrode's oxidation stability in comparison to the thin MXene layer. (g) The resistance decrease (ΔR) and initial resistance (R_0) of the PL-MXene electrode are shown against time and PVPh concentration, 200 hours after undergoing air oxidation. (h) Evolution of the resistance variations over time for the PL-MXene electrode under oxidation stability tests at 50% humidity and 70 °C. Reproduced with permission from ref. 141. Copyright 2021, American Chemical Society.

oxidation stability, with percentage changes shown in Fig. 5c. The results showed obvious proof that polymer passivation preserves MXene from oxidization. Even 180 days later, the relative resistance change, $(R - R_0/R_0)\%$, is ~20% in polymer-passivated MXene as compared to 800% in pristine MXene. The UV-vis spectra of the pristine MXene film after 30 days show the same transmittance as that on day 1; however, the transmittance rises to ~89% after 180 days (Fig. 5d). The high transmittance may be associated with TiO_2 formation due to the oxidized $Ti_3C_2T_x$ MXene.[151] In contrast to this, a negligible change in transmittance was noticed in the passivated MXene film after 180 days (Fig. 5e), indicating that almost no TiO_2 is formed and MXene oxidation is suppressed due to polymer passivation.

In another study, a polymer laminated MXene (PL-MXene) electrode was fabricated to analyze the impact of polymer lamination on electronic applications.[141] MXene flakes dispersed in water were spin-coated on a glass substrate silanized with a self-assembled monolayer of (3-aminopropyl)triethoxysilane (APTES).

Subsequently, poly(4-vinyl phenol) (PVPh) was prepared as a barrier layer on the MXene film.[141] The PL-MXene film, coated with a PVPh layer (~60 nm) on an MXene layer (~18 nm), exhibits a very smooth surface with an RMS roughness of ~1.4 nm. After 200–600 hours of air exposure, the resistance of bare MXene increases by 310% and 470%, respectively (Fig. 5f). In contrast, PL-MXenes with PVPh coatings showed minimal resistance change, between 27% and 38% after 200 hours, with only slight increases after 600 hours, demonstrating excellent oxidation resistance (Fig. 5g). Even at 70 °C temperature and 50% relative humidity, PL-MXenes with PVPh coatings maintained good stability, showing a $\Delta R/R_0$ change of 35% to 60%

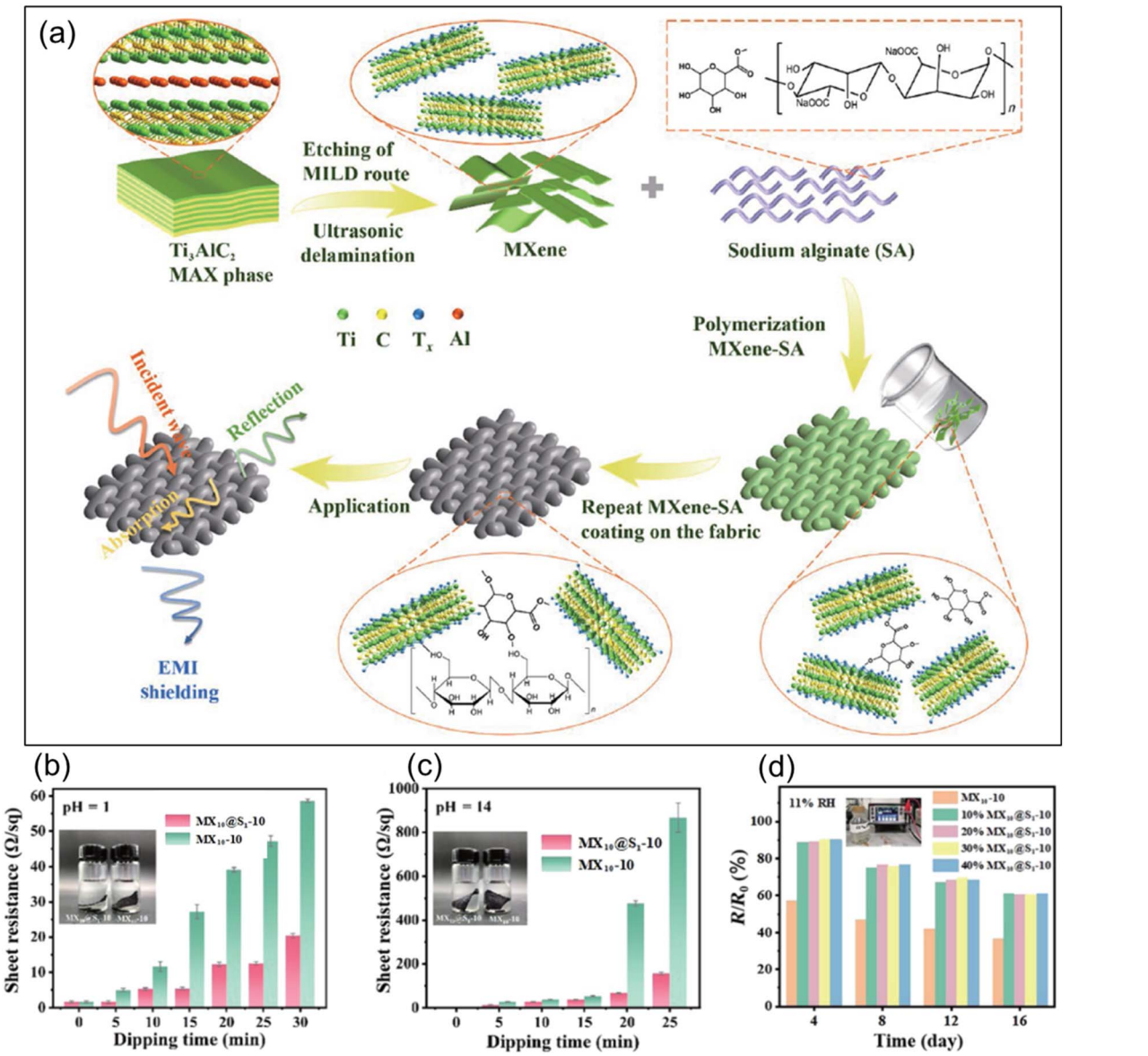

Fig. 6 (a) Schematic synthesis of MXene and illustration of the single-step fabrication strategy for sodium alginate–MXene films. Sheet-resistance (R/R_0) variation upon treating in (b) HCl (pH = 1) and (c) NaOH (pH = 14), and (d) change in R/R_0 for MX_{10}-10 and MX_{10}@S_1-10 with varying SA content at 11% RH and 25 °C. Reproduced with permission from ref. 150. Copyright 2024, Springer Nature.

after 200 hours, while bare MXene showed a drastic increase of 600% (Fig. 5h).

4.3 MXene–sodium alginate nanocomposites

Sodium alginate (SA) effectively stabilizes MXenes against oxidation. Alginate-stabilized MXenes maintain their conductivity and offer improved oxidation resistance. These MXene–alginate nanocomposites are particularly useful in flexible EMI shielding applications. Fig. 6a shows a schematic illustrating the fabrication process of the MXene–SA composite.[150] Linen fabric, chosen for its eco-friendly properties, was used as a substrate for MXene composite modification. Before applying the composite, the fabric was treated with decontamination powder to ensure effective loading. Hydrogen bonding between SA and MXene was achieved *via* functional groups on the MXene surface, enhancing the composite's mechanical strength and oxidation stability. MXene–SA composites and MXene alone were subjected to acidic and basic conditions to assess their environmental stability and oxidation resistance. After 30 minutes in HCl (pH = 1), the sheet resistance of MX_{10}@S_1-10 (MXene with SA) increased to 20.4 ± 0.7 Ω per sq, whereas MX_{10}-10 (MXene without SA) showed a much higher increase to 58.63 ± 0.047 Ω per sq (Fig. 6b). In NaOH (pH = 14), the resistance of MX_{10}@S_1-10 rose to 155.33 ± 7.02 Ω per sq after 25 minutes, compared to a significant rise to 867.67 ± 66.38 Ω per sq for MX_{10}-10 (Fig. 6c). This demonstrates that the MXene–SA composite offers superior protection against oxidation in both acidic and basic environments. The results manifest that

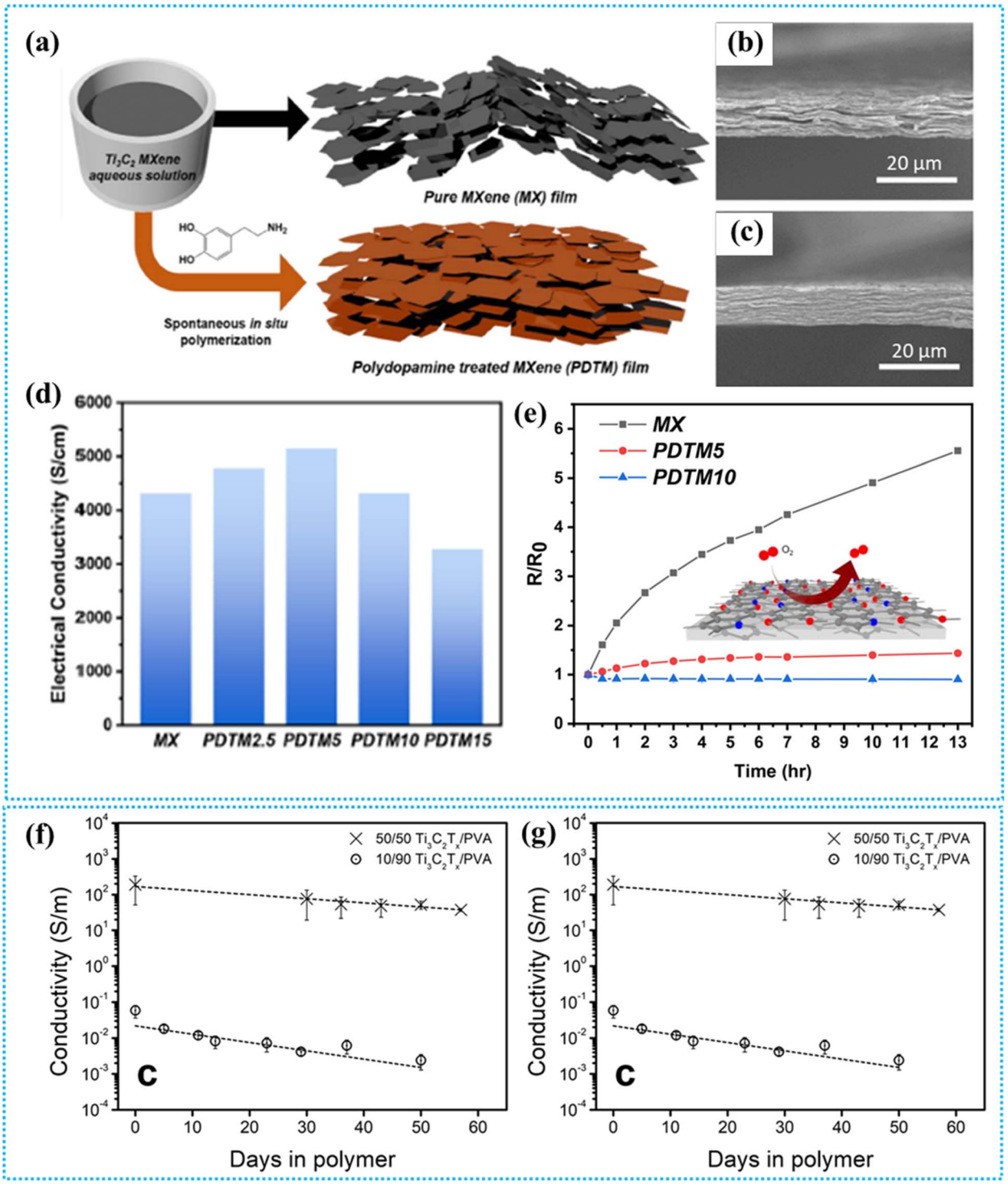

Fig. 7 (a) Schematic showing the production process and the morphological changes between pure and polydopamine-treated MXene films, (b) and (c) cross-sectional SEM images of pure- and PDTM-treated MXene, (d) electrical conductivity of the MXene film with varied PDTM concentrations (0–15%), and (e) change in electrical resistance during heating (170 °C) in air. Reproduced with permission from ref. 148. Copyright 2020, American Chemical Society. The conductivity variation of (f) pristine MXene films and (g) MXene/PVA films in air.[151]

MX_{10}@S_1-10 has much better stability than MX_{10}-10 even under harsh conditions such as acidic and alkaline. The coating of MXene sheets with SA inhibited the direct interaction of ambient oxygen, moisture, or corrosive solutions, resulting in improved oxidation stability.

The oxidation stability of the fabricated MXene composites was further studied by measuring their sheet resistance after storing under humid conditions at ambient temperature (25 °C). MX_{10}-10 and MX_{10}@S_1-10 were stored under humid conditions (RH) of 11%, 33%, 75.5%, and 97.6% with varied SA

amounts of 10%, 20%, 30%, and 40% for evaluating their stability. There is a change in the resistance of the MX_{10}-10 composite with time at 11% RH, with the resistance ratio decreasing to 36.67% from 57.48%. The resistance ratio decreased from 88.56% to 60.99% for $MX_{10}@S_1$-10 upon the addition of 10% SA (Fig. 6d). $MX_{10}@S_1$-10 has a higher resistance ratio than MX_{10}-10, indicating that $MX_{10}@S_1$-10 has a higher stability under varied humid and corrosive conditions.

4.4 Mussel-derived dopamine polymerization

Researchers addressed the oxidation vulnerability of MXene-based materials by utilizing mussel-derived dopamine polymerization.[148] Dopamine derived from mussels effectively overcomes oxidation by enhancing interfacial interaction and ordering in MXene films. Dopamine forms a thin sticky layer on the surfaces of MXene flakes by *in situ* polymerization and binding caused by spontaneous interfacial charge transfer. Effective oxygen and moisture screening also significantly increases the ambient stability of MXene films. It is interesting to note that angstrom thick polydopamine enhances MXene films' inherent high electrical conductivity. Fig. 7a shows the fabrication procedure and morphological distinction between pure- and polydopamine-treated MXene (PDTM) films. SEM cross-sectional images show that pure MXene has random, misaligned layers, while PDTM5 films exhibit well-aligned, consistent MXene sheets (Fig. 7b and c). Neighboring MXene flakes are aligned in their organized stacking by the polydopamine nanobinder, which bridges them together and creates a highly ordered MXene structure.[156] After applying a polydopamine coating, internal voids and misfits could be mostly eliminated.[157] As a result, the dopamine coating increased the apparent density of hybrid films, resulting in in-plane electron transfer. Furthermore, dopamine hybridization enhances MXene's electrical conductivity; PDTM5 has the greatest conductivity of 5141 S cm^{-1} as shown in Fig. 7d. The enhanced flake alignment, enhanced film densification, and increased electron density all contribute to in-plane electron transport.[158] Polydopamine-treated MXene films exhibit significantly reduced oxidation under ambient conditions and elevated temperatures, as shown in Fig. 7e. The PDTM5 film experiences a much smaller increase in sheet resistance at 170 °C compared to the pure MXene film, which shows a five-fold resistance increase in 13 hours. The PDTM10 film demonstrates even lower resistance, likely due to thermally induced crystallization of the polydopamine layer, which also limits oxygen and moisture infiltration.

The thin dopamine layer protects MXene from oxidation while maintaining electrical performance and enhancing interfacial contact.

4.5 Can all polymers prevent MXene oxidation?

As discussed above, while most polymers support MXene stability, not all polymers can effectively prevent oxidation. Polymers with a hydrophilic nature are mostly unable to prevent oxidation in MXenes as hydrophilicity allows water and oxygen molecules to penetrate the composite and the MXene surface. Habib *et al.* studied the oxidation stability of vacuum-filtered $Ti_3C_2T_x$ films and MXenes/PVA films and used the electrical conductivity as an indicator to estimate their stability.[151] The study monitored the decline in the electrical conductivity of $Ti_3C_2T_x$/PVA composites over time and compared it with that of pristine MXene films exposed to air (Fig. 7f and g). Two different weight ratios of PVA were used to assess the impact of polymer concentration on the stability of MXenes: 50–50 wt% $Ti_3C_2T_x$ to PVA and 10–90 wt% $Ti_3C_2T_x$ to PVA. The study reported that the pristine MXene maintained only 2% of its initial conductivity in air after 9 weeks (Fig. 7f). The conductivity of the 50–50 wt% sample decreased to about 40% of its original value by day 30 and 20% by day 57, while that of the 10–90 wt% sample dropped to roughly 7% by day 29 and 4% by day 50 (Fig. 7g). Both samples exhibited a rapid decline in conductivity during the first four weeks, followed by a slower decrease, indicating a reduction in oxidation rates due to diminishing reactive sites. This consistent trend across both composite samples and the $Ti_3C_2T_x$ film suggests that the oxidation mechanism is mostly unaffected by polymer content, and the hydrophilic PVA does not provide an effective protective barrier against oxidation.

5. Synergistic effects on nanocomposite properties

Typically, the main benefit of composite membranes lies in their tailored properties, allowing the use of specific materials for particular applications. MXene materials can serve as optimal nanofillers, enhancing MXene/polymer membranes with a range of properties such as increased mechanical strength,[159] better thermal performance,[160] enhanced conductivity,[161] *etc.* Moreover, the oxidation of MXene materials is significantly reduced due to their effective encapsulation within the polymer.[162] MXenes can be combined with two types of polymers: cationic and neutral.[163] The cationic polymer (*e.g.* PDDA) can form electrostatic interactions with negatively charged MXene nanosheets, resulting in a relatively loose structure with some voids, similar to the MXene-only film. In contrast, the neutral polymer (*e.g.* PVA) can rely on hydrogen bonding, leading to a compact layered structure (Fig. 8a). Using negatively charged polymers can enhance the dispersion of MXene nanosheets due to electrostatic repulsion. Molecular dynamics simulations reveal the synergy of hydrogen and ionic bonding agents in effectively transferring local stress while providing substantial slippage space for MXene nanosheets.[164]

5.1 Mechanical properties

The mechanical properties represent a crucial factor for polymer-based composites, which can be effectively enhanced by incorporating inorganic fillers. The distinctive characteristics and nanostructures of nanomaterials, along with their reactivity, have made them appealing candidates as fillers to strengthen polymer-based membranes across various types of polymers. Usually, free-standing MXenes often experience inadequate mechanical characteristics and weak interactions among the nanosheets, which can lead to structural failure due

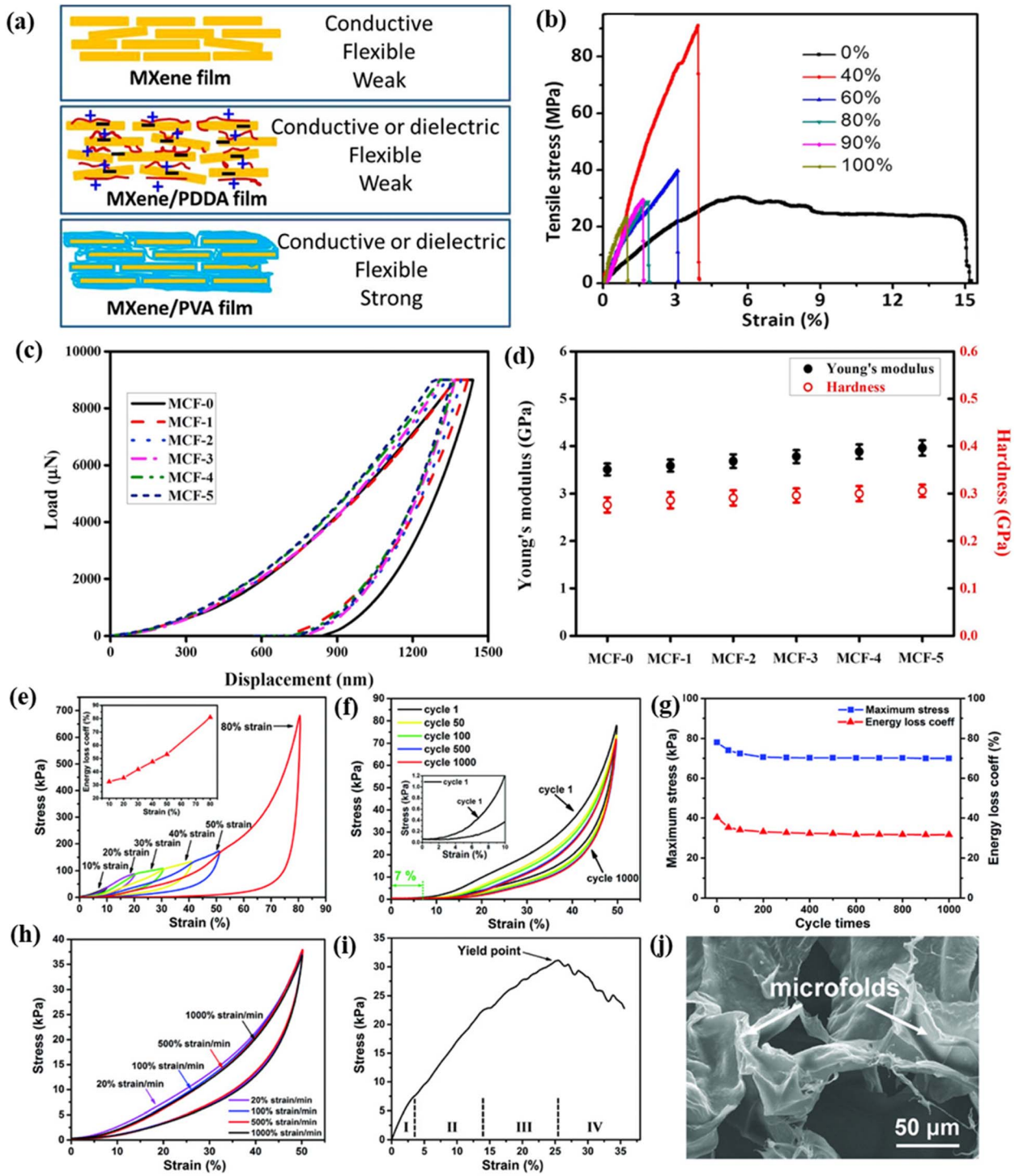

Fig. 8 Mechanical properties of the MXene–polymer nanocomposite. (a) Schematic representation of MXene-based functional films demonstrating tunable mechanical characteristics of flexible, free-standing $Ti_3C_2T_x$, $Ti_3C_2T_x$/PVA, and $Ti_3C_2T_x$/PDDA films. (b) Stress–strain curves illustrating the performance of $Ti_3C_2T_x$/PVA films with varying $Ti_3C_2T_x$ content.[163] (c) Load–displacement curves showcasing the performance of the MCF/epoxy EMI shielding nanocomposites; (d) hardness and Young's modulus measurements for the MCF/epoxy EMI shielding nanocomposites, illustrating their mechanical properties. Reproduced with permission from ref. 165. Copyright 2019, Elsevier Ltd. (e) Compressive stress–strain (σ–ε) curves for the aerogel (MXene to PAA ratio 1 : 4) at various strains, with an inset showing energy loss coefficients at these strains. (f) Fatigue performance of the aerogel (MXene to PAA ratio 1 : 1) subjected to 1000 cycles at 50% strain. (g) Changes in elastic stress and energy loss coefficients over 1000 cycles at 50% strain. (h) Stress–strain curves of the aerogel (MXene to PAA ratio 2 : 1) evaluated at different compressive strain rates (20, 100, 500, and 1000% min^{-1}). (i) Tensile stress–strain curve for the aerogel (MXene to PAA ratio 2 : 1); (j) SEM image illustrating the fracture morphology of the MXene/PI aerogel. Reproduced with permission from ref. 166. Copyright 2018, Wiley.

to capillary forces during the polymer impregnation process. Introducing 10 wt% PVA improves the tensile strength of the $Ti_3C_2T_x$/PVA film by 34%, reaching 91 ± 10 MPa, around four-fold that of the pure $Ti_3C_2T_x$ film, when the PVA loading was increased to 60 wt%[163] (Fig. 8b). The enhanced stiffness and strength indicate effective stress transfer to the embedded $Ti_3C_2T_x$ nanosheets, suggesting some interfacial bonding, likely aided by the OH group terminations on $Ti_3C_2T_x$. The Young's modulus of $Ti_3C_2T_x$/PVA films can be adjusted by varying the $Ti_3C_2T_x$-to-PVA ratio. Hollow cylinders made from these films can support substantial weights; a cylinder with a 6 mm diameter and 10 mm height can support about 4000 times its weight (~1.3 MPa) and a similar cylinder with 90 wt% $Ti_3C_2T_x$/PVA can support approximately 15 000 times its weight (~2.9 MPa).

To explore this issue in greater depth, researchers have created MXene composite frameworks by adding crosslinking agents to connect MXene nanosheets. Researchers combined resorcinol and formaldehyde with $Ti_3C_2T_x$ to form a composite framework.[165] The organic precursors polymerized on hydrophilic $Ti_3C_2T_x$, creating a crosslinked $Ti_3C_2T_x$/C foam (MCF) structure after pyrolysis. This framework exhibited a well-connected structure with impressive mechanical strength, supporting 500 times its weight. Using a similar polymer impregnation method with epoxy precursors, a dense $Ti_3C_2T_x$/C/epoxy film structure was also produced. The MCF samples were labeled as MCF-0 to MCF-5, with increasing $Ti_3C_2T_x$ MXene content from 0 to 1.64 wt%, respectively. The SEM images show that adding $Ti_3C_2T_x$ MXene to the MCF resulted in a reduction of cell density due to crosslinked, folded sheets, while further MXene addition increased cell density and decreased sheet size.

The polymerization of resorcinol and formaldehyde on hydrophilic $Ti_3C_2T_x$ MXene effectively fused the carbon structure and MXene, enhancing crosslinking density and carbon junctions. The load–displacement curves (Fig. 8c) show that increasing $Ti_3C_2T_x$ MXene content reduces the indentation depth of MCF/epoxy EMI shielding nanocomposites, enhancing their resistance to indentation. As $Ti_3C_2T_x$ MXene content increases, Young's modulus and hardness improve by 13% and 11%, respectively, due to the superior mechanical properties of MXenes and the improved stress transfer within the crosslinked MCF network (Fig. 8d). The higher cell density from additional MXene further strengthens the cross-linked structure, boosting the mechanical performance of the nanocomposites. Liu *et al.* improved the flexibility and mechanical stability of $Ti_3C_2T_x$/PI foam by using polyimide (PI) to bridge $Ti_3C_2T_x$ nanosheets, achieving compressibility and stretchability through freeze-drying $Ti_3C_2T_x$/poly(amic acid) (PAA) followed by polymerization.[166] An aqueous solution of hydrophilic PAA and $Ti_3C_2T_x$ was freeze-dried, followed by thermal annealing to polymerize PAA into PI. Strong polar interactions between PI and $Ti_3C_2T_x$ tightly bonded the two components, resulting in a durable $Ti_3C_2T_x$/PI foam with excellent mechanical properties, including compression, torsion, and 180° bending. The MXene/PI aerogel demonstrates strong interfacial bonding between MXene and PI, resulting in superior mechanical properties compared to neat MXene aerogel. Fig. 8e shows the compressive stress–strain curves, where the MXene/PI aerogel exhibits excellent reversible compressibility up to 80% strain (MXene to PAA ratio 1 : 4), unlike the pristine MXene aerogel, which suffers from irreversible deformation due to weak interactions between its layers. The MXene/PI aerogel also has a high energy loss coefficient (η), reaching 80.9% at 80% strain, indicating strong energy absorption. This makes it highly effective for shock absorption, as demonstrated by its ability to protect a glass plate from fracturing after a heavy impact while maintaining its original shape. The MXene/PI aerogel was tested for fatigue resistance through long-term compression-release cycles. After pre-stabilizing the aerogel with several loading–unloading cycles, it maintained over 90% of maximum stress with only 7% volume deformation after 1000 cycles at a fixed strain of 50% (Fig. 8f), indicating excellent structural robustness. While the maximum stress and energy loss coefficient slightly decreased during initial cycles, they stabilized over 1000 cycles (Fig. 8g). Additionally, the aerogel retained its compressibility at various strain rates (20, 100, 500, and 1000% min^{-1}), with stress–strain curves showing close overlap (Fig. 8h). Uniaxial tensile tests show that the MXene/PI aerogel achieves a tensile strain of 26% and a maximum stress of 31.1 kPa, attributed to enhanced sheet-to-sheet interactions with PI (Fig. 8i). The tensile stress–strain curve consists of four stages: (1) elastic deformation, where stress increases linearly with strain; (2) densification, marked by continuous stress increase as the porous network compacts; (3) a plateau region with slower stress increases due to friction and adhesion; and (4) fracture, characterized by decreasing stress with fluctuations, indicating structural failure. Fractured surfaces with pleated cell walls illustrate the role of micro-folds in tolerating cyclic tensile deformation (Fig. 8j). Some of the mechanical properties of MXene–polymer nanocomposites are summarized in Table 2.

5.2 Electrical properties

In any device application, conductivity is a crucial property, and MXenes excel in this regard, achieving an impressive electrical conductivity of ~24 000 S cm^{-1}.[178] Among the MXenes, $Ti_3C_2T_x$ stands as a pinnacle, characterized by its exceptional electrical conductivity and multifaceted utility across diverse applications. Most polymers are insulators, but adding MXene flakes can improve their electrical conductivity. The addition of MXenes to polymers can separate the layers of MXenes and promote bonding at the molecular level between MXene and the polymer. It was found that the electrical conductivity of PVA increases from 0.04 to 2.2 × 10^4 S m^{-1} when the MXene ($Ti_3C_2T_x$) content varies from 40 wt% to 90 wt% in the polymer matrix.[163] The relationship between the MXene content in the polymer matrix, *e.g.* polyacrylamide (PAM), and electrical conductivity is expressed as[179]

$$\sigma = k(m - m_{th})^{\alpha}$$

In this equation, σ represents the electrical conductivity of nanocomposite ($Ti_3C_2T_x$/PAM) membranes, k is a constant, m denotes the MXene loading amount, m_{th} is the percolation

Table 2 Mechanical properties of MXene–polymer nanocomposites

S. no.	Polymer	MXene	MXene concentration	Mechanical property (MPa)	Improvement percentage (%)	Ref.
1	Natural rubber	$Ti_3C_2T_x$	6.71 vol%	~18 (tensile stress)	700	167
2	Epoxy resin	$Ti_3C_2T_x$	1.0 wt%	98 (flexural strength)	66	168
3	PEDOT:PSS	$Ti_3C_2T_x$	$Ti_3C_2T_x$: polymer (3 : 1)	30.18 (tensile strength)	503.6	169
4	Polyvinyl alcohol (PVA)	$Ti_3C_2T_x$	2 wt%	~48 (tensile stress)	77.8	170
5	Polyurethane (PU)	$Ti_3C_2T_x$	0.5 wt%	~18 (tensile strength)	20	171
6	Thermoplastic polyurethane (TPU)	$Ti_3C_2T_x$	0.5 wt%	20.6 (tensile strength)	47.1	172
7	PVC	$Ti_3C_2T_x$	15 wt%	57.3 (tensile strength)	174.1	173
8	PVA	$Ti_3C_2T_x$	0.5 wt%	13 (tensile strength)	—	174
9	Epoxy	Ti_3CN	90 wt%	12.8 GPa (Young's modulus)	—	175
10	Epoxy	$Ti_3C_2T_x$	15 wt%	4.32 GPa (Young's modulus)	20.8	176
11	Epoxy	$Ti_3C_2T_x$	4.25 wt%	3.96 GPa (Young's modulus)	13	165
12	Polypropylene	$Ti_3C_2T_x$	2.0 wt%	18.4 (tensile strength)	35.3	177
13	PVA	$Ti_3C_2T_x$	40	91 (tensile strength)	313.6	163

threshold required for conductivity enhancement, and α is the scaling exponent.

The role of MXene in inducing electrical conductivity in MXene–polymer nanocomposites has been theoretically predicted for various nanocomposites like polypropylene (PP)/MXene, nitrile butadiene rubber (NBR)/MXene, natural rubber (NR)/MXene, polystyrene (PS)/MXene, and polyacrylamide (PAM)/MXene.[180] A proposed model predicts electrical conductivity, assuming a MXene nanosheet thickness of ~500 nm. The percolation threshold (φ_p), calculated using the interphase thickness, aligns with experimental values. The φ_p is given by the following equation:

$$\varphi_p = \frac{(40t)^2}{(D + 20t_i)^2}$$

where t is the thickness, t_i the interphase depth, and D the MXene diameter. Uniform MXene dispersion lowers the percolation threshold, while clustering increases it. Based on theoretical predictions, the interphase thickness for NBR/MXene, PP/MXene, PS/MXene, NR/MXene, and PAM/MXene nanocomposites is 10, 10, 34, 17, and 5 nm, respectively. The proposed model yields a tunneling distance of 0.76 to 7.5 nm, which is below the 10 nm maximum threshold for tunneling conductivity. For all MXene-based nanocomposites, the theoretical calculations match experimental values (Fig. 9a–d).

Yu *et al.* developed an MXene organohydrogel incorporating glycerol (Gly), featuring an MXene network for electron conduction, binary solvent channels for ion conduction, and multiple solvent-polymer–MXene interfaces for EMI applications.[181] The conductivity of the MXene hydrogel rises sharply from 0.099 to 0.442 S m^{-1} with increasing MXene content from 0.1 to 2.2 wt%, before slightly decreasing to 0.394 S m^{-1} (Fig. 9e). This trend reflects the balance between enhanced electron transport and reduced ion conduction due to smaller ion channels at higher MXene concentrations.

MXenes, when combined with cellulose nanofibers (CNFs), form a composite paper that demonstrates significant improvements in electrical conductivity.[182] As the D-$Ti_3C_2T_x$ content increases, the conductivity rises sharply, reaching 739.4 S m^{-1} at 90 wt%. Even at 50 wt%, the conductivity is 9.691 S m^{-1}, exceeding the 1 S m^{-1} required for effective EMI shielding applications (Fig. 9f). While the insulating nature of CNFs slightly reduces the overall conductivity compared to pure D-$Ti_3C_2T_x$, their one-dimensional structure aids in the alignment of MXene nanosheets, ensuring a connected and efficient conductive network. This nanocomposite exhibits a tensile strength of 135.4 MPa, a fracture strain of 16.7%, and a high folding endurance of up to 14 260 cycles.

MXene-based nanocomposites display both isotropic and anisotropic electrical properties, depending on their structural alignment and processing conditions. When hybridized with materials like CNTs and PVDF, these composites can exhibit anisotropic conductivity, with high in-plane conductivity and lower through-plane conductivity in films, while achieving isotropic conductivity in foams. Le *et al.* prepared PVDF/CNT/MXene films and introduced foam structures using CO_2-assisted foaming at various saturation temperatures (T_{sat}) and different MXene content levels. CNTs intertwine with MXenes to form a 3D conductive network, further improving electrical performance. PVDF is selected for its pyroelectric effect, high dielectric constant, mechanical stiffness, and thermal stability. The in-plane conductivity ($\sigma_{\parallel}$) and through-plane conductivity ($\sigma_{\perp}$) of PVDF/CNT/MXene films initially increase with MXene content but level off due to contact resistance between fillers. With 1 wt% MXene, $\sigma_{\parallel}$ reaches a peak value (~17 S m^{-1}) due to optimal MXene alignment, while $\sigma_{\perp}$ remains lower due to poor conductivity between layers. Higher MXene content (12 wt%) leads to aggregation, reducing $\sigma_{\parallel}$ and increasing $\sigma_{\perp}$ slightly. Composite foams, prepared at T_{sat} = 171 °C, show increased $\sigma_{\perp}$ and decreased $\sigma_{\parallel}$ compared to films, with more random filler orientation enhancing through-plane connectivity. Larger cell sizes at higher T_{sat} reduce filler contact, lowering both conductivities. Some of the electrical properties of MXene–polymer nanocomposites are summarized in Table 3.

5.3 Thermal properties

MXenes exhibit anisotropic properties due to their structural makeup, with strong covalent bonds within the basal plane

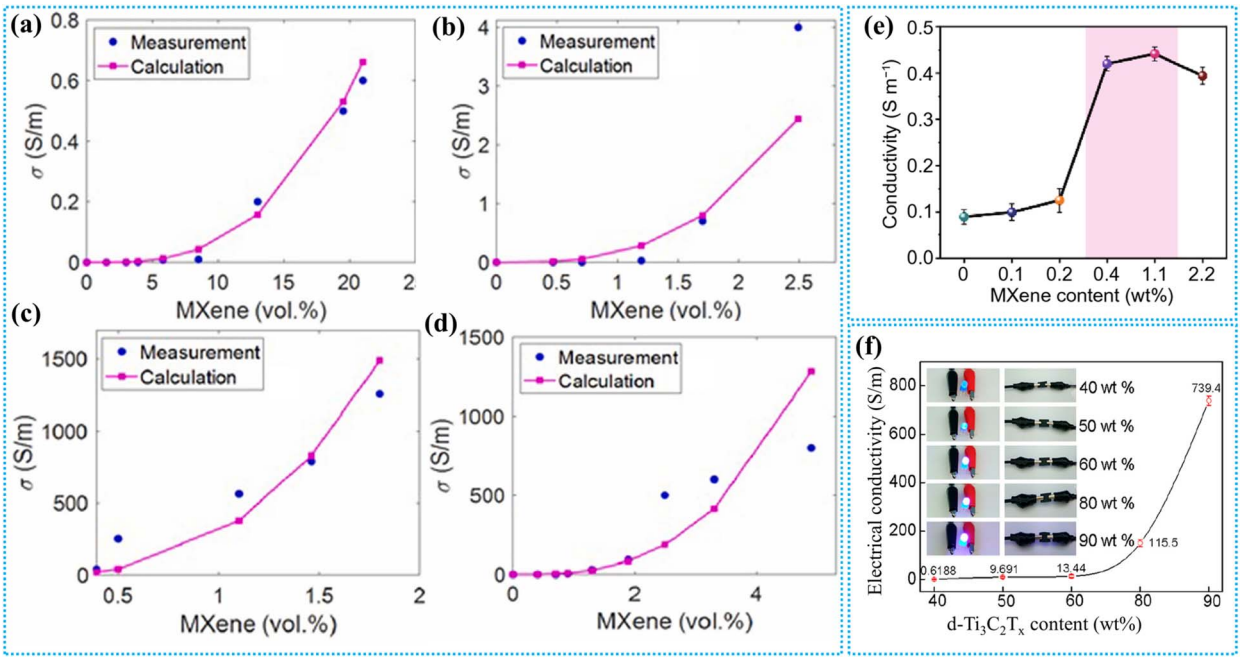

Fig. 9 Electrical properties of MXene–polymer nanocomposites. (a–d) Empirical findings and conductivity predictions for NBR/MXene, PP/MXene, PS/MXene, and NR/MXene nanocomposites, respectively. Reproduced with permission from ref. 180. Copyright 2024, Elsevier Ltd. (e) Conductivity variation of the MXene hydrogel with MXene content.[181] (f) Electrical conductivity *vs.* D-$Ti_3C_2T_x$ content for D-$Ti_3C_2T_x$/CNF composite sheets. Reproduced with permission from ref. 182. Copyright 2018, American Chemical Society.

providing high in-plane strength, while weaker interlayer forces allow easy exfoliation.[189] This anisotropy results in higher thermal conductivity within the plane, making MXenes ideal for heat dissipation in different applications.[190] MXenes, particularly Ti_3C_2, have thermal conductivities that often surpass those of many metals, making them ideal for enhancing heat transfer in composites. When incorporated into polymers, MXenes improve thermal conductivity by forming interconnected networks that facilitate efficient heat conduction. The effectiveness of these composites depends on the polymer type; those that form hydrogen bonds with MXenes, like PVA and PVDF, enhance thermal transfer through better interfacial bonding. The loading amount of MXenes also influences conductivity, with significant improvements occurring when a continuous network is established at higher concentrations. First-principles density functional calculations show that MXenes exhibit thermal conductivities greater than most metals and low-dimensional semiconductors, making them promising additives for enhancing the thermal conductivity of polymer composites. Earlier studies demonstrate that a $Ti_3C_2T_x$/PVA membrane (12.71 wt% PVA) demonstrated a thermal conductivity of 47.6 W m^{-1} K^{-1}, which was lower than that of pristine Ti_3C_2 (55.8 W m^{-1} K^{-1}).[191] Cao *et al.* found that the thermal conductivity of $Ti_3C_2T_x$/PVDF membranes exhibited minimal increase at low MXene loading (<1.0 wt%) but surged at higher levels.[192] This increase is attributed to the extensive

Table 3 Electrical properties of MXene–polymer nanocomposites

S. no.	Polymer	MXene	MXene concentration	Electrical conductivity (S m^{-1})	Ref.
1	Natural rubber	$Ti_3C_2T_x$	6.71 vol%	1400	167
2	PEDOT:PSS	$Ti_3C_2T_x$	88 wt%	340.5	169
3	Epoxy	$Ti_3C_2T_x$	15 wt%	105	176
4	Epoxy	$Ti_3C_2T_x$	4.25 wt%	184	165
5	PDMS	$Ti_3C_2T_x$	2.5 vol%	550	183
6	PVA	$Ti_3C_2T_x$	90 wt%	22 433	163
7	PEO	$Ti_3C_2T_x$	1 wt%	210×10^{-6}	184
8	PAM	$Ti_3C_2T_x$	6 wt%	3.3×10^{-2}	185
9	PVA	$Ti_3C_2T_x$	0.14 wt%	590×10^{-6}	186
10	Polystyrene	$Ti_3C_2T_x$	0.26%	1081	187
11	PVDF–TrFE–CFE[a]	$Ti_3C_2T_x$	19.5 wt%	37.4	188

[a] poly(vinylidene fluoride–trifluoroethylene) (PVDF–TrFE).

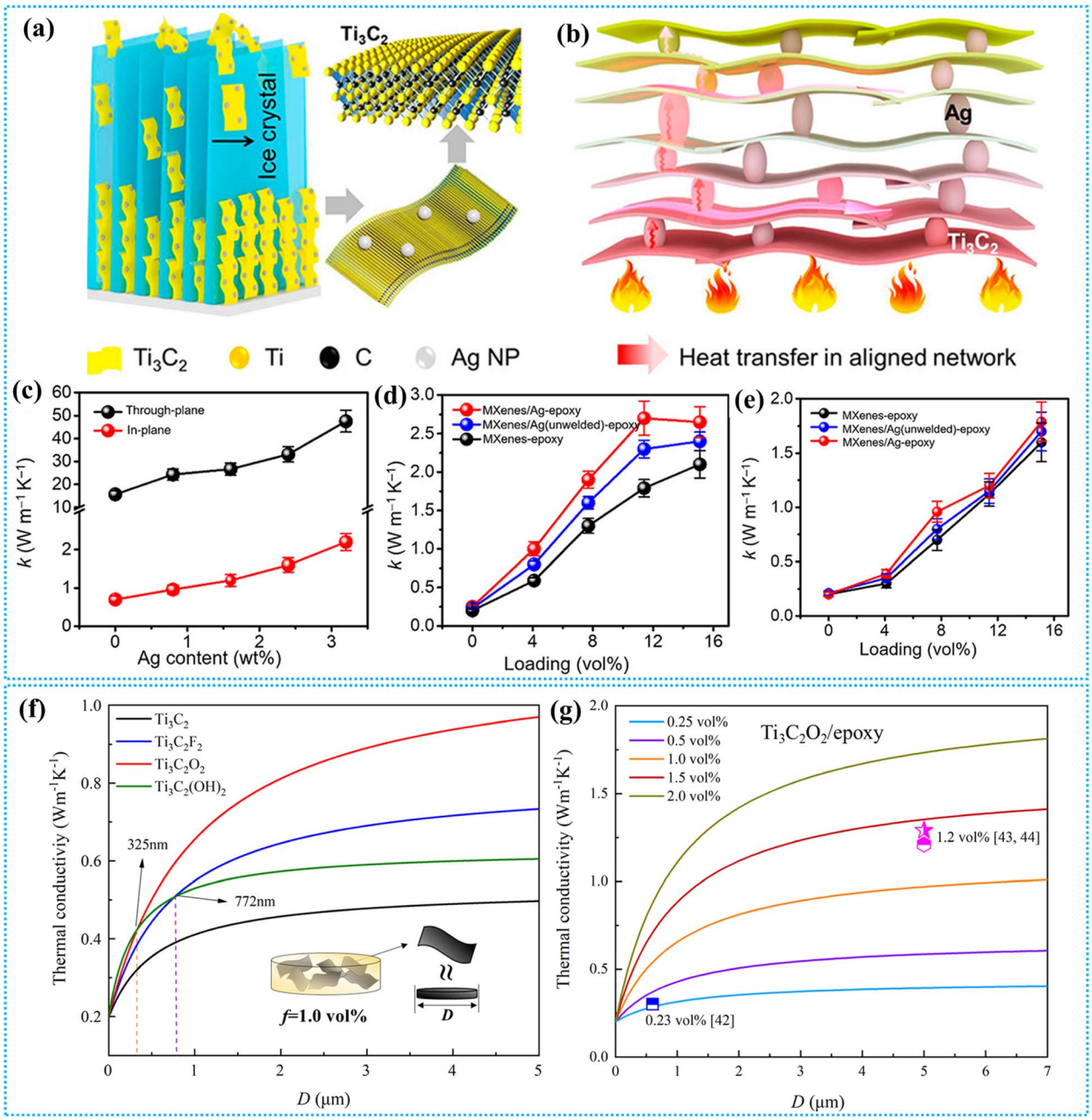

Fig. 10 Thermal properties of MXene–polymer nanocomposites. (a) Illustration of the ice-template technique for aligning MXene/Ag nanofillers. (b) Effective heat transfer in both in-plane and through-plane directions within the welded MXene/Ag aerogel skeleton due to material and structural synergy. (c) Thermal conductivities of MXene films with varying Ag loadings. (d) Through-plane conductivity comparisons of MXene–epoxy, MXene/Ag (unwelded)–epoxy, and MXene/Ag–epoxy nanocomposites. (e) In-plane conductivity comparisons of MXene–epoxy, MXene/Ag (unwelded)–epoxy, and MXene/Ag–epoxy nanocomposites. Reproduced with permission from ref. 193. Copyright 2020, American Chemical Society. (f) Thermal conductivity of $Ti_3C_2T_x$/epoxy composites at 1.0 vol% filler content. (g) Thermal conductivities of $Ti_3C_2O_2$/epoxy composites with varying volume content and filler size. Reproduced with permission from ref. 194. Copyright 2022, Elsevier Ltd.

surface area of Ti_3C_2 flakes and the formation of hydrogen bonds with PVDF, which effectively reduce interfacial thermal resistance and enhance thermal conductivity.

To improve the thermal conductivity of MXene/epoxy nanocomposites, Ji *et al.* designed 3D MXene/Ag aerogels using the ice templating method (Fig. 10a) as heat transfer skeletons for epoxy nanocomposites by *in situ* decorating Ag nanoparticles on exfoliated MXene nanosheets to improve contact[193] (Fig. 10b). The vertically aligned MXenes, with a high through-plane thermal conductivity of 472 W m^{-1} K^{-1}, form a thermally conductive network when combined with Ag, which has a thermal conductivity of 430 W m^{-1} K^{-1} and low soldering temperature. The resulting MXene/Ag/epoxy nanocomposite exhibits a through-plane thermal conductivity of 2.65 W m^{-1}

Table 4 Thermal properties of MXene–polymer nanocomposites

S. no.	Polymer	MXene	MXene concentration	Thermal conductivity (W mK^{-1})	Improvement percentage (%)	Ref.
1	PVA	$Ti_3C_2T_x$	2 wt%	—	18.7	170
2	Thermoplastic polyurethane (TPU)	$Ti_3C_2T_x$	1 wt%	—	8.4	172
3	PVC	$Ti_3C_2T_x$	15 wt%	3.45	∼1050	173
4	PVA	$Ti_3C_2T_x$	2 wt%	—	8.2	174
5	Epoxy	Ti_3CN	5 wt%	—	2.7	175
6	Epoxy resin	$Ti_3C_2T_x$	1.0 wt%	—	−0.55	168
7	Polypropylene	$Ti_3C_2T_x$	2.0 wt%	—	11.8	177
8	PDMS	$Ti_3C_2T_x$	2.5 vol%	0.694	220	183
9	PVDF	$Ti_3C_2T_x$	5 wt%	0.363	100	196
10	PVA	$Ti_3C_2T_x$	—	47.6	—	197
11	Epoxy	$Ti_3C_2T_x$	15 wt%	7.60	∼100	198
12	Epoxy	$Ti_3C_2T_x$	1 wt%	0.587	141.3	199

K^{-1}, a 26.2% increase compared to that of the MXene–epoxy nanocomposite, along with improved mechanical and thermal expansion properties. The films demonstrate distinct thermal conductive behaviors in the in-plane and through-plane directions, with in-plane thermal conductivity rising to 47.57 W m^{-1} K^{-1} at 3.2 wt% Ag nanoparticle loading compared to 15.64 W m^{-1} K^{-1} for pristine MXene films. In the through-plane direction, the thermal conductivity increases from 0.7 to 2.2 W m^{-1} K^{-1} (Fig. 10c), enhancing efficient heat dissipation in practical applications; however, Ag nanoparticle loading beyond 3.2 wt% leads to film fragility. The thermal conductivities of MXene/Ag/epoxy nanocomposites, measured *via* the laser flash technique, exhibited enhancements in both in-plane (Fig. 10d) and through-plane (Fig. 10e) directions upon incorporating MXene/Ag fillers. The through-plane thermal conductivity reaches 2.65 W m^{-1} K^{-1} at 15.1 vol% filler loading, representing a >1200% increase compared to pure epoxy resin. This suggests that Ag nanoparticles improve thermal conductivity by promoting effective heat transfer channels within the nanocomposite. The observed anisotropic thermal behavior is attributed to the two-dimensional structure of MXenes, which results in distinct heat transfer mechanisms along the horizontal and vertical orientations of the film.

Terminal groups on MXenes can impact thermal conductivity by reducing phonon scattering and enhancing interfacial interactions with epoxy matrices.[194,195] Wang *et al.* used molecular dynamics and effective medium theory to analyze four MXenes, Ti_3C_2, $Ti_3C_2F_2$, $Ti_3C_2O_2$, and $Ti_3C_2(OH)_2$, and their epoxy composites.[194] The study found that $Ti_3C_2O_2$ achieves the highest thermal conductivity of 140.25 W m^{-1} K^{-1}, while $Ti_3C_2(OH)_2$ exhibits the lowest interfacial thermal resistance (ITR), improving composite conductivity at optimal flake sizes (Fig. 10f). The study assumes MXene flakes as disk shapes with a diameter and thickness of 0.98 nm. It was proposed that the effective thermal conductivities of the nanocomposites initially increase sharply with the lateral size of fillers, eventually leveling off after reaching a critical size. Among the composites, $Ti_3C_2O_2$/epoxy demonstrates the highest thermal conductivity, while Ti_3C_2/epoxy exhibits the lowest due to its intrinsic thermal conductivity and high ITR. The results indicate two intersections between $Ti_3C_2(OH)_2$/epoxy and the –O and –F terminated MXenes, suggesting that below critical sizes (325 nm for –O and 772 nm for –F), interfacial thermal conductance plays a more significant role in enhancing thermal performance. Additionally, in the $Ti_3C_2O_2$/epoxy system, a filler volume content below 2 vol% is optimal to avoid agglomeration, with thermal conductivity increasing linearly before reaching a plateau as the MXene size increases (Fig. 10g). Some of the thermal properties of MXene–polymer nanocomposites are summarized in Table 4.

6. Synthesis strategies for MXene–polymer nanocomposites

MXenes can be integrated with a wide range of polymers, facilitating the tailoring of nanocomposite materials for specific applications. The interaction force between the MXene matrix and polymers in nanocomposite synthesis primarily involves hydrogen bonding, van der Waals interactions, electrostatic interactions, and π–π stacking, depending on the functional groups present on both MXene surfaces and the polymer chains.[94] The MXene surface terminations (*e.g.*, –O, –OH, and –F) can form hydrogen bonds with polymers containing polar groups like –OH, –COOH, $–NH_2$, *etc.* Additionally, electrostatic interactions may occur when charged polymers are used, especially in systems where MXenes have surface charges.[92] van der Waals forces contribute to non-covalent binding, while polymers with aromatic groups can engage in π–π interactions with MXene layers. These interactions are key to enhancing compatibility, mechanical strength, and functional properties in MXene–polymer nanocomposites. MXene–polymer composites can be fabricated using different processing techniques, such as solution casting,[68,77] melt blending,[200,201] electrospinning,[80] *etc.*, allowing for the production of complex shapes, thin films, coatings, or fibers. This versatility in processing enables the integration of MXenes into a wide range of devices and structures.[202–205]

6.1 Surface grafting/modification of MXenes

Due to the abundant functional groups at the surface of MXenes, it becomes easier to functionalize them with different

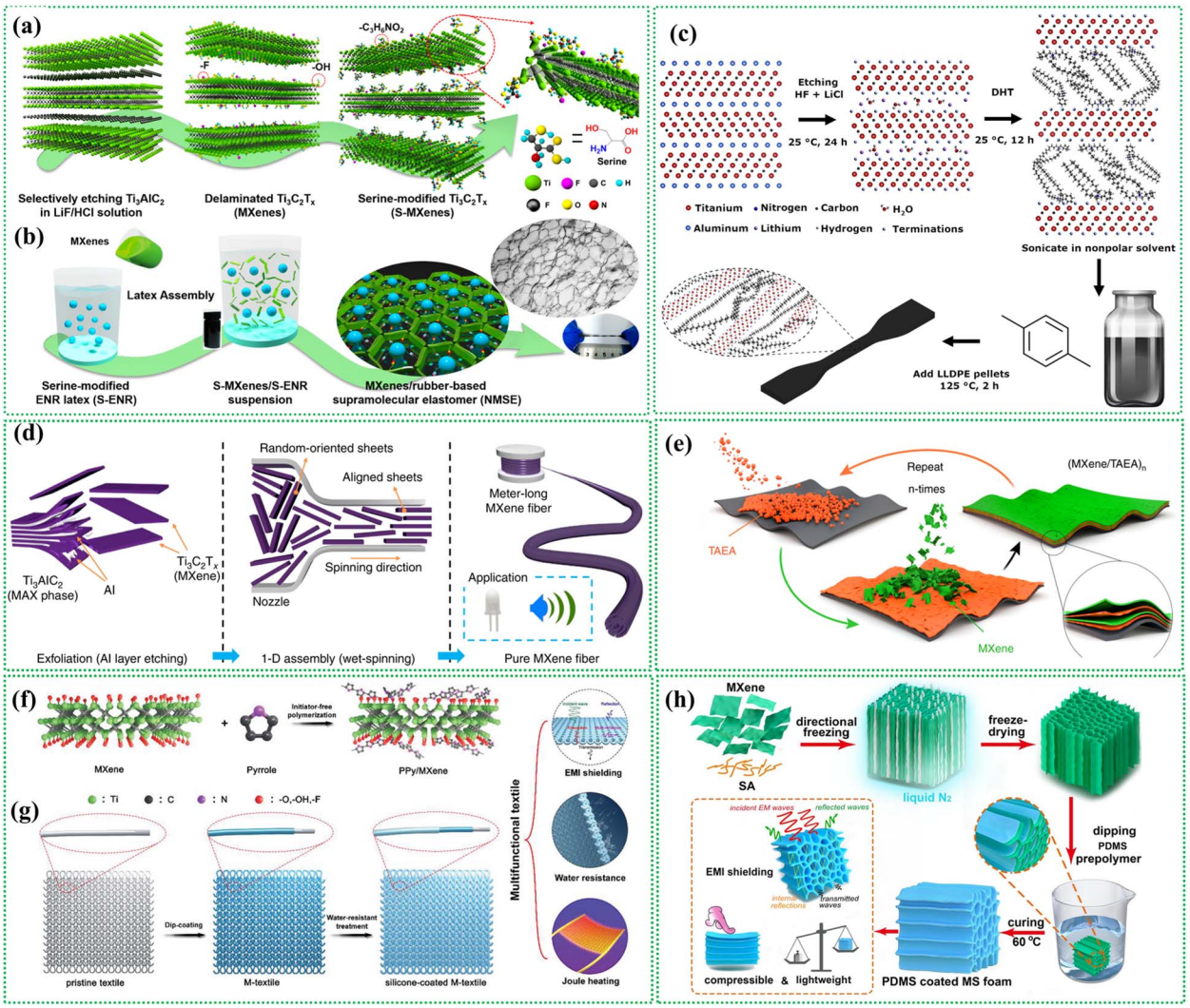

Fig. 11 MXene–polymer nanocomposite synthesis. (a) The surface modification of MXene nanosheets is achieved through an esterification reaction with serine. (b) MXene network in NMSE is constructed using the latex assembly method. Reproduced with permission from ref. 209. Copyright 2020, American Chemical Society. (c) MXene–polymer blending. MXene multilayers are then treated with DHT to enhance their functionality. The functionalized MXene nanosheets are dispersed in a nonpolar solvent and subsequently utilized in the solution processing of LLDPE.[201] (d) Electrospinning technique. MXene material is concentrated in an aqueous solution and then assembled into a fiber. This fiber was aligned in the axial direction using a wet-spinning process.[212] (e) The process of LBL self-assembly of $(MXene/TAEA)_n$ multilayer films on planar substrates is depicted schematically.[213] (f) *In situ* polymerization MXene–polymer hybrids. Schematic illustration of the modification process of MXene with *in situ* polymerized PPy. (g) Fabrication of PPy/MXene-decorated PET textile, along with the subsequent process of creating multifunctional silicone-coated M-textile. Reproduced with permission from ref. 82. Copyright 2018, Wiley. (h) Schematic showing the process of fabrication an MXene/SA hybrid aerogel and its subsequent PDMS-coated MXene/SA foam. Reproduced with permission from ref. 214. Copyright 2024, Elsevier Ltd.

organic molecules. First-principles calculations revealed that unmodified Ti_3C_2 MXene can cleave and decompose monomers effectively. In contrast, surface-functionalized $Ti_3C_2F_2$, Ti_3C_2FO, and $Ti_3C_2O_2$ bind weakly with monomers due to van der Waals forces, while $Ti_3C_2(OH)_2$ shows a stronger binding affinity.[206] In the surface modification process, MXene sheets are functionalized or chemically modified to introduce specific groups or moieties on their surfaces. These modified MXene sheets are then mixed or dispersed within a polymer solution or melt. During polymerization or crosslinking, the functionalized MXene sheets become covalently bonded or physically intertwined with the polymer chains, leading to the formation of a nanocomposite material.[207,208] A protein-inspired supramolecular elastomer was developed for intelligent sensing applications, utilizing self-healable Ti_3C_2 MXene blended with rubber (serine-grafted epoxidized natural rubber) (S-ENR) latex.[209] The study created a self-healing elastomer inspired by proteins for smart sensing. MXene nanosheets were esterified with serine using EDC and DMAP at 100 °C for 3 hours to produce S-MXene (Fig. 11a). Serine-modified epoxidized natural rubber (ENR) latex was synthesized by reacting serine with ENR latex at 100 °C for 3 hours. S-MXenes/S-ENR nanocomposites

were prepared by combining S-MXene with S-ENR latex, stirring, sonicating, and drying to form a 3D network film (Fig. 11b). Besides this, another surface modification technique involving the covalent attachment of polyethylene glycol carboxylic acid (PEG6-COOH) onto MXenes through esterification chemistry was introduced. The surface modification of $Ti_3C_2T_x$ using PEG6-COOH with high ligand loading significantly improves the dispersibility of MXene flakes in a wide range of non-polar organic solvents (*e.g.*, 2.88 mg mL^{-1} in chloroform) without inducing oxidation or altering the structural ordering of $Ti_3C_2T_x$ two-dimensional layers.[208] Besides these, there are other reports on MXenes surface modifications for MXene–polymer hybridization.[208,210]

6.2 Solution blending

In this method, MXenes and polymers are dispersed in a compatible solvent and mixed *via* stirring, ultrasonication, or high-shear mixing. Then the solvent is removed by evaporation, vacuum drying, or freeze-drying to form a solid MXene–polymer composite. Carey *et al.* conducted a study where they prepared a dispersion of alkylated 2D MXene in nonpolar solvents using the blending method.[201] The study investigated the pseudocapacitive behavior of the resulting nanocomposite material. In this process, after the MXene etching, the Li^+ ions present inside the multilayers are ion-exchanged with di(hydrogenated tallow)benzyl methyl ammonium chloride (DHT) (Fig. 11c). The resulting multilayers can be easily dispersed in nonpolar solvents. These can be easily processed with a linear low-density polyethylene nanocomposite (LLDPE) for many applications. A notable advantage of this hybrid assembly is that it remains dispersed for more than 10 days without sedimentation even in nonpolar solvents. Jiao *et al.* conducted a study to prepare photothermal healable, stretchable, and conductive $Ti_3C_2T_x$ MXene composite films using the vacuum filtration method, to achieve efficient EMI shielding.[211] To determine the optimal ratio between waterborne polyurethane (WPU) and natural rubber latex (NR latex), a series of composite films were prepared with varying WPU : NR mass ratios. These composite films were respectively denoted as WNM as they contain WPU, NR, and MXene. The next step involved obtaining WPU/NR composite emulsions by mixing specific proportions of WPU and NR latex emulsions in an ice bath. Subsequently, a $Ti_3C_2T_x$ suspension was gradually introduced into the WPU/NR composite emulsions. This step allowed the incorporation of $Ti_3C_2T_x$ at various volume fractions.

The WNM films were obtained through vacuum filtration, followed by natural drying. Recently, Pan *et al.* have reported a wearable and flexible MXene and PEDOT:PSS conducting polymer nanocomposite for continuous noninvasive monitoring of sweat glucose.[215] The addition of a 0.1% mass fraction of MXene has significantly improved the conductivity of the composite. In this study, ethylene glycol has been utilized to increase the cross-linking and film-forming properties of the nanocomposite. The nanocomposite hydrogel sensor showed a sensitivity of 21.7 μA mM^{-1} cm^{-2} within the concentration range of 1–94 μM and a sensitivity of 8.3 μA mM^{-1} cm^{-2} within the range of 94–1294 μM. Importantly, this glucose biosensor demonstrated outstanding electrochemical performance in sweat, which was highly correlated with the corresponding findings of the glucometer.

6.3 Electrospinning method

The electrospinning technique can prepare polymer fibers with diameters in the nanoscale range. MXene–polymer nanocomposites can be effectively synthesized using electrospinning techniques.[80,216] MXene fibers can also be synthesized using the wet-spinning technique. Eom *et al.* devised a technique for producing pure MXene fibers without additional binders.[212] This method involves a large-scale wet-spinning assembly, where MXene sheets are dispersed in water at high concentrations, preventing aggregation or phase separation issues (Fig. 11d). The coagulation process plays a pivotal role in the fabrication of these fibers. By introducing ammonium ions during coagulation, the researchers have assembled MXene sheets into highly flexible, meter-long fibers. These fibers exhibit an exceptionally high level of electrical conductivity, making them promising candidates for various applications in advanced materials. Besides, MXenes can be incorporated into polymer solutions used for electrospinning to produce MXene–polymer composite nanofibers. Recently, a study was conducted on an electrospun flexible triboelectric nanogenerator that utilized metallic MXene nanosheets and poly(vinyl alcohol) (PVA).[217] To prepare the PVA–MXene solution, a 10% (w/v) PVA solution and 1.0 g of PVA were mixed with 10 mL of distilled water at 90 °C while stirring for ~1 h. Subsequently, MXene was added to the PVA aqueous solution and stirred thoroughly to achieve a homogeneous PVA/MXene mixture. Electrospinning was performed using a 5 mL syringe and needle with a 0.68 mm inner diameter at an applied voltage of 18 kV. The combination of MXene nanosheets and PVA in the composite material imparts outstanding electrical properties, enhancing its electronegativity and conductivity. For the positive friction layer, silk fibroin (SF) was selected as the material for electrospinning nanofiber films due to its biocompatibility, biodegradability, and significant triboelectric properties.

6.4 Layer-by-layer (LBL) assembly

This method involves the sequential deposition of alternating layers of $Ti_3C_2T_x$ MXenes and polymers onto a substrate. The MXene and polymer layers are formed through techniques such as dip coating, spin coating, spray deposition, *etc.* The coating process can be repeated to achieve the desired thickness and control the MXene-to-polymer ratio in the composite. A method for the vacuum-assisted LBL self-assembly of pillared two-dimensional multilayers comprising MXene and a small molecule called tris(2-aminoethyl)amine (TAEA) was developed.[213] In this process, $(MXene/TAEA)_n$ multilayers were prepared, where n represents the number of bilayers formed in the self-assembled structure. In this method, $Ti_3C_2T_x$ MXene and TAEA solutions with a concentration of 1 g L^{-1} were used. Porous substrates were placed on a cellulose membrane fixed in

an adjustable-flow vacuum system. Using airbrushes, atomized solutions were sprayed onto the substrates. The cycle of spraying TAEA, rinsing with water, and then spraying MXene was repeated to create $(MXene/TAEA)_n$ films of the desired thickness (Fig. 11e). For larger surfaces of 3D CNF aerogel and melamine foam, a rapid-LBL assembly method was used. MXene and TAEA solutions were poured on top of the aerogel or foam and forced through by applying vacuum pressure. $(MXene/TAEA)_n$ multilayer films can be prepared through LBL self-assembly onto fibers and foams. Another study was conducted titled LBL assembly of polyaniline nanofibers (PNF) and $Ti_3C_2T_x$ MXene electrodes for electrochemical energy storage.[218] In this research, the LBL assembly technique was used to create thin-film electrodes by stacking PNF and $Ti_3C_2T_x$ MXene materials. The resulting electrodes were intended for applications in electrochemical energy storage, aiming to enhance the performance of energy storage devices such as batteries or supercapacitors.

6.5 *In situ* polymerization

In this method, the monomers of a polymer are introduced into a solution containing MXene, and polymerization occurs *in situ*, meaning within the same environment as the MXene particles.[81,82,214] This leads to the formation of a homogeneous mixture of MXene and polymer, creating a nanocomposite material with MXene uniformly dispersed throughout the polymer matrix.[219] The choice of the polymer depends upon the end requirement. If a conducting polymer is chosen, it will result in a nanocomposite, which may have applications as an active electronic material, whereas an insulating polymer will result in a final product with limited or reduced conductivity. In a study reported by Wang *et al.*, the fabrication of MXene-decorated multifunctional and water-resistant textiles with remarkable electromagnetic interference (EMI) shielding and Joule heating performance was investigated. To achieve this, PPy modified MXene sheets using *in situ* polymerization (Fig. 11f) were utilized, which were deposited onto poly(ethylene terephthalate) textiles.[82] Subsequently, a silicone coating was applied to the textiles to enhance their conductivity and hydrophobicity. Highly conductive and water-resistant textiles exhibited high EMI shielding efficiency and excellent Joule heating performance (Fig. 11g). In another study, Wu and co-workers developed compressible, durable, and conductive PDMS-coated MXene/sodium alginate (SA) foams (MS) for high-performance electromagnetic interference (EMI) shielding. The researchers used MXene and SA to fabricate the foam and then coated the foam with PDMS to enhance its properties for EMI shielding.[214] $Ti_3C_2T_x$/SA hybrid aerogels were fabricated as follows: $Ti_3C_2T_x$ suspension (20 mg mL^{-1}) was added to different amounts of SA (0, 4, 12, 28, and 48 mg) with stirring at 500 rpm for 5 h to achieve homogeneous and high viscosity suspensions. The resulting suspensions were poured into Teflon molds and rapidly frozen on a copper cylinder immersed in liquid nitrogen. Subsequently, the directionally frozen samples were freeze-dried at −60 °C under 10 Pa for 48 h to yield

Table 5 MXene–polymer nanocomposites and their applications

S. no.	MXene	Polymer used	Synthesis technique	MXene concentration	Application of the nanocomposite	Reference
1	$Ti_3C_2T_x$	PEDOT:PSS	Electrogelation method	0 to 60 wt%	Sensing	220
2	$Ti_3C_2T_x$	PEDOT:PSS	Ice templating method	0, 1, and 3 wt%	Electrical stimulation	221
3	$Ti_3C_2T_x$	PEDOT:PSS	Mixing/blending	10–90 wt%	EMI shielding	222
4	$Ti_3C_2T_x$	PEDOT:PSS	LBL assembly	—	Energy storage/capacitive sensors	88
5	$Ti_3C_2T_x$	PEDOT:PSS	LBL assembly (spray)	29–76.6 wt%	Multifunctional	223
6	V_2CT_x	PEDOT:PSS	Mixing/blending	—	Solar cells	224
7	Nb_2CT_x	PEDOT:PSS	Solution mixing	MXene : PEDOT:PSS (1 : 5, 1 : 7, and 1 : 9)	Solar cells	225
8	$Ti_3C_2T_x$	PDMS	Dip-coating and curing	1, 3, and 5 wt%	EMI shielding skins	226
9	$Ti_3C_2T_x$	PDMS	Mixing/curing	20–50%	Pressure sensor	227
10	V_2CT_x	PDMS	Coating	—	EDL transistor	228
11	$Ti_3C_2T_x$	PU[b]	Mixing	1 : 1	EMI shielding	229
12	$Ti_3C_2T_x$	PU[b]	LBL assembly	—	EMI shielding and Joule heating	230
13	$Ti_3C_2T_x$	Epoxy	Coating	0-2 wt%	Anti-corrosion	231
14	$Ti_3C_2T_x$	Polypyrrole	*In situ* polymerization	MXene : PPy (9 : 1, 8 : 2 and 7 : 3)	Supercapacitors	232
15	$Ti_3C_2T_x$	Doxorubicin	Surface modification	1 : 2	Tumor targeting	233
16	$Ti_3C_2T_x$	Chitosan	Electrospinning	0–0.75 wt%	Antibacterial	234
17	$Ti_3C_2T_x$	Silane	Surface modification	1 : 1	Water purification	235
18	$Ti_3C_2T_x$	PANI/PU	Electrospinning	0–10%	Zn-ion batteries	236
19	$Ti_3C_2T_x$	Polypyrrole	Polymerization	1 : 1 and 2 : 1	Pseudocapacitive electrodes	81
20	$Ti_3C_2T_x$	PEG	3D printing	—	Tissue engineering	237
21	$Ti_3C_2T_x$	PVA	Blending	40–90%	Flexible electronics	16
22	$Ti_3C_2T_x$	PVA	Solvent exchange	2.50%	Strain sensors	238
23	$Ti_3C_2T_x$	SA	Ultrasonic mixing	5–30 mg mL^{-1}	Flexible electronic sensors	239
24	$Ti_3C_2T_x$	Polypropylene	Hot-pressing	25%, 56%, and 70%	Flame-retarding/EMI shielding	240
25	$Ti_3C_2T_x$	TAEA[a]	LBL self-assembly	—	Supercapacitors	213

[a] Tris(2-aminoethyl)amine (TAEA). [b] Polyurethane (PU).

unidirectional aerogels. These MS porous architectures were coated with PDMS by a vacuum-assisted impregnation method. To create the PDMS-coated MS foam, a mixture of 10 g PDMS prepolymer, 1 g curing agent, and 30 mL *n*-hexane was thoroughly mixed in a beaker for 30 min. The resulting mixture was cured at 60 °C for 12 h, resulting in the formation of a thin PDMS layer on the MXene nanosheets of the MS aerogel, creating the PDMS-coated MS foam (Fig. 11h). The resulting PDMS-coated MXene/SA foam exhibited excellent compressibility, durability, and electrical conductivity, making it a promising candidate for effective EMI shielding applications. Besides these, Table 5 summarizes different polymers utilized in the synthesis of MXene–polymer nanocomposites, along with their respective applications.

Combining MXenes with a wide variety of polymers makes it possible to enhance and tailor the properties of MXenes and these can alter the properties of the resulting composite material as desired.[241–243]

7. Applications of MXene–polymer nanocomposites

The addition of polymers to MXenes can significantly improve their performance and expand their applications in various fields. By incorporating polymers with good mechanical strength and flexibility, the resulting MXene–polymer hybrids exhibit enhanced mechanical properties, making them suitable for applications requiring flexibility, stretchability, and impact resistance.[54,244,245] These applications include flexible electronics, wearable devices, and flexible coatings.[60,83,202,246] Polymers can enhance the electrochemical performance of MXenes in energy storage devices. The combination of MXenes' high electrical conductivity with polymers' ion transport properties can enhance the charge storage capacity of these devices.[247,248] Polymers enhance MXene dispersion, prevent restacking, and improve synergy, boosting overall material properties.[249]

7.1 MXene–polymers for energy storage applications

MXene–polymer composites offer several advantages in energy storage devices. Polymers can provide mechanical stability to electrode materials. This improved mechanical stability leads to enhanced cycling performance and a longer lifespan of energy storage devices.[250] Due to van der Waals forces, MXenes layers tend to restack and agglomerate, resulting in reduced accessible surface area and hindered ion diffusion due to lack of active sites.[91,251] Polymers in MXene–polymer composites help to disperse and stabilize MXene layers, preventing restacking and preserving the high surface area of MXenes.[16] Polymers can facilitate ion diffusion within electrode materials.[252] Polymers can enhance the compatibility of MXene electrodes with different electrolyte systems. Certain polymers can act as ion-conductive additives or binders that promote ion transport and enhance the stability of electrolyte–electrode interfaces. The performance of electrodes, which were fabricated using PEDOT (poly(3,4-ethylene dioxythiophene)) deposited $Ti_3C_2T_x$ sheets, exhibited an improvement compared to electrodes made with pristine $Ti_3C_2T_x$.[253]

Polyaniline@MXene-based positive electrodes have been investigated for asymmetric supercapacitor applications.[250] An electrode is prepared by casting a homogeneous polyaniline layer onto a 3D porous $Ti_3C_2T_x$ MXene. This enabled the stable operation of MXene at positive potential due to the increased work function after combining with polyaniline. The resulting flexible polyaniline@MXene positive electrode offers a high volumetric capacitance of 1632 F cm^{-3} at 5000 mV s^{-1}. In another study, pseudocapacitive electrodes were developed by performing oxidant-free polymerization of PPy between the layers of $Ti_3C_2T_x$ MXene.[81] Hybrid electrodes of $Ti_3C_2T_x$ and PPy achieved up to 416 F g^{-1} capacitance in 1 M H_2SO_4.

MXene/PPy (2 : 1 and 1 : 1 ratios) nanocomposites, prepared by mixing delaminated $Ti_3C_2T_x$ and PPy, were utilized for supercapacitor applications. Cyclic voltammetry (CV) curves of the hybrid samples revealed a strong pseudocapacitive behavior. The supercapacitors based on a 2 : 1 ratio nanocomposite demonstrated higher capacitance than those of pristine MXene with a 1 : 1 ratio due to optimized composition. These supercapacitors outperformed PVA–$Ti_3C_2T_x$ electrodes, achieving ~99% coulombic efficiency and 92% capacitance retention over 25 000 cycles. Nyquist plots confirmed good ionic conductivity, with slightly higher diffusion resistance in PPy-containing films, attributed to robust bonding, effective ion/electron transport, and the protective role of MXene.

Besides $Ti_3C_2T_x$ MXene, Ti_2C MXene has also demonstrated excellent energy storage capabilities. Xue *et al.* developed ultrafast, metal-free, on-paper micro-supercapacitors (MSCs) using a composite of conductive PEDOT:PSS and capacitive Ti_2C MXene.[254] They developed more effective direct ink writing (DIW) by combining PEDOT:PSS with Ti_2CT_x, leveraging its higher specific capacitance and compatibility with PEDOT:PSS's hole transport paths (Fig. 12a). Unlike $Ti_3C_2T_x$, this blend avoids conductivity degradation, enabling improved conductivity, reduced restacking, and high-rate electrochemical performance even with thick electrodes. At a 1000 mV s^{-1} scan rate, PEDOT:PSS–Ti_2C MSCs (10 layers, ≈5 μm thick) achieved a volumetric capacitance of ≈30.6 F cm^{-3}, which is nearly double that of pure Ti_2C MSCs and 6 times higher than that of PEDOT:PSS MSCs, confirming their synergistic interaction. CV curves maintained excellent rectangularity, and capacitance increased linearly with the number of layers at lower scan rates (Fig. 12b and c). These MSCs retained >96% of their capacitance after 10 000 cycles at a high scan rate of 1000 mV s^{-1}. They also exhibited an extended voltage window of up to 6 V and maintained outstanding performance even at an ultrafast scan rate of 10 V s^{-1}. This work highlights the potential of Ti_2C when integrated with polymers for eco-friendly, high-performance power sources for paper-based, portable, and wearable electronics. Additionally, flexible solid-state micro-supercapacitors can be fabricated by electrochemically polymerizing MXene-facilitated PEDOT composite films, and these composite films can be utilized along with MnO_2 to create pseudocapacitive asymmetric micro-supercapacitors.[256]

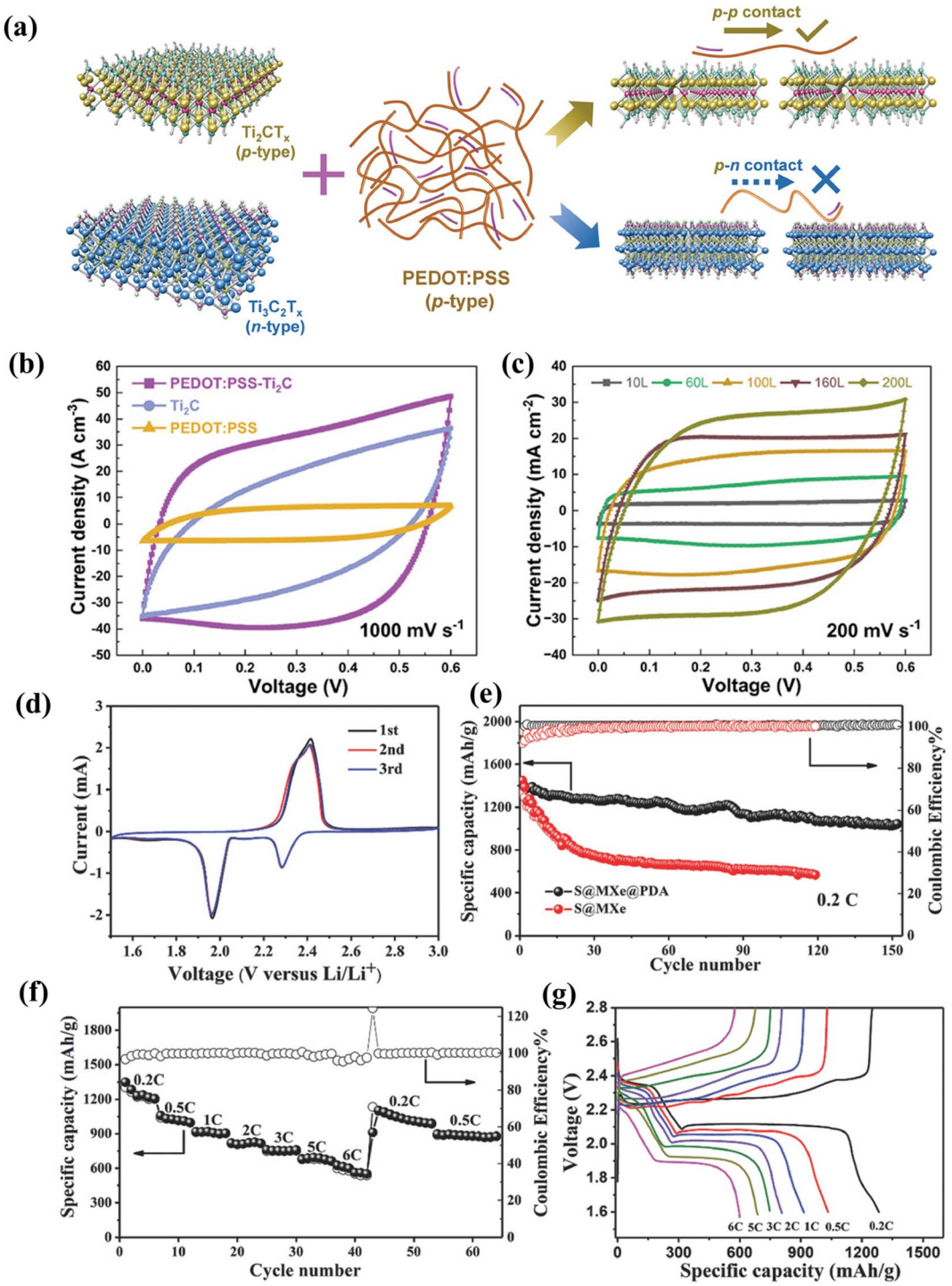

Fig. 12 (a) Schematic of interactions between PEDOT:PSS and MXenes (Ti_2C and Ti_3C_2). (b) CV curves of 10 L MSCs with Ti_2C, PEDOT:PSS, and PEDOT:PSS–Ti_2C electrodes. (c) CV curves of PEDOT:PSS–Ti_2C MSCs at 200 mV s^{-1} with different layer numbers.[254] (d) CV curves of S@MXene@PDA at 0.2 mV s^{-1} (first three cycles). (e) Cycling performance of S@MXene@PDA *vs.* S@MXene at 0.2C. (f and g) Rate performance and voltage profiles at 0.2–6C. Reproduced with permission from ref. 255. Copyright 2018, Wiley.

MXene–polymer nanocomposites also offer advantages in batteries, as demonstrated by Yao *et al.* in Li–S batteries with MXene–polydopamine (S@MXene@PDA) cathodes.[255] The dual polysulfide confinement strategy effectively suppresses shuttling, supports high sulfur loading, and ensures strong conductivity and lithium polysulfide adsorption for improved performance. The polar amine sites of the PDA layer enable strong chemical adsorption of polysulfides, localizing them on the electrode surface. Additionally, PDA enhances electrolyte wetting, uptake, and ionic conductivity, improving Li^+

transport. Fig. 12d shows the CV curves of the S@MXene@PDA cathode at 0.2 mV s^{-1}, with reduction peaks at 2.27 and 1.98 V corresponding to the formation of Li_2S_x and Li_2S_2/Li_2S. Fig. 12e displays long-term cycling stability at 0.2C, with S@MXene@PDA achieving 1044 mA h g^{-1} after 150 cycles (73% retention), outperforming S@MXene (565 mA h g^{-1}, 39% retention) due to better polysulfide confinement. Fig. 12e and f demonstrate the rate performance of S@MXene@PDA, showing stable capacities at 1349–624 mA h g^{-1} from 0.2 to 6C, with minimal capacity loss when returning to lower rates, indicating fast kinetics and stability.

Besides these, MXene–polymer hybrids can also be utilized for all-solid-state batteries and fuel cells.[19,205,257,258]

7.2 MXene–polymer nanocomposites in sensors and flexible electronics

MXene–polymer nanocomposites offer several advantages over MXene-only systems in the field of sensors.[32,60,259,260] The incorporation of polymers in MXene-based sensors can improve the sensing performance by enhancing selectivity, flexibility, sensitivity, and response time depending upon their sensing nature.[261–263] Polymers can provide a selective environment for target analytes by interacting with specific molecules, gases, or ions.[264,265] The integration of MXene–polymer nanocomposites has shown significant promise in enhancing the performance of pressure and gas sensors due to the higher conductivity and surface area of MXenes. In a study, a bioinspired interlocked structure was developed to achieve high deformability in 2D MXene/natural microcapsule-based flexible pressure sensors using polyimide (PI) and PDMS.[262] To prepare a Ti_3C_2 MXene/natural microcapsule nanofilm, a 0.2 g portion of natural microcapsule (NMC) was dispersed in 10 mL of ethanol to create a well-mixed solution. 10 ml of Ti_3C_2 MXene solution was then added to the NMC solution, and the mixture was stirred for 2 hours to ensure uniform dispersion of Ti_3C_2 MXenes and NMC. The mixture was subsequently filtered through a polypropylene membrane to create a composite film. This film was air-dried for 30 minutes at room temperature and carefully peeled off from the polypropylene membrane, resulting in a flexible Ti_3C_2/NMC composite film (Fig. 13a).

Polymeric $Ti_3C_2T_x$ MXene nanocomposites have exhibited promising applications in room-temperature ammonia gas sensing.[265] The PEDOT:PSS/MXene composites were prepared *via* a simple *in situ* polymerization process in/on $Ti_3C_2T_x$ MXene and subsequently utilized to fabricate a gas sensor on a PI substrate. The synthesis involved adding EDOT to an appropriate amount of $Ti_3C_2T_x$ MXene suspension, followed by the introduction of ammonium persulfate (APS) and poly(4-styrene sulfonate) (PSS). The mixture was stirred for 24 hours at room temperature and 1000 rpm, producing a black PEDOT:PSS/MXene composite solution (Fig. 13b). These MXene–polymer nanocomposites are used to create wearable capacitive pressure sensors, with $Ti_3C_2T_x$ MXene and poly(vinylidene fluoride–trifluoroethylene) (PVDF–TrFE) as the dielectric layer between PEDOT:PSS and polydimethylsiloxane electrodes, facilitating reliable human physiological signal acquisition.[261] MXene powder in DMF was sonicated for 1 hour to form a homogeneous suspension, mixed with PVDF–TrFE to create a solution with up to 13 wt% MXene, and electro-spun into nanofibers. For the sensor, PDMS was spin-coated and cured on glass, followed by PEDOT:PSS spin-coating and DMSO treatment. The PEDOT:PSS film was peeled off, with CNS placed between two PEDOT:PSS layers, and carbon tape electrodes were added (Fig. 13c).

Self-healing sensors based on MXene–polymer nanocomposites have attracted significant attention due to their unique capabilities in autonomously repairing damage and restoring functionality.[266] Polymers provide flexibility and conformability to MXene-based sensors, enabling their integration into various form factors and substrates. These composites combine the exceptional properties of MXene, such as high electrical conductivity and mechanical strength, with the self-healing properties of polymers.[267] A study recently developed a conductive MXene nanocomposite hydrogel with healable and degradable properties for advanced epidermal sensors.[267] The hydrogel was created by combining MXene, poly(acrylic acid) (PAA), and amorphous calcium carbonate (ACC). In the synthesis, PAA and calcium chloride were dissolved in water and stirred, followed by the addition of an MXene solution. A carbonate solution was then added, forming an MXene–PAA–ACC hydrogel. After formation, the hydrogel was washed thoroughly until the water was clear.

Besides these, there are many other reports on MXene–polymer composites given in Table 6 with diverse applications.[32,243,260,268]

MXene–polymer composites can lead to the development of lightweight, flexible, and high-performance electronic devices with enhanced mechanical properties, tailored electrical conductivity, and improved protection against environmental factors.[16,59] The synergistic effects between MXenes and polymers can be used in next-generation flexible electronic devices with diverse applications, including wearable electronics, flexible displays, EMI shielding, conformable sensors, and piezoelectric applications.[50,60,278–281] Zhang *et al.* investigated a flexible MXene-decorated fabric (M–CF) featuring interwoven conductive networks. The study explored the fabric's multifunctional capabilities, specifically focusing on integrated Joule heating, electromagnetic interference shielding, and strain-sensing performance.[59] By incorporating MXene into the fabric's structure, the researchers aimed to enhance its electrical and thermal properties, making it a versatile material for various applications related to heating, shielding, and sensing. After etching the MXene, inks were uniformly sprayed onto the surface of pretreated cotton fabrics (Fig. 14a). To achieve different loading contents of MXene on the fabric, they adjusted the spray-drying cycles. By varying the MXene content in the cotton fabric, they aimed to optimize and find the most suitable MXene loading for achieving the desired multifunctional applications like EMI shielding, Joule heating, sensing, *etc.* (Fig. 14b). The EMI shielding properties of the samples were studied within a frequency range of 8–12 GHz, employing a waveguide method. The average EMI shielding effectiveness of the 2 wt% MXene-based sample is ~25 dB, while for 4 and 6

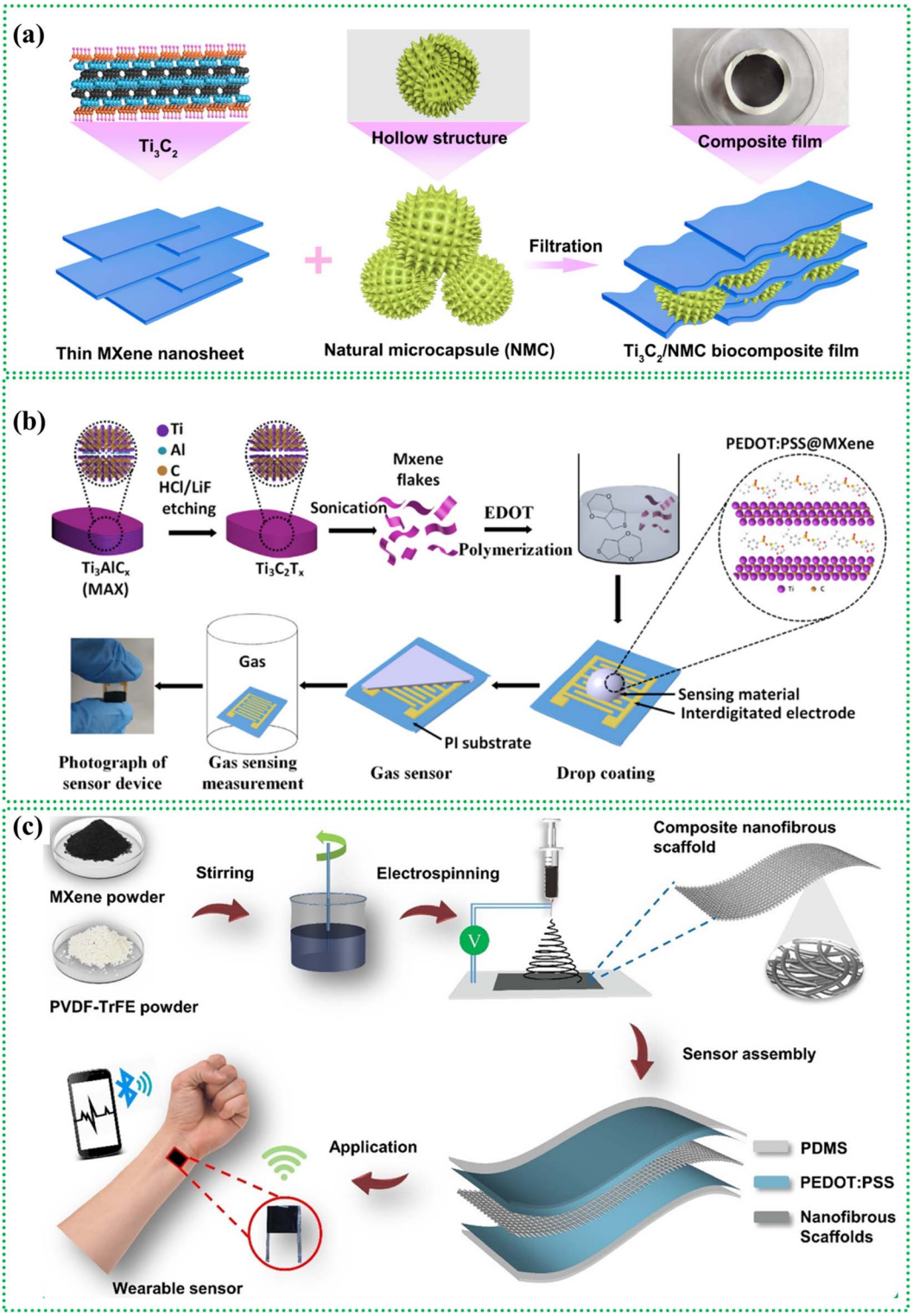

Fig. 13 MXene–polymer nanocomposite-based sensors. (a) Schematic diagram illustrating the fabrication process of the Ti_3C_2/NMC biocomposite film. Reproduced with permission from ref. 262. Copyright 2019, American Chemical Society. (b) The schematic illustration depicts the synthesis process of PEDOT:PSS/MXene composites and the subsequent fabrication process of the gas sensor based on these composites. Reproduced with permission from ref. 265. Copyright 2020, American Chemical Society. (c) Schematic diagram illustrating the fabrication process of the composite nanofiber scaffold (CNS)-based pressure sensor. Reproduced with permission from ref. 261. Copyright 2020, American Chemical Society.

Table 6 The comparison of several MXene-based composites as sensors

S. no	Components	MXene contents (wt%)	Fabrication technique	Structure type	Sensor type	Mechanical strength	Gauze factor	Ref.
1	$Ti_3C_2T_x$/PDMAEMA	78	Surface modification	Accordion	Temperature	—	—	269
2	$Ti_3C_2T_x$/poly(*N*-isopropylacrylamide)/polyacrylamide	—	*In situ* polymerization	Porous network	Temperature and strain	0.4 MPa	—	270
3	$Ti_3C_2T_x$/PDADMA/BPEI	90.7	Physical mixing	Layer-by-layer	pH	—	116 kΩ pH^{-1}	271
4	$Ti_3C_2T_x$/PEDOT/PVDF	5	*In situ* polymerization	Sandwich	Pressure	—	0.51 kP a^{-1}	261
5	$Ti_3C_2T_x$/PVA/PDMS	0.2	Physical mixing	Sandwich	Pressure	—	1.5 kPa^{-1}	272
6	$Ti_3C_2T_x$/PVDF–TrFE	38	Physical mixing	Sandwich	Pressure	—	2213.68 kPa^{-1}	273
7	$Ti_3C_2T_x$/PDA/AgNWs	16.7	Physical mixing	Brick-and-mortar	Strain	—	200	274
8	$Ti_3C_2T_x$/PVA/poly(vinylpyrrolidone)	1	Physical mixing	Porous network	Strain	300 kPa	19.18	275
9	$Ti_3C_2T_x$/poly(acrylic acid) (PAA)/amorphous calcium carbonate (ACC)	0.07	Physical mixing	Porous network	Strain	180 kPa	10.79	276
10	$Ti_3C_2T_x$/PAA	2	Physical mixing	Porous network	Strain	30 kPa	0	277

wt%, it measured 33 and 36 dB, respectively. The sensors based on 2 wt% MXene led to maximum resistance change under the same bending strain, making the nanocomposite ideal for detecting small human activities. The optimized 2 wt% M–CF sensor maintained consistent resistance change for more than 5000 cycles of bending and releasing. Attached to a finger, the MXene-based sensor consistently detected resistance changes during bending movements and accurately recorded a pulse rate of 80 beats per minute.

Polymer lamination can effectively mitigate MXene oxidation, as evidenced by their application in various devices. Lee *et al.* demonstrated that laminating a thin poly(4-vinylphenol) (PVPh) layer as a protective film on MXene (PL-MXene) protects it from the external environment.[50] This combination was utilized for the electroluminescent (EL) display, whose structure is demonstrated in Fig. 14c. The relative luminance variance ($\Delta L/L_0$) of devices with PL-MXene and bare MXene electrodes over time is shown in Fig. 14d. Besides these, there are many other reports on the usage of MXene–polymer nanocomposites in the domain of flexible devices with a wide variety of applications.[244,248,256,258,279,282,283]

MXene–polymer nanocomposites are also studied for piezoelectric applications. Piezoelectric sensors can transform the plentiful mechanical energy that surrounds us into electrical energy, and mechanical energy harvesters are seen to be one of the most appealing energy harvesting technologies. Nevertheless, their poor electrical performance is preventing them from being used practically. Because the electrical performance of an energy harvester may be enhanced by harvesting the applied mechanical energy in two harvesters concurrently, hybridization of two distinct mechanical energy harvesters such as MXene and any other piezoelectric material may offer a solution to this problem.

An overall schematic representation of the hybridization generator integrating MXene and barium titanate as conductive fillers in the PDMS matrix (HG-MBP) is shown in Fig. 14e.[284] HG-MBP was made of MXene/$BaTiO_3$, polyimide (PI), and aluminum (Al), as seen in Fig. 14e.

The electrode, substrate, piezoelectric layer, and triboelectric layer are all PDMS (MBP) composite films. As seen in the inset photographic image of Fig. 14e, the superior flexibility of HG-MBP was verified with a high bending angle using a bending test. This resulted from the intrinsic properties of the MBP composite film, which has a thickness of 125 ± 10 μm and contains 2D and nano-scaled materials, such as MXene sheets and $BaTiO_3$ nanoparticles, inside the PDMS matrix with high elasticity. A schematic of MXene is shown in Fig. 14g(i). Additionally, X-ray diffraction (XRD) analysis was performed to verify that MXene was successfully synthesized. As shown in Fig. 14g(ii), a high open-circuit voltage of 80 V, a short-circuit current of 14 μA, and a power density of 13.5 W m^{-2} were achieved after determining the ideal MXene concentration. An example of this is the successful control of a 3D printer-modeled robot hand using the finger joint motions of a real hand that has HG-MBPs attached. The k-means clustering approach was also used in the development of the object recognition system, which distinguishes between various

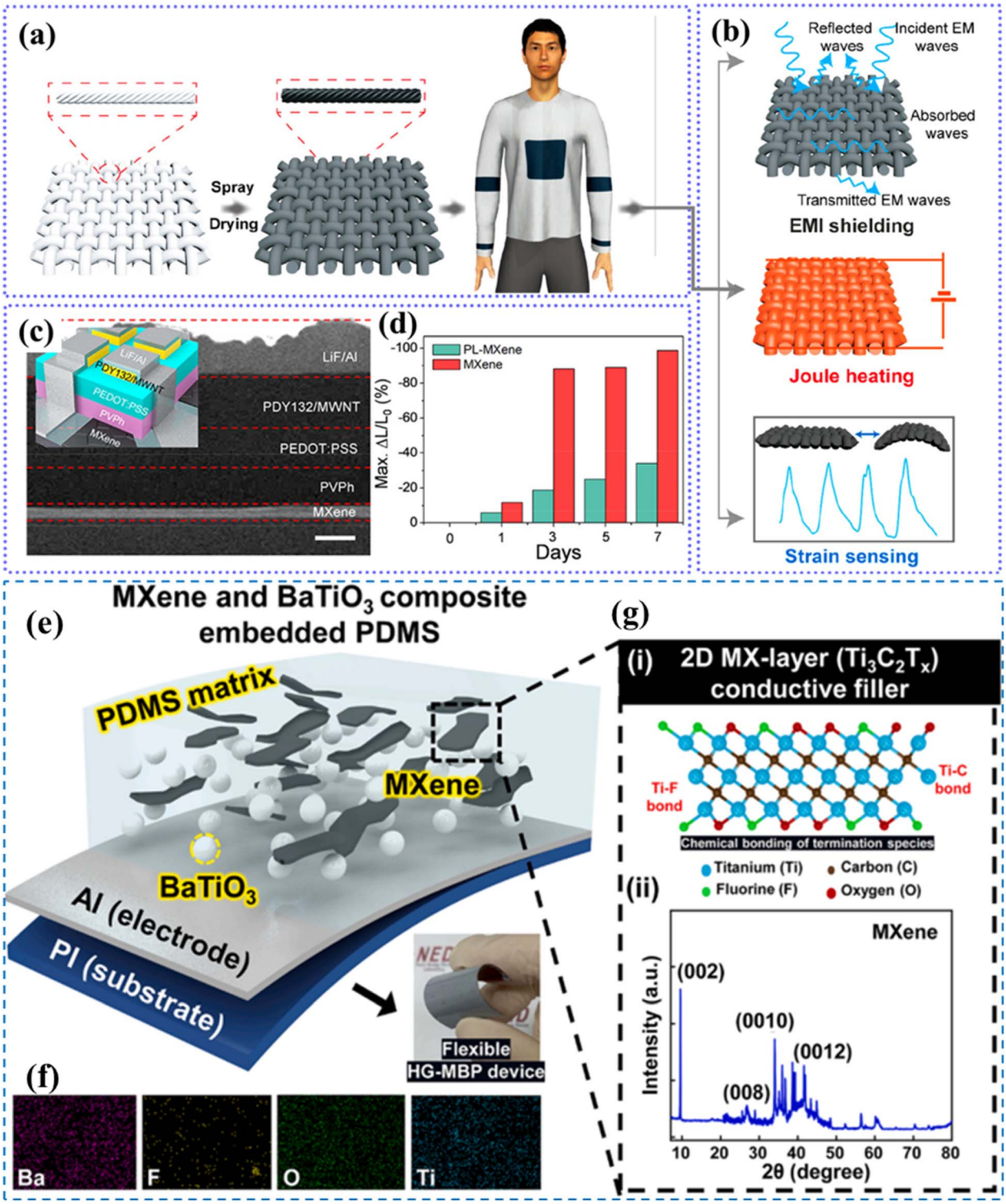

Fig. 14 MXene–polymer nanocomposites in flexible electronics. (a) Multifunctional MXene-decorated cotton woven fabrics fabricated by employing the spray-coating method, where the MXene material is applied to the cotton woven fabric to impart multifunctional properties like EMI shielding, Joule heating, strain sensing, *etc.* (b) Demonstration indicating the applications of MXene coated flexible fabrics in different areas. Reproduced with permission from ref. 59. Copyright 2020, American Chemical Society. (c) SEM image showing the cross-sectional view of an organic AC-EL display with a PL-MXene electrode (scale bar: 50 nm). The inset provides a schematic representation of the PL-MXene organic AC-EL display. (d) Maximum ΔL (luminance change) to L_0 (initial luminance) ratio of bare MXene and PL-MXene organic AC-EL displays as a function of air exposure duration (days).[50] Copyright 2020, American Chemical Society. (e) General schematic representation of the manufactured HG-MBP with the Al electrode connected to the PI substrate spin-coated with a MBP composite film. The inset graphic illustrates the constructed HG-BMP's flexibility. (f) MXene and $BaTiO_3$ particles implanted in the PDMS matrix as shown in a cross-sectional EDX picture. (g) (i) MXene's schematic chemical bond structure and (ii) XRD result.[284]

materials with a high classification accuracy of 93.33%. These findings demonstrate the great potential of the suggested HG-MBP as a material detection sensor and human gesture manipulation system, which is anticipated to be used as a next-generation e-skin in the human–machine interface.

MXene exhibits a better piezoelectric effect on poly(-vinylidene fluoride-*co*-trifluoroethylene) (PVDF–TrFE) compared to polyvinylidene fluoride (PVDF). Generally the (beta-phase) β-phase in PVDF crystals exhibits the best piezoelectric properties, although achieving this phase in PVDF is still challenging.[285,286] However, PVDF–TrFE inherently possesses a larger content of the electroactive β-phase than PVDF due to its higher steric hindrance.[287] The incorporation of MXene into PVDF–TrFE further promotes the nucleation of this phase, leading to improved piezoelectric properties.[288] This enhancement is less significant in PVDF due to its lower initial β-phase content. The dielectric constant significantly increases, while dielectric loss decreases in PVDF–TrFE as a result of the interaction between the polymer matrix and the surface functional groups of MXene. PVDF–TrFE/MXene composites exhibit enhanced mechanical flexibility and durability, making them more suitable for applications in flexible electronics and wearable devices. Fatemeh M. *et al.*[288] reported the fabrication of acoustic energy harvesters using electrospinning of the piezoelectric polymer PVDF–TrFE onto fabric-based electrodes. The incorporation of $Ti_3C_2T_x$ MXene flakes effectively induced polarization locking within the electro-spun PVDF–TrFE, optimizing its electromechanical performance. The resulting device was mechanically robust, lightweight, and flexible, enabling efficient energy harvesting and sound detection within the 50 to 1000 Hz frequency range and at sound pressure levels between 60 and 95 dB. The device demonstrated an impressive sensitivity of 37 V Pa^{-1}, outperforming previous PVDF-based acoustic harvesters. It achieved a peak output power of 19 mW cm^{-3} at 200 Hz and 95 dB. This advancement highlights the potential of MXene-enhanced PVDF–TrFE composites in powering small electronic devices, including implantable biomedical devices, smart wearables, and remote Internet-of-things (IoT) systems. The comparison of PVDF/MXene and PVDF–TrFE/MXene composites is given in Table 7. Numerous studies that reported the applications of PVDF–TrFE/MXene-based piezoelectric nanogenerators can be found here.[289–292]

Zhao and colleagues used rolling,[281] hot pressing, and electrospinning techniques to create a high-performance MXene/PVDF composite film with a β-phase of more than 95 weight percent. The MXene/PVDF-based sensor showed an exceptional voltage sensitivity of up to 0.0480 V N^{-1}. It is important to remember that the MXene used in this work was generated *via* HF etching, which left it with rich surface groups. The favorable impact may be primarily ascribed to the hydrogen bonding interaction that favors all trans planar conformation (β-phase) during PVDF crystallization and is brought about by the –OH groups of the MXene and F atoms of PVDF chains. The directed distribution and orderly stacking of MXene flakes, which facilitated the transfer, storage, and release of electric charge, were further examined by Han and colleagues.[280] Furthermore, this study discussed the –F groups of the MXene with interfacial compatibility, which are typically considered as significant surface functional group for modulating the surface chemistry of MXenes.

Even though adding MXenes to composites increases their piezoelectricity for improved sensing properties, if the MXene level is over the percolation threshold, the composite's performance drastically declines.[300,301] This may be explained by the fact that when the amount of conductive MXene is too high, many connections are created that degrade the performance. Increased MXene content may result in additional β phases but a conductive route inside the composite. Additionally, a lower MXene content results in fewer β phases. One important component for improving performance is the percolation threshold. Li and colleagues used molecular dynamics to simulate MXene/PVDF composite material systems with varying MXene levels based on the Forcite model.[302] They then computed the free volume fraction (FFV) to demonstrate the impact of MXene sheets on the shape of the macromolecular chain. The space between molecules is known as free volume. When a suitable number of MXene sheets were introduced into the PVDF polymer system, the polymer system's FFV dropped to its lowest value, indicating that there was less room for macromolecular chains to move.

Table 7 The comparison of several MXene-based composites as piezoelectric nanogenerators

Components	MXene content (wt%)	Device dimensions	Source	Fabrication technique	Sensitivity	Power density	Ref.
PVA/$Ti_3C_2T_x$	—	8 × 8 mm^2	0.5 Hz	Electrospinning	—	42 mW m^{-2}	293
Glycine/Nb_2CT_x	—	100 mm^2	0.6 Hz, 10 N	Crystallization	5 pC N^{-1}	—	294
PVDF/$Ti_3C_2T_x$	—	1 × 1 cm^2	96.5 dB, 0.2 N	Crystallization	0.4 nA kPa^{-1}	—	295
PVDF/$Ti_3C_2T_x$	0.4 wt%	2.5 cm × 3.0 cm	1–3 Hz	Electrospinning	43 pC N^{-1}	—	281
PVDF/$Ti_3C_2T_x$	1.0 wt%	2 × 20 mm	1–10^7 Hz	Microinjection molding		18.9 μW cm^{-2}	280
PVDF/$Ti_3C_2T_x$	0.01–0.05 g L^{-1}	2 cm × 2 cm	4.7 N, 5 Hz	Spin- and spray-coating	—	14 μW cm^{-2}	296
PVDF/$Ti_3C_2T_x$	5–25 wt%	20 mm × 20 mm	1–8 Hz	Electrospinning	—	11.213 W m^{-2}	297
PVDF/CNT/$Ti_3C_2T_x$	0.05–0.2 wt%	2 × 1.5 cm^2	1–500 MΩ	Electrospinning	—	18.08 W m^{-2}	298
PVDF–TrFE/$Ti_3C_2T_x$	0.05–0.2 wt%	12.56 cm^2	200 Hz, 95 dB	Electrospinning	37 V Pa^{-1}	0.207 mW m^{-2}	288
PVDF–TrFE/$Ti_3C_2T_x$	0.02–0.5 wt%	2.4 cm^2	5 kPa, 1 Hz	Printing	−52.0 pC N^{-1}	—	299
PVDF–TrFE/$Ti_3C_2T_x$	2.0 wt%	1 × 1 cm^2	20 N, 1 Hz	Electrospinning	—	3.64 mW m^{-2}	285
PVDF–TrFE/$Ti_3C_2T_x$	16% (w/v)	15 × 1.3 mm	7 N, 6 Hz	Electrospinning	—	4.02 W m^{-2}	289

Additionally, the optimized sensor demonstrated a sensitivity of up to 55.42 mV kPa^{-1}.

Due to their varied inherent characteristics, MXenes give composite materials new functions in addition to improving piezoelectric performance. In addition to their electrical benefits, MXenes are biocompatible, which makes them appropriate for a range of biomedical applications.[303,304] MXene-based composites can be employed safely in settings that require interactions with biological systems thanks to their biocompatibility. MXenes are promising materials for advanced composite technologies because of their improved piezoelectricity and bio-friendly qualities, which help to close the gap between high-performance materials and environmentally and biologically compatible solutions. By using MXenes' high electrical conductivity to increase electron transfer rates, Fu and colleagues were able to generate and transport electrical charges under mechanical stress, improving the piezoelectric response.[305] Furthermore, the MXenes in the composite not only generated sufficient heat to eradicate bacteria but also produced singlet oxygen, which may also have a highly effective sterilizing effect. This suggests that it has significant potential for use in biomedical and self-powered body monitoring applications. A comparison of several MXene–polymer composites in the field of piezoelectric nanogenerators is given in Table 7.

7.3 MXene–polymer nanocomposites in 3D/4D printing

MXene polymer composites offer great promise for 3D/4D printing applications, integrating MXene's exceptional properties of high electrical conductivity and mechanical strength with the versatility and tunability of polymers.[26,64,306] Enabled by 3D/4D printing technology, these composites showcase dynamic and shape-changing capabilities in response to external stimuli, paving the way for advanced engineering and smart applications.[307,308]

Programmable micro-supercapacitors can be developed using 3D printing of a composite ink consisting of PEDOT:PSS/MXene/ethylene glycol (PME).[26] In Fig. 15a, the design and preparation procedure of 3D printed PME gel composites for micro-supercapacitors is illustrated. By mixing MXene and ethylene glycol (EG), and PEDOT:PSS solution, an ink was prepared. During the fabrication process, the ink was transferred to a syringe and extruded under pressure through a needle to construct thick interdigitated electrodes for MSCs. To achieve controlled solidification and form a highly interconnected 3D framework, a cold plate-based freezing technique was applied during the printing process. In this process, PEDOT:PSS (Fig. 15b) plays a significant role, and by appropriately bridging the PEDOT structures, an integrated porous structure is created for the optimization of ion/electron transport kinetics in the fabricated gel (Fig. 15c).

In addition to the development of 3D printing, 4D printed hydrogels using MXene and PEDOT:PSS have been developed, showcasing high-efficiency pseudocapacitive energy storage capabilities.[309]

MXene hydrogels were prepared *via* self-assembly by mixing $Ti_3C_2T_x$ MXene suspension with PEDOT suspension, followed by sonication. A solution containing DMSO, sulfuric acid, sodium L-ascorbate, and deionized water was added and stirred. The mixture was then poured into molds and heated to form $Ti_3C_2T_x$ MXene hydrogels. These hydrogels were further treated with sulfuric acid to improve mechanical strength and washed to remove impurities. The optimization involved adjusting the MXene content, DMSO volume, sulfuric acid concentration, and sodium L-ascorbate ratio. The method offers numerous advantages, especially remarkable versatility and feasibility in synthesizing various MXenes such as Nb_2CT_x, $Ti_3C_2T_x$, and $Mo_2Ti_2C_3T_x$.

An approach to 3D printing using MXene and poly(vinyl alcohol) (PVA) composites using MXene-surfactant ink has also been proposed for energy storage applications. Through the controlled deposition of highly conductive MXene particles onto a PVA matrix, the fabricated sample exhibited conductive behavior.[63] In a separate study, Li *et al.* demonstrated the production of elastic nanocomposites by encapsulating 3-(trimethoxysilyl)propyl methacrylate-modified MXene nanosheets within a photocurable polyurethane acrylate resin (PAR) matrix using digital light processing 3D printing. By adjusting the MXene content in the PAR, the mechanical properties of the elastomers were tailored. The resulting MXene–PAR nanocomposites, containing 0.1% w/w fillers, exhibited a remarkable tensile strength and elongation at a break of 23.3 MPa and 404.3%, respectively, representing a significant increase of 100.8% and 37.8%, compared to the control.[310] Some other reports on MXene–polymer composites in 3D/4D printing are also available in the literature.[307,311]

7.4 MXene–polymer nanocomposites in EMI shielding

EMI shielding is the most extensively explored area among the applications of MXene–polymer nanocomposites. These composites offer several advantages in the field of EMI shielding.[312,313] MXene–polymer composites exhibit lightweight, conductivity, and improved mechanical properties, making them highly suitable for EMI shielding applications.[313,314] Polymers provide the advantage of tunability in MXene–polymer composites, allowing the customization of EMI shielding performance for specific applications or requirements.[29,313] By selecting appropriate polymers with specific dielectric properties, the composite's overall electrical conductivity and impedance matching can be tailored to provide optimal shielding performance within desired frequency ranges.[29,204] Polymers in MXene–polymer composites provide chemical resistance and durability, enhancing the longevity and performance of EMI shielding materials. The polymer matrix acts as a protective layer, shielding the MXene flakes from environmental factors such as moisture, chemicals, or oxidation.[315]

Different structures of MXene/polymer composites offer distinct mechanisms for EMI shielding depending on various factors.[315] In multilayer MXene/polymer composites, multiple MXene layers are stacked within the polymer matrix (Fig. 16a). The interlayer spacing and alignment influence the EMI shielding. Electromagnetic waves penetrate the composite and get reflected or scattered at the interfaces between the MXene

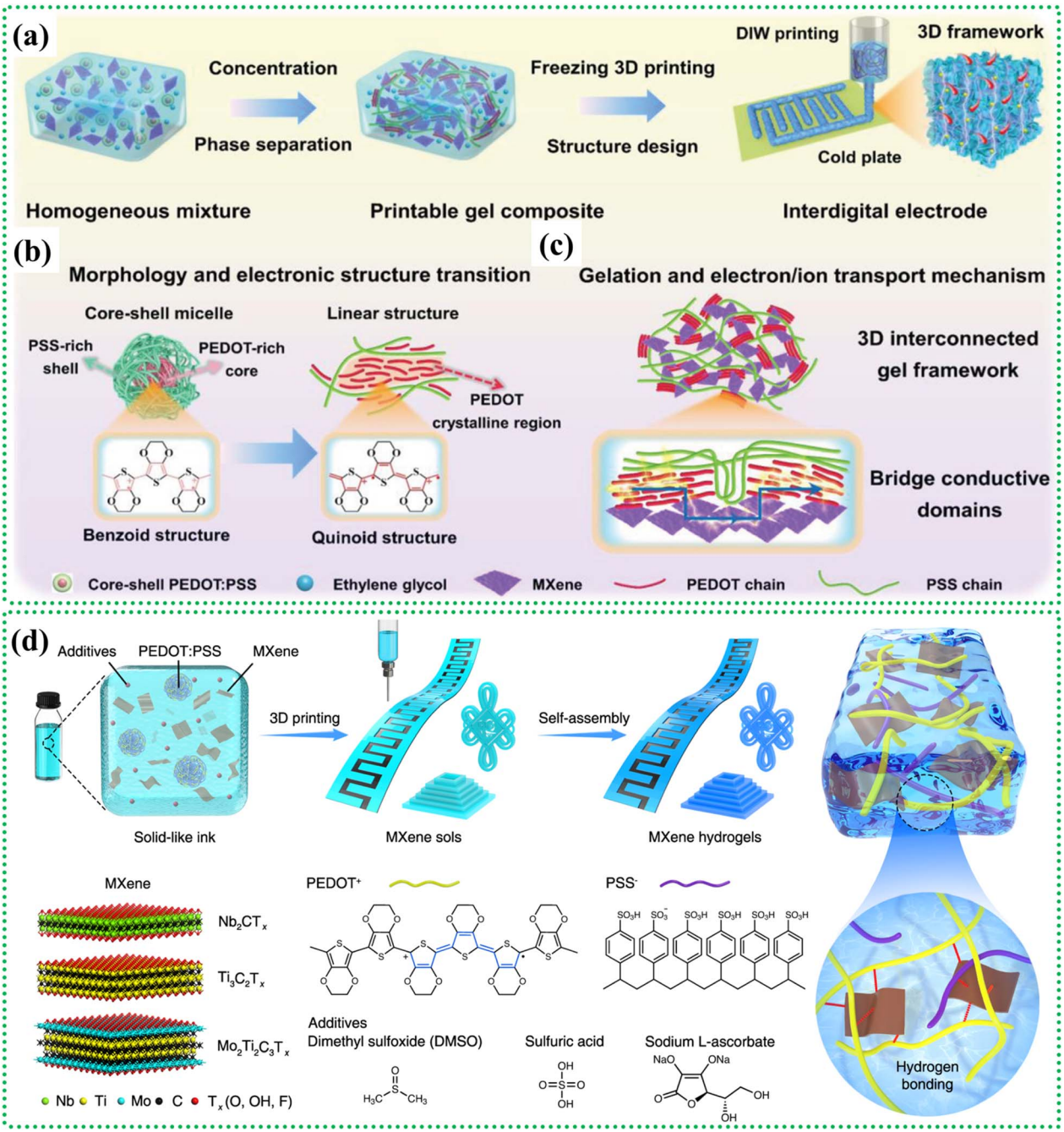

Fig. 15 3D/4D printing applications. (a) A schematic illustration of the preparation of 3D printable PME gel composite inks and interdigital electrodes is depicted. (b) The morphology and electronic structure transition of PEDOT:PSS within the PME gel composites. (c) A schematic illustration of the gelation process and the mechanism for enhancing electron/ion transport in the PME gel composites. Reproduced with permission from ref. 26. Copyright 2023, Wiley. (d) Composite inks comprising MXenes, PEDOT:PSS, and additives are utilized for 3D printing designed patterns. Through a self-assembly process, these inks transform into MXene hydrogels.[309]

layers and the polymer. This multiple reflection and scattering lead to effective EMI attenuation. Porous MXene/polymer composites have voids or pores within the material (Fig. 16b). These voids can trap and dissipate electromagnetic waves, reducing their propagation. The interconnected porous network of MXene also enhances the electrical conductivity, further improving the EMI shielding efficiency. In segregated MXene/polymer composites, MXene and polymer phases exist as distinct domains within the material (16c). The MXene domains act as conductive pathways, while the polymer regions provide structural support. This phase separation enhances electrical conductivity and enables effective EMI shielding by creating a conductive network to dissipate electromagnetic energy. Some MXene/polymer composites include magnetic particles or other conductive additives (Fig. 16d). MXene/polymer composites with conductive and magnetic fillers show excellent EMI-

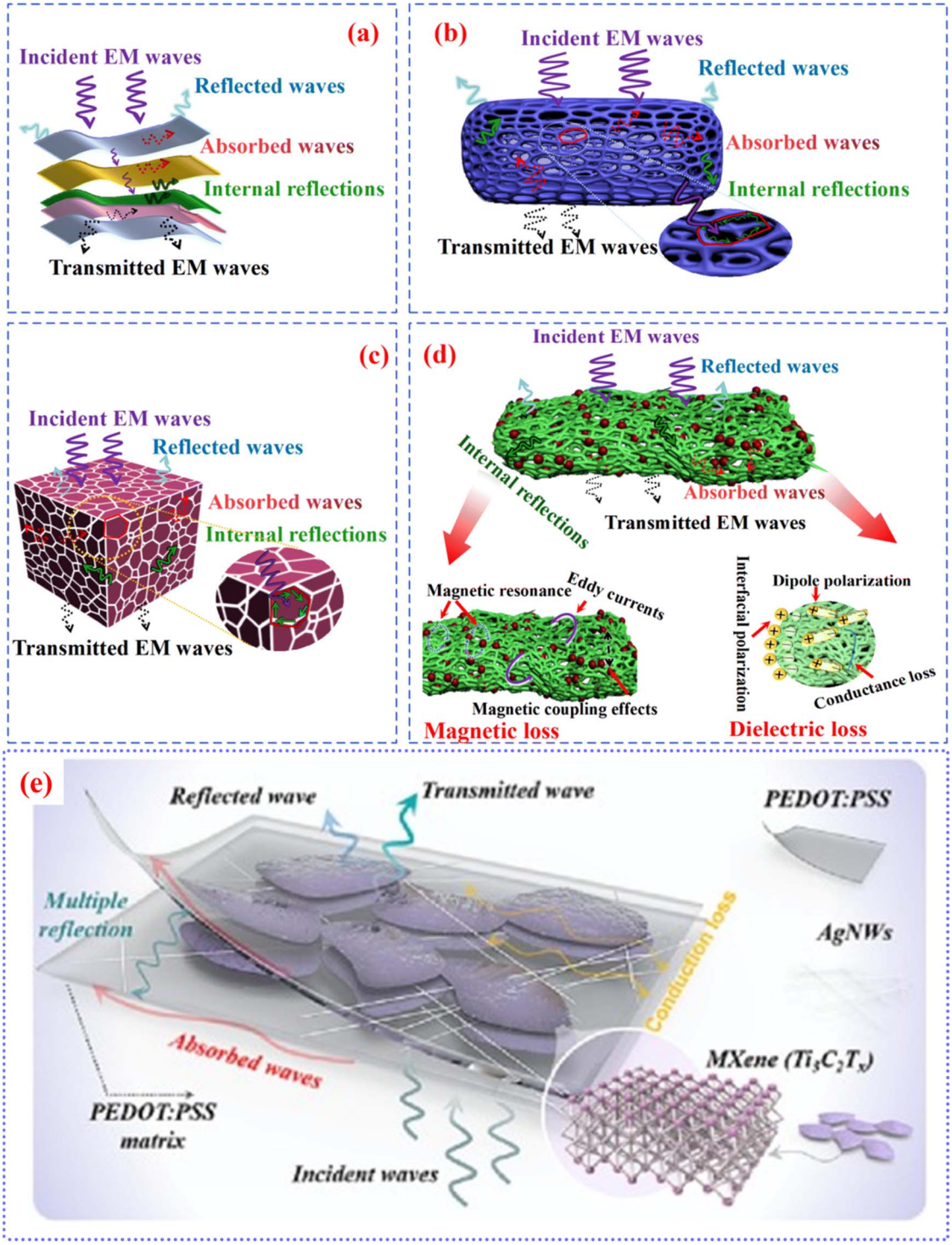

Fig. 16 EMI shielding mechanisms vary among different structures of MXene/polymer composites. (a) Multiple MXene layers lead to reflection and scattering, effectively attenuating EMI. (b) The interconnected MXene network and voids trap and dissipate electromagnetic waves, reducing their propagation. (c) Separate MXene and polymer domains create conductive pathways, ensuring efficient EMI shielding. (d) The inclusion of magnetic or conductive fillers enhances impedance matching, improving EMI absorption.[315] (e) Diagram depicting electromagnetic microwave dissipation in the MXene/AgNW/PEDOT:PSS coating. Reproduced with permission from ref. 316. Copyright 2023, Elsevier Ltd.

shielding performance. The conductive network induces an impedance mismatch at the composite/air interface, leading to high reflection. Magnetic materials enhance impedance matching at the conductive filler/air interface, increasing EMW absorption. These additives enhance the electromagnetic absorption and scattering properties of the composite.

To address the challenges posed by harsh freezing and high-humidity environments for polymeric EMI shielding materials,

Chang *et al.* developed ultrathin, flexible MXene/Ag nanowires/PEDOT:PSS composite coatings.[316] Fabricated *via* drop-casting and hydrophobic spraying, these coatings achieve an EMI shielding effectiveness of 31.5 dB at ~10 μm thickness. These nanocomposite coatings also offer excellent electro/photothermal properties, water repellency, interfacial adhesion, and mechanical durability, making them suitable for cold and damp conditions. The shielding mechanism of the MXene/AgNWs/PEDOT:PSS coating is shown in Fig. 16e.

As an electromagnetic wave strikes the MXene/AgNWs/PEDOT:PSS coating, most of it reflects due to impedance mismatch. The penetrating portion interacts with dense charge carriers, leading to significant polarization and conduction losses. The 1D AgNWs bridge the gaps between MXene nanosheets, creating conduction networks that enhance electron hopping and migration, thus increasing conduction losses. Additionally, the lamellar microstructures cause the wave to bounce between MXene layers, further dissipating energy due to impedance mismatch at the PEDOT:PSS/MXene interfaces.

In a recent study, $Ti_3C_2T_x$ MXene composite films were developed for efficient EMI shielding, featuring photothermal healing, stretchability, and high conductivity.[211] By increasing the MXene content in waterborne polyurethane (WPU), natural rubber, and MXene-based composite (WNM) films, the conductivity increased sharply, which led to high EMI shielding for the WNM composite, exhibiting an EMI shielding efficiency (SE) of 76.1 dB at a thickness of 336 ± 15 μm for the X-band, whereas, for the Ku-band, the EMI SE value is ~80 dB. The EMI shielding mechanism in the composite films is based on induced polarization due to the MXene functional groups. The local dipoles between Ti and surface groups (–F and –OH), especially –F on MXene surfaces, induce dipole polarization, leading to attenuation of penetrated EMWs through interfacial polarization loss. Additionally, polarized interfaces between the honeycomb-like MXene network and the polymeric matrix enhance polarization loss, further improving EMI shielding performance. The honeycomb-like MXene network structure contributes to the exceptional EMI shielding performance of the WNM films across a wide frequency range.

These advantages of MXene–polymer composites in EMI shielding make them highly attractive for various industries, including flexible electronics,[317] telecommunications,[318] and aerospace,[319] where effective protection against electromagnetic interference is crucial.[320] The synergistic effects between MXenes and polymers enable the development of lightweight, flexible, and high-performance EMI shielding materials with improved properties and capabilities.

7.5 MXene–polymer nanocomposites for anti-corrosion applications

The exceptional characteristics of $Ti_3C_2T_x$, such as its unique layered structure and large specific surface area, along with remarkable electrical and mechanical properties, make it highly promising for anti-corrosion applications.[66,321,322] To utilize the inherent anticorrosion properties of pristine $Ti_3C_2T_x$ nanosheets, these were incorporated in the form of single- to few-layer $Ti_3C_2T_x$ nanosheets into a waterborne epoxy coating (WEC) through simple physical mixing. Zhang *et al.* conducted a study on the surface functionalization of $Ti_3C_2T_x$ and its application in aqueous polymer nanocomposites to enhance corrosion protection.[322] In this approach, they utilized [3-(2-aminoethyl)aminopropyl] trimethoxy silane (AEAPTES), a silane coupling agent, to modify the $Ti_3C_2T_x$ MXene. This modification aimed at adjusting the wettability of $Ti_3C_2T_x$ to improve its compatibility with the polymer matrix in the nanocomposites.

In another study, a few-layer amino-functionalized $Ti_3C_2T_x$ nanosheets (k-Ti_3C_2) were combined with an interpenetrating polymer network (IPN) to create k-Ti_3C_2/IPN composite coatings and the tribological characteristics of these coatings were examined[323] (Fig. 16a). The wear rates of the k-Ti_3C_2-0.75 (0.75 wt% amino functional $Ti_3C_2T_x$) composite coating decreased by 82.41% before UV aging and 74.55% after UV aging, compared to the pure IPN coating, under dry friction conditions. Additionally, during the tribo-corrosion test in a 3.5 wt% NaCl solution, the k-Ti_3C_2-0.75 composite coating exhibited the highest open circuit potential (OCP) and the lowest coefficient of friction (COF) among all coatings, both before and after UV aging.

In a recent study, the anticorrosion and anti-wear behavior of an inorganic-organic multilayer protection system consisting of an epoxy coating incorporating $Ti_3C_2T_x$ MXene was investigated. The researchers designed and prepared this protective system to enhance its effectiveness against corrosion and wear.[66] The hydrophilic nature of $Ti_3C_2T_x$ allowed it to maintain stable dispersions within the epoxy matrix. This characteristic played a vital role in creating an effective physical barrier for anti-corrosion purposes. Ti_3C_2/epoxy coatings with different Ti_3C_2 contents (0.5, 1, and 2 wt% $Ti_3C_2T_x$/epoxy) were obtained *via* the curing reaction of epoxy resin with an amine curing agent (Fig. 17a). The mechanism of protection from corrosion with Ti_3C_2 content was proposed as demonstrated in Fig. 17b and c. With no MXene content, the corrosion probability is high and as the MXene content increases, the corrosion inhibition efficiency increases. But as the Ti_3C_2 content was increased to 2.0 wt%, irregular corrosion particles began to accumulate once more and corrosion inhibition efficiency decreased. This indicates that beyond the optimal content, MXene tends to agglomerate, adversely impacting the anti-corrosion performance. Hence, Ti_3C_2 nanosheets can effectively enhance the corrosion resistance of the coatings, but only when added in the optimal amount. The Tafel plots display the corrosion behavior of the uncoated Q345 sample (polished steel), pure epoxy, and $Ti_3C_2T_x$/epoxy composites with different $Ti_3C_2T_x$ ratios (Fig. 17d).

Following a 96-hour immersion in a 3.5% NaCl solution, it was observed that the $Ti_3C_2T_x$ provided enhanced corrosion protection on steel substrates compared to pure epoxy coatings. This improvement in anti-corrosion properties was attributed to MXene flakes in an optimized concentration, acting as thin film barriers that hindered the diffusion of electrolytes and provided effective corrosion protection to the substrate. The anti-corrosion performance can also be achieved through well-

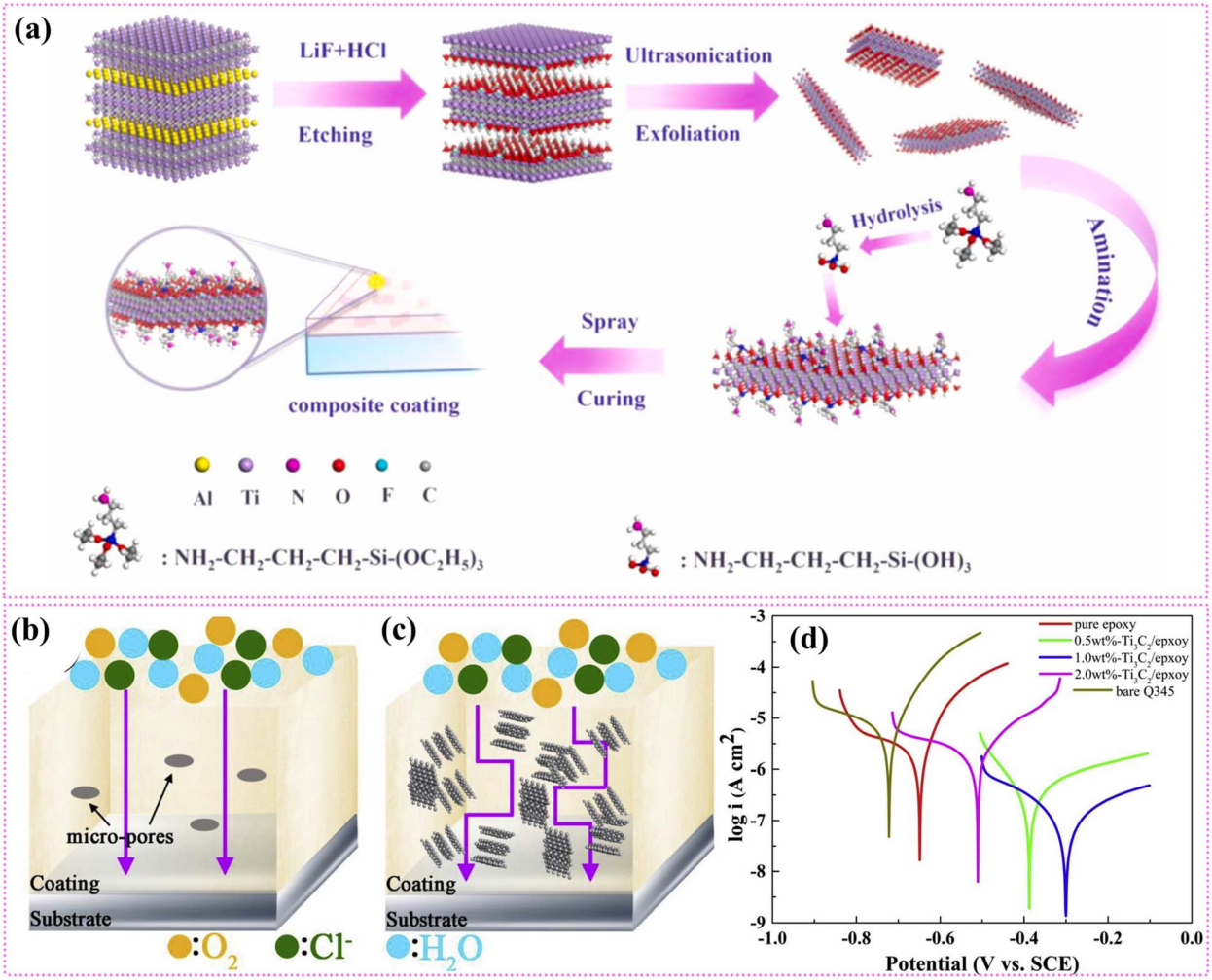

Fig. 17 The anti-corrosion performance of MXene–polymer composites. (a) Synthesis of k-Ti_3C_2/IPN coatings. Reproduced with permission from ref. 323. Copyright 2021, Elsevier Ltd. Schematic representation of the corrosion process in two scenarios: (b) without a Ti_3C_2 containing epoxy coating and (c) with a Ti_3C_2 containing epoxy coating. (d) Tafel plots of the samples immersed in 3.5% NaCl for 96 hours. Among the uncoated and coated samples, the 1 wt%-coated sample exhibited the most superior protection. This was evident from the substantial positive shift in the potential value (E_{corr}) and the lowest corrosion current (I_{corr}). The potential was measured relative to the saturated calomel electrode, utilized as the reference electrode. Reproduced with permission from ref. 66. Copyright 2019, Elsevier Ltd.

dispersed MXene–polymer composite coatings, made possible by covalent modification and ambient electron-beam curing.[241]

7.6 MXene–polymer nanocomposites in biomedical applications

Polymer-functionalized MXenes exhibit exceptional properties that make them highly valuable for various applications in the medical sector. The big advantage is that polymers have better compatibility and hence these nanocomposites can also be applied to numerous biomedical applications.[282,324] The applications include antimicrobial treatments, photothermal therapy (PTT), drug delivery systems, diagnostic imaging techniques, biosensors, and bone regeneration processes. MXene polymer nanocomposites have shown great promise in biomedical applications. These nanocomposites combine the unique properties of MXene materials, such as excellent conductivity, high surface area, and antibacterial activity, with the versatility and biocompatibility of polymers. They hold potential for various biomedical uses, including tissue engineering,[237,325] cancer therapy,[326–328] drug delivery systems,[207,329] biosensors,[330] and antimicrobial coatings.[331,332] MXene polymer nanocomposites offer exciting opportunities for advancing medical technologies and improving healthcare outcomes.

7.6.1 Antimicrobial applications. The hydrophilic nature and anionic surface properties of MXenes enhance their interaction with bacterial cell membranes. Through hydrogen bonding, the functional groups of MXenes interact with lipopolysaccharide molecules on the cell membrane, leading to cell inactivation. This interaction hinders nutrient intake, effectively inhibiting bacterial growth. Additionally, the formation of a conductive bridge over the lipid bilayer facilitates the transfer of reactive electrons from the bacterial cell to the external environment, ultimately causing cell death.[74,75] The application of $Ti_3C_2T_x$, a high aspect ratio material, as a coating on PVDF

membranes resulted in notable improvements in hydrophilicity, as evidenced by a reduced contact angle of 37°. Additionally, the presence of large pores in the membrane was mitigated. As a result, the viability and growth of *E. coli* (Gram-negative bacteria) were reduced by approximately 73%, while *B. subtilis* (Gram-positive bacteria) experienced a growth inhibition of around 67%.[74]

A study on the tunable antibacterial activity of a polypropylene (PP) fabric coated with $Ti_3C_2T_x$ MXene flakes, coupling the nano-blade effect with reactive oxygen species (ROS) generation, was conducted.[75] In this study, an antibacterial medical fabric using a straightforward self-assembly process was developed, wherein delaminated $Ti_3C_2T_x$ MXene flakes were arranged on the surface of PP fibers (Fig. 18a). By varying the amount of MXene in the coating solution from 1 to 32 mg mL^{-1}, edge-on assembly of MXene flakes on the PP surface was achieved, allowing the monitoring of band gap evolution for a restacked structure. Characterization of the PP/$Ti_3C_2T_x$ nanocomposite revealed highly effective antibacterial properties, a robust coating, and excellent chemical/thermal stability. *In vitro* microbiological studies against both Gram-positive *Staphylococcus aureus* and Gram-negative *Escherichia coli* demonstrated that PP/$Ti_3C_2T_x$ reduced bacterial viability by up to 100%. This effect was attributed to a synergistic combination of physical contact causing membrane stress and light-induced ROS generation. The antibacterial mechanism in PP/$Ti_3C_2T_x$ fabrics involved synergistic membrane stress mediated by the physical contact of sharp edges (nano-blade effect) of MXene flakes, along with the generation of ROS (Fig. 18b). Before this, $Ti_3C_2T_x$ MXene exhibited antibacterial properties. Rasool *et al.* investigated $Ti_3C_2T_x$ against *E. coli* and *B. subtilis* using bacterial growth curves and agar plates.[74] $Ti_3C_2T_x$ showed higher antibacterial efficiency against both *E. coli* and *B. subtilis* compared to graphene oxide. The concentration-dependent antibacterial activities of $Ti_3C_2T_x$ in aqueous suspensions are shown in Fig. 18c. The top frame (right side-top, Fig. 18c(A–F)) shows photographs of agar plates, where after a 4-hour treatment, the *E. coli* bacterial cells were subjected to recultivation with different concentrations of $Ti_3C_2T_x$: 0 μg mL^{-1} (A), 10 μg mL^{-1} (B), 20 μg mL^{-1} (C), 50 μg mL^{-1} (D), 100 μg mL^{-1} (E), and 200 μg mL^{-1} (F). The bottom frame (right side-down, Fig. 18c(A–F)) shows

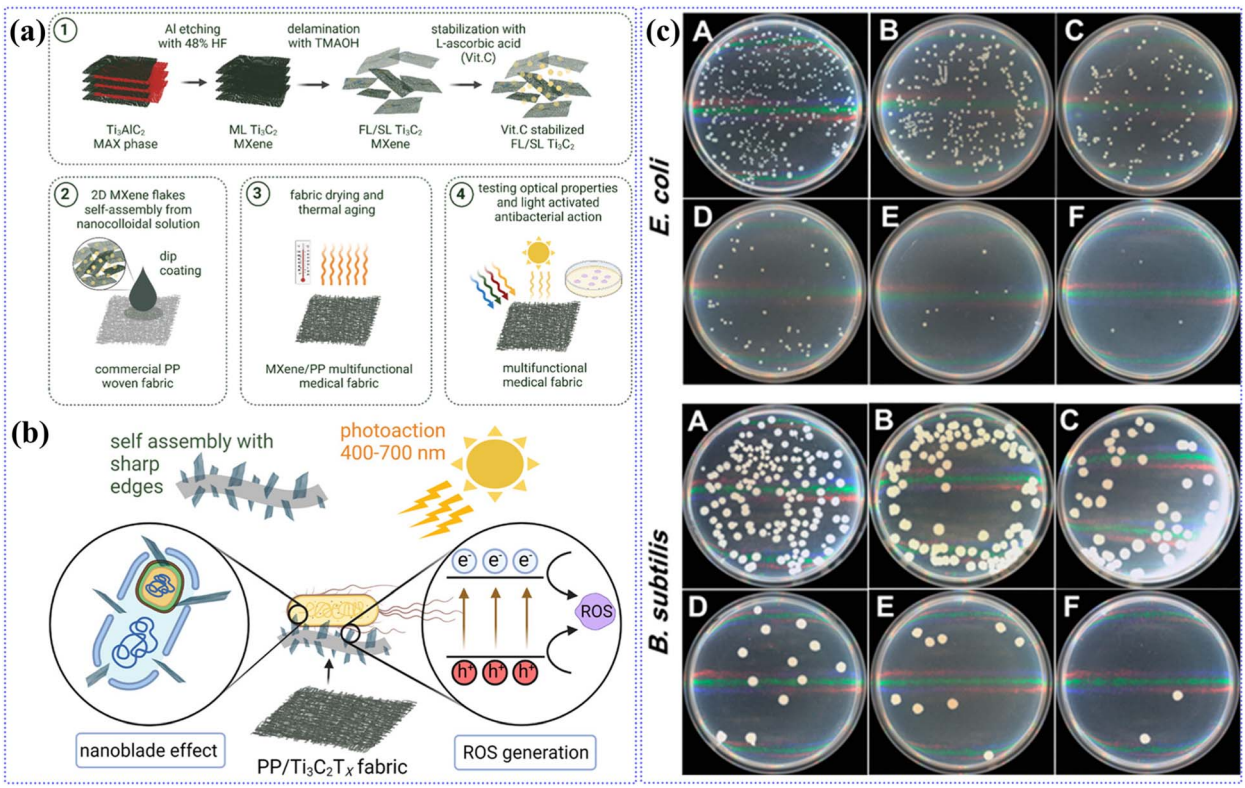

Fig. 18 Antibacterial activity of MXene–polymer nanocomposites. (a) Illustration showing a facile approach to obtaining $Ti_3C_2T_x$-modified PP medical fabrics (PP/$Ti_3C_2T_x$ nanocomposites) with exceptional antibacterial properties, adjustable optical characteristics, and impressive thermal and chemical stability. (b) Schematic diagram showcasing the antibacterial activity of PP/$Ti_3C_2T_x$ nanocomposites, highlighting the synergistic effect of the physical nanoblade action and the generation of reactive oxygen species. Reproduced with permission from ref. 75. Copyright 2022, American Chemical Society. (c) Concentration-dependent antibacterial activities of $Ti_3C_2T_x$ in aqueous suspensions. The top frame (right side-top, figure (A–F)) shows photographs of agar plates, where after a 4-hour treatment, the *E. coli* bacterial cells were subjected to recultivation with different concentrations of $Ti_3C_2T_x$: 0 μg mL^{-1} (A), 10 μg mL^{-1} (B), 20 μg mL^{-1} (C), 50 μg mL^{-1} (D), 100 μg mL^{-1} (E), and 200 μg mL^{-1} (F). The bottom frame (right side-bottom, figure (A–F)) displays photographs of agar plates with *B. subtilis* bacterial cells treated similarly. The study utilized bacterial suspensions in deionized water as a control, without the presence of $Ti_3C_2T_x$ MXene. Reproduced with permission from ref. 74. Copyright 2016, American Chemical Society.

photographs of agar plates with *B. subtilis* bacterial cells treated similarly. At a concentration of 200 μg mL^{-1}, $Ti_3C_2T_x$ resulted in over 98% bacterial cell viability loss within 4 hours of exposure, as validated by regrowth curve analysis and colony forming unit (CFU) assays. Electron microscopic analysis and lactate dehydrogenase (LDH) release assay revealed damage to the cell membrane, leading to the release of cytoplasmic materials.

MXenes can be utilized for their antibacterial properties, as shown in a study where micrometer-thick $Ti_3C_2T_x$ MXene membranes were prepared by filtration onto a polyvinylidene fluoride (PVDF) support.[333] To assess their bactericidal effects, the modified $Ti_3C_2T_x$ membranes were tested against *E. coli* and *B. subtilis* using two methods: bacterial growth on the membrane surface and exposure of the membrane to bacterial suspensions. The results showed that the fresh $Ti_3C_2T_x$ MXene membranes exhibited an antibacterial rate of over 67% against *E. coli* and 73% against *B. subtilis*, compared to the control PVDF membrane, under the same conditions. Interestingly, the aged $Ti_3C_2T_x$ membrane displayed even higher efficacy, with over 99% growth inhibition observed for both bacterial strains.

7.6.2 Drug delivery and photothermal therapy. MXene–polymer nanocomposites have promising applications in drug delivery, anticancer, antibacterial biofilms, *etc.*[332,334] Rabiee *et al.* developed an innovative nanocarrier using inorganic MXene/MOF-5 (metal–organic frameworks) nanostructures for co-delivery of the drug doxorubicin (DOX) and gene pCRISPR.[335] This study presents a nanocarrier approach for efficient co-delivery of drugs and genes for biomedical applications. To

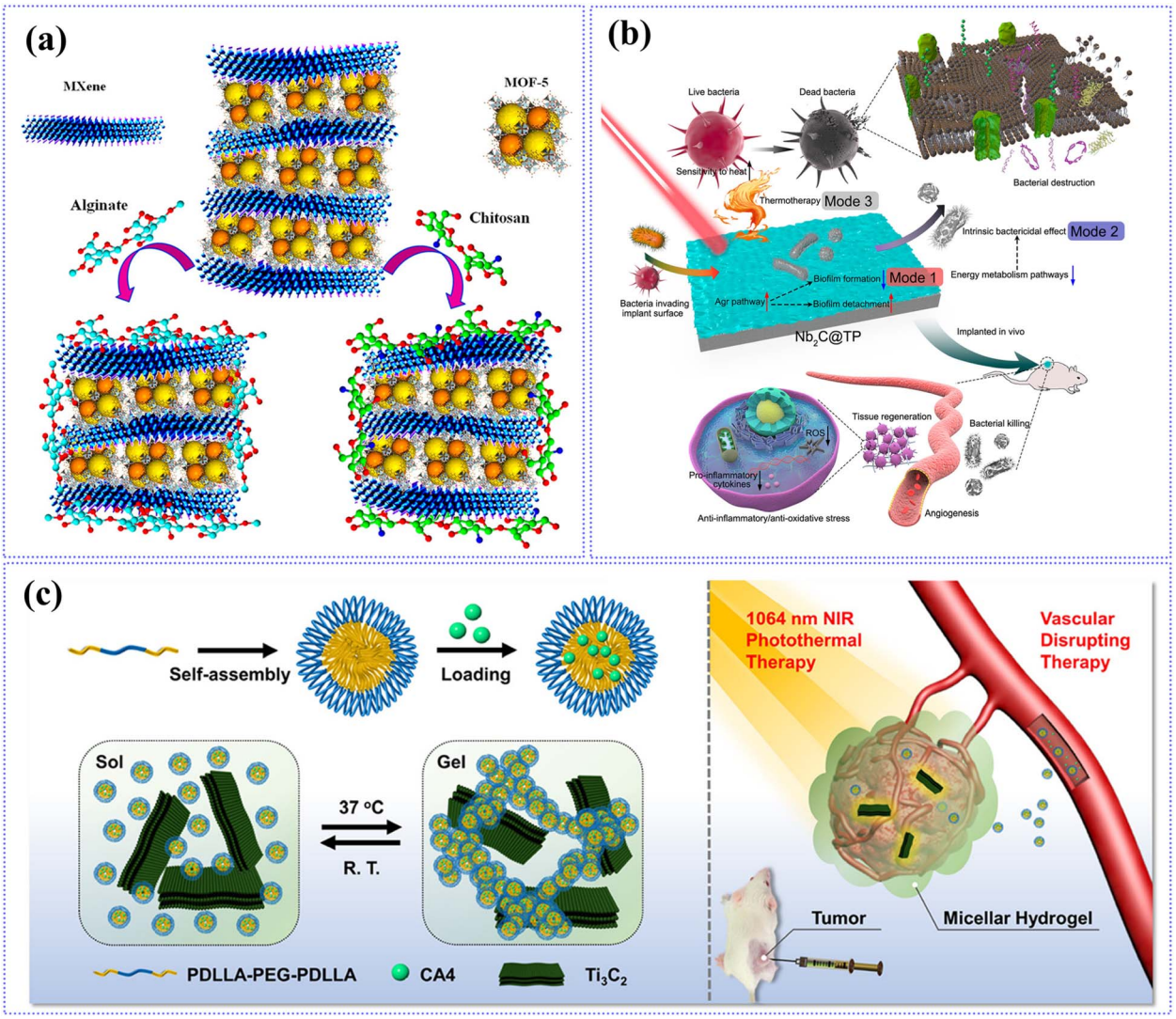

Fig. 19 Biomedical applications of MXene polymer nanocomposites in drug delivery and photothermal therapy. (a) Schematic illustration of MXene/MOF-5 and its alginate and chitosan nanostructures. The modification process involves the integration of chitosan and alginate onto the nanocarriers, resulting in stimuli-responsive properties and the incorporation of a capping agent. Reproduced with permission from ref. 335. Copyright 2021, American Chemical Society. (b) The trimodal bacterial killing strategy of Nb_2C@TP. This strategy involves biofilm resistance, intrinsic bactericidal effects, and thermal ablation of bacteria. Additionally, Nb_2C@TP demonstrates promising *in vivo* tissue regeneration properties. Reproduced with permission from ref. 336. Copyright 2021, American Chemical Society. (c) The schematic illustration of injectable PLEL-based micellar hydrogels co-delivered with CA4 and Ti_3C_2 for synergistic NIR-II photothermal and vascular disrupting therapy. Reproduced with permission from ref. 337. Copyright 2020, American Chemical Society.

enhance bioavailability and interaction with pCRISPR, the nanomaterial was coated with alginate and chitosan. The doxorubicin delivery and cytotoxicity of the polymer-coated nano-systems were evaluated on HEK-293, PC_{12}, $HepG_2$, and HeLa cell lines. The chitosan-coated nanocarriers demonstrated superior cell viability, with over 60% relative cell viability in all tested cell lines. The alginate-coated nanocarriers ranked second, showing more than 50% relative cell viability across all cell lines. The cytotoxicity was dose-dependent, with longer treatment times, leading to reduced cell viability. The nanocarriers were modified to become suitable, stimuli-responsive, and equipped with a capping agent. To achieve this, chitosan and alginate were used to modify the nanocarriers (Fig. 19a). Polymer solutions of alginate and chitosan were prepared and reacted in the dark for 7 hours. The resulting suspensions were mixed with drug-free (MXene/MOF-5) and drug-loaded (MXene/MOF-5-DOX) nanocarriers for 6 hours at room temperature. After 24 hours on various cell lines, MXene/MOF-5 showed cell viabilities of 38.7–14.3% at 0.1 μg mL^{-1} and 27.6–9.9% at 10 μg mL^{-1}, with a drug payload efficiency of 35.7%. Chitosan-based nanocarriers achieved a green fluorescent protein (GFP)-positive efficiency of 25.8% in gene delivery studies. Yang *et al.* developed a clinical implant based on a Nb_2C MXene/titanium plate (Nb_2C@TP) for bacterial infection removal and for regeneration of tissues.[336] This implant offers practical multimodal anti-infection functions. The Nb_2C nanosheets (NSs) were decorated onto amidated TPs (TPs–NH_2) *via* electrostatic interactions, resulting in the formation of Nb_2C@TP. Nb_2C@TP plays a crucial role in suppressing bacteria through multiple modes (Fig. 19b). When bacteria attempt to attack the implant surface, Nb_2C@TP activates the accessory gene regulator (Agr), which prevents bacterial adherence and promotes biofilm detachment. Nb_2C@TP directly induces bacterial death by regulating the essential metabolic pathways such as the tricarboxylic acid (TCA) cycle and the phosphotransferase system (PTS) pathway. These combined mechanisms effectively combat bacterial infection.

Researchers have created a biodegradable nanocomposite micellar hydrogel delivery system with unique functionalities of NIR-II photothermal ablation and vascular disruption, enabling minimally invasive antitumor therapy using $Ti_3C_2T_x$ and poly(D,L-lactide)–poly(ethylene glycol)–poly(D,L-lactide) (PDLLA–PEG–PDLLA, PLEL) triblock copolymer micelle.[337] Ti_3C_2 and CA4 (natural polymer) were selected as the photothermal therapy (PTT) agent and vascular disrupting agent (VDA), respectively, for the development of the nanocomposite micellar hydrogel with dual functionalities in minimally invasive antitumor therapy (Fig. 19c).

The micellar hydrogel system exhibits an impressive photothermal conversion efficiency (41.4% in the 1064 nm window, utilizing a laser power of 1.0 W cm^{-2}). Additionally, the hydrogel demonstrates prolonged retention at the tumor site, enabling sustained release of therapeutic agents, thereby facilitating comprehensive and effective treatment.

Additionally, MXenes can also be used to create smart 3D network nanoplatforms by integrating Ti_3C_2 MXene with cellulose hydrogels, showcasing light-induced bimodal photothermal/chemotherapy anticancer activity.[327] When incorporating the anticancer drug doxorubicin hydrochloride (DOX), the cellulose/MXene hydrogels exhibit a remarkable ability to enhance the release rate of DOX, significantly accelerating its delivery. Dai *et al.* designed composite nanosheets based on Ta_4C_3 MXene for multiple imaging-guided photothermal tumor ablation. The rational selection of MXene composition and surface functionalization facilitated the achievement of this innovative approach.[328] In the study, a redox reaction was initiated on the surface of Ta_4C_3 MXene, leading to the *in situ* growth of manganese oxide nanoparticles (MnO_x/Ta_4C_3). This growth was facilitated by the reducing properties of the nanosheets. Through careful selection of the MXene composition and additional functionalization, the resulting MnO_x/Ta_4C_3–SP composite nanosheets served as high-performance contrast agents. They enabled simultaneous use in computed tomography (CT) for tantalum-based imaging, tumor microenvironment-responsive T1-weighted magnetic resonance imaging (MRI) using the MnO_x component, and photoacoustic imaging.

The advantages of MXene–polymer nanocomposites in photothermal therapy enable more efficient, targeted, and controlled treatment of diseases, particularly cancer. The combination of the photothermal properties of MXenes with the tunability, biocompatibility, and targeting capabilities of polymers opens new possibilities for non-invasive, localized, and personalized therapeutic approaches.

7.7 Water desalination and purification membranes

MXene–polymer composites offer many advantages in water purification and desalination applications over MXene.[69] These composites can be easily synthesized, coated onto membranes, or formed into filters or adsorbents.[338] Polymers can provide a porous and interconnected network within the composite, increasing the surface area available for adsorption.[205,339] Numerous studies have provided evidence that laminar membranes exhibit anomalous transport phenomena, such as ultrafast and precise ion selectivity, when the *d*-spacing is comparable to the diameter *D* of hydrated ions.[340]

MXene–polymer nanocomposites can be utilized to create a super-hydrophilic and underwater super-oleophobic $Ti_3C_2T_x$ MXene-based composite membrane. This can be achieved through vacuum-assisted self-assembly of MXene nanosheets on a porous polyvinylidene fluoride (PVDF) substrate, followed by *in situ* mineralization of the photocatalyst β-FeOOH on the membrane surface.[70] The resulting membrane was treated with HCl and dried under vacuum. The MXene@CS/TA membrane was prepared by mixing chitosan and tannic acid solutions at pH 3, immersing MXene in the solution for 12 hours and then rinsing and drying at 30 °C under vacuum. The membrane was subsequently mineralized in $FeCl_3$ solution, resulting in the MXenes/TA–FeOOH membrane, which exhibited high permeation flux and superior separation efficiency for various oil-in-water emulsions.

Wang *et al.* demonstrated a novel approach to stabilizing the $Ti_3C_2T_x$ laminar architecture using alginate hydrogel pillars.[341] A hybrid SA–$Ti_3C_2T_x$ membrane with a lamellar structure was

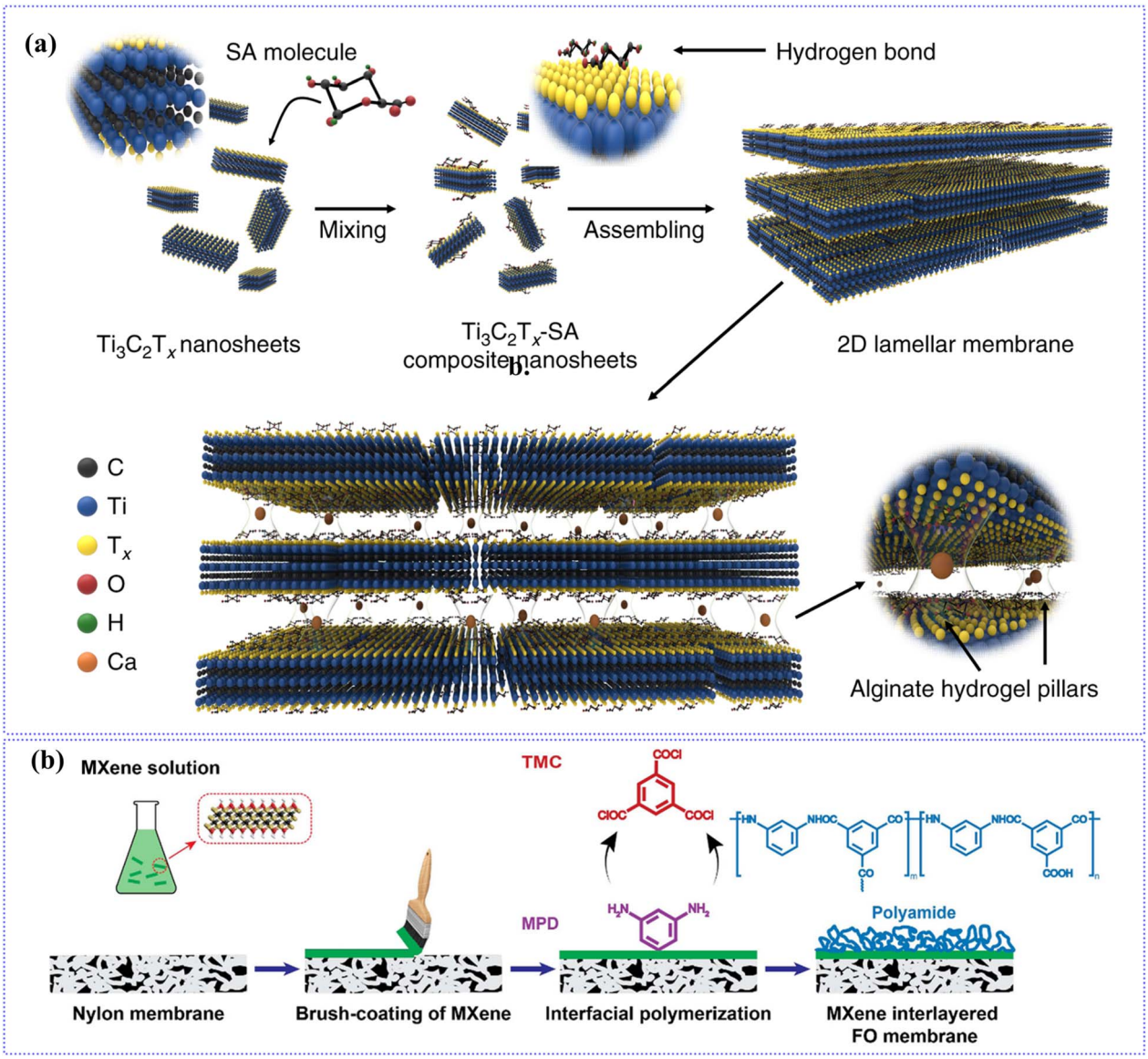

Fig. 20 MXene–polymer nanocomposites in water purification/filtration membranes. (a) Fabrication process of the sodium alginate (SA) and $Ti_3C_2T_x$ membrane. Initially, the SA solution was mixed with the $Ti_3C_2T_x$ colloidal solution, leading to firm and homogeneous attachment of SA molecules onto the nanosheet surface through hydrogen bonding. Subsequently, the composite SA–$Ti_3C_2T_x$ nanosheets were assembled into a hybrid membrane with a lamellar structure. Finally, the SA–$Ti_3C_2T_x$ membrane was immersed in various multivalent Mn^+ cross-linking solutions (Ca^{2+}, Ba^{2+}, Mn^{2+}, and Al^{3+}) to obtain a cross-linked membrane with hydrogel pillars in the interlayer spacing.[341] (b) Schematic of the fabrication process for MXene/nylon substrates. It involves brush-coating MXene onto the surface of commercial nylon membranes, creating a thin MXene layer on the nylon substrate. Subsequently, a polyamide membrane is fabricated on top of the MXene/nylon substrate, resulting in the final MXene/nylon/polyamide composite membrane. Reproduced with permission from ref. 338. Copyright 2020, American Chemical Society.

prepared by mixing sodium alginate (SA) solution with a diluted $Ti_3C_2T_x$ colloidal solution and filtered using a PVDF membrane. Subsequently, the SA–$Ti_3C_2T_x$ membrane was immersed in various multivalent Mn^+ cross-linking solutions for 4 hours to obtain a cross-linked membrane having hydrogel pillars in the interlayer spacing (Fig. 20a). The flexible membrane was then dried at room temperature under a vacuum, peeled from the PVDF support, and stored under a vacuum. Pillaring the membrane with Ca-alginate results in the nanochannel with diameters of 7.4 ± 0.2 Å, resulting in a membrane that exhibited exceptional permeation cut-off and outstanding sieving properties for different cations of varying valencies. The membrane exhibited high promise for acid recovery due to its outstanding H^+/Fe^{2+} selectivity, making it useful for traditional ion exchange membranes. Additionally, an ultrathin Mn-alginate pillared membrane with the same *d*-spacing displayed 100% Na_2SO_4 rejection along with high water permeance.

Additionally, MXene–polymer nanocomposites can be utilized to develop a high-performance forward osmosis (FO) membrane by interlayering $Ti_3C_2T_x$ MXene with polyamide.[338] The fabrication process involved a scalable and straightforward

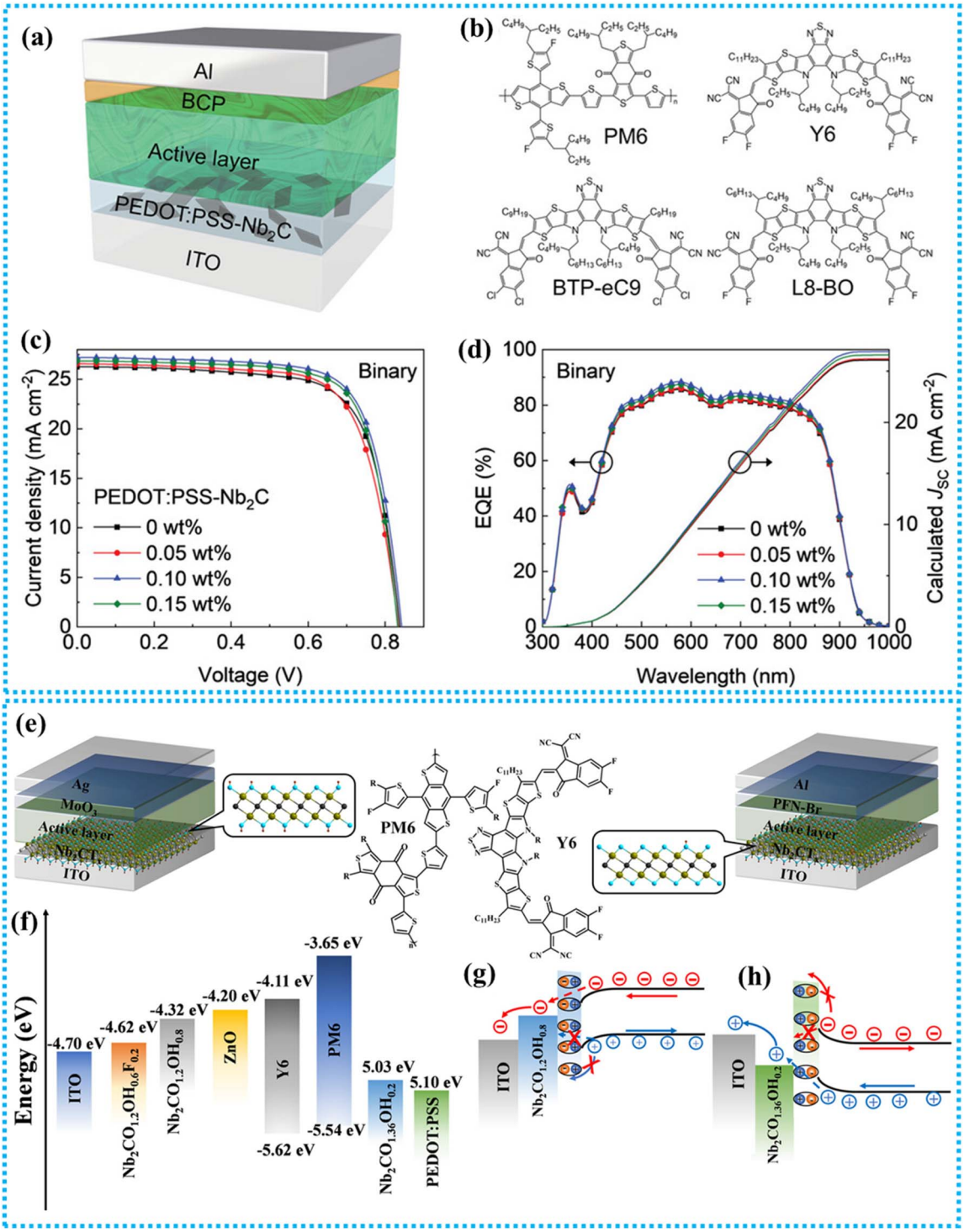

Fig. 21 MXene–polymer-based solar cells. (a) PEDOT:PSS–Nb_2C hybrid HTL device construction. (b) The chemical structure of various NFAs and the polymer donor PM6, L8-BO, Y6, and BTP-eC9. (c) *J*–*V* properties and (d) EQE spectra obtained for the solar cells using the PM6:BTP-eC9 binary active layer with varying Nb_2C MXene doping ratios in PEDOT:PSS. Reproduced with permission from ref. 346. Copyright 2023, Wiley. (e) Diagram of the PSC device architecture showing the chemical structure of PM6, Y6, ETL, HTL, and Nb_2CT_x. (f) Nb_2CT_x is utilized as the ETL and HTL in the schematic energy level diagram of solar cells. (g) Using $Nb_2CO_{1.2}OH_{0.8}$ as the ETL and (h) $Nb_2CO_{1.36}OH_{0.2}$ as the HTL, charge transfer, and extraction in solar cells. Reproduced with permission from ref. 348. Copyright 2021, American Chemical Society.

brush-coating of MXene on nylon substrates, followed by an interfacial polymerization step (Fig. 20b). The resulting FO membrane exhibited high water permeability and low specific salt flux when tested with a sodium chloride draw solution. It also demonstrated exceptional performance in organic solvent forward osmosis, showing a significant flux with low specific salt flux using a lithium chloride draw solution. Additionally, the membrane proved effective for seawater desalination and industrial textile wastewater treatment applications.

All in all, the incorporation of polymers into MXene-based materials for water purification and desalination offers improved adsorption capacity, selectivity, stability, membrane performance, antifouling properties, scalability, and environmental compatibility[342,216,343]. These advantages make MXene–polymer composites promising candidates for addressing water scarcity, ensuring clean water supply, and advancing sustainable water treatment technologies.

7.8 MXene–polymer nanocomposites for solar cell applications

MXene integrated with polymers can be ideal for solar cell applications due to their ability to preserve inherent electronic properties and ensure strong interaction with polymer matrices.[344] This compatibility enhances electrical conductivity, making MXene–polymer composites highly promising for advancing flexible electronics and photovoltaic devices. Nb_2CT_x is a significant member of the MXenes family, which exhibits distinct chemical and physical characteristics as well.[345] Deng *et al.* reported a PEDOT:PSS–Nb_2C hybrid hole transport layer (HTL) to improve the device performance of organic solar cells (OSCs).[346] They employed PEDOT:PSS–Nb_2C hybrids with varying doping MXene ratios (0.05, 0.10, and 0.15 wt%) by directly mixing the Nb_2C colloidal aqueous solution with PEDOT:PSS. A 40 nm-thick HTL layer was produced by spin coating the ITO/glass substrates with PEDOT:PSS aqueous solution or the PEDOT:PSS–Nb_2C hybrid solution for 60 seconds at 3000 rpm, followed by deposition of the active material, electron transport layer (ETL), and electrode, respectively. Fig. 21a and b present the schematic layout of the fabricated device and the chemical structures of various non-fullerene acceptors (NFAs) and the polymer donor PM6. A higher WF was observed in the case of the PEDOT:PSS–Nb_2C hybrid film (5.3 eV), as compared to the PEDOT:PSS film (5.0 eV). It is clear that the increased WF better fits the WF of PM6 (5.5 eV), which decreases leakage current by suppressing charge recombination and facilitating hole extraction.[347] Fig. 21c and d show *J–V* characteristics and external quantum efficiency (EQE) spectra acquired for the OSCs with different Nb_2C MXene ratios in PEDOT:PSS employing the PM6:BTP-eC9 binary active layer.

Through the use of solution-processable Nb_2C MXene and by using different NFAs (PM6:Y6, PM6:BTP-eC9, and PM6:BTP-eC9:L8-BO), surface treatments have improved PCE for OSCs based on binary and ternary systems of active layers. It was proposed that Nb_2C MXene added to PEDOT:PSS HTL may efficiently aid in PEDOT and PSS phase separation, enhancing PEDOT:PSS's conductivity. For OSCs based on the ternary active layer of PM6:BTP-eC9:L8-BO, the doping ratio of Nb_2C MXene in PEDOT:PSS was tuned to reach a maximal PCE of 19.33%, which is currently the highest value among those of single junction OSCs employing 2D materials. The hybrid HTL improves performance by reducing interface recombination, enhancing hole mobility, and boosting charge extraction efficiency.

A similar study by Huang *et al.* reported the use of Nb_2CT_x that investigated the use of additional MXenes in the photovoltaic area by treating Nb_2CT_x with alkali and annealing treatments to modify its WF by controlling the surface functional groups.[348] Following a KOH treatment, –F in pure Nb_2CT_x may be substituted with –OH, lowering the WF from 4.62 ($Nb_2CO_{1.2}OH_{0.6}F_{0.2}$) to 4.32 eV ($Nb_2CO_{1.2}OH_{0.8}$). The WF increased to 5.03 eV ($Nb_2CO_{1.36}OH_{0.2}$) as a result of the removal of some –OH groups and the transformation of others into –O groups upon annealing at 500 °C. Additionally, this is the first time that these Nb_2CT_x groups have been used as the ETL and HTL in PM6:Y6-based polymer solar cells (PSCs), achieving a stellar PCE of 15.22% (ETL) and 15.03% (HTL). These Nb_2CT_x are applied to PSCs based on PM6:Y6 as a buffer layer, where Nb_2CT_x with KOH treatment is used as the ETL, and Nb_2CT_x with annealing treatment is used as the HTL. Fig. 21e shows the schematic of the PSC structures with tuned Nb_2CT_x ($Nb_2CO_{1.2}$-$OH_{0.8}$ and $Nb_2CO_{1.36}OH_{0.2}$) used as the ETL and HTL. Fig. 21f shows the energy level diagram with Nb_2CT_x used as the ETL and HTL. From this, it can be seen that $Nb_2CO_{1.2}OH_{0.8}$ (or $Nb_2CO_{1.36}OH_{0.2}$) exhibits a well-matched energy level compared to $Nb_2CO_{1.2}OH_{0.6}F_{0.2}$ in PSCs, which reduces the electron (or hole) barrier height. Moreover, for $Nb_2CO_{1.2}OH_{0.8}$, the dipolar interlayer induced by –OH will form an electric field pointing from the active layer toward Nb_2CT_x, which will facilitate the transport of electrons but block the transport of holes (Fig. 21g). On the other hand, with $Nb_2CO_{1.36}OH_{0.2}$, the dipolar interlayer created by –O will provide an electric field that points from Nb_2CT_x in the direction of the active layer, facilitating the movement of holes but preventing the motion of electrons (Fig. 21h).

V_2C MXene has also demonstrated great potential for solar cell applications due to its exceptional electrical properties, superior mechanical qualities, and high transmittance.[73] V_2C MXene exhibits excellent hydrophilicity, adjustable work function, strong electrical conductivity, and better transparency. Gu *et al.* improved the properties of organic solar cells by placing a layer of V_2C material between ITO and PEDOT:PSS, significantly improving the performance of PM6:BTP-eC9-based devices.[73] Using a 2D nanosheet material V_2C in combination with PEDOT:PSS, a high-performance V_2C/PEDOT:PSS composited HTL was created, offering superior transmittance and strong electrical conductivity. In addition, the V_2C/PEDOT:PSS composite HTL outperformed the pure PEDOT:PSS interface layer in terms of device performance and photovoltaic properties. In comparison to the 17.41% efficiency of the pure PEDOT:PSS interface device, the V_2C/PEDOT:PSS-based composite interface device exhibited a notable rise to 18.17%. According to the carrier dynamics study, the addition of the V_2C layer increased the number of charge-transfer paths with PEDOT:PSS, which enhanced charge transfer and collection and

even reduced the performance of charge combinations. The findings showed that adding 2D material V_2C, which has excellent conductivity and permeability, offers an efficient way to improve the performance of solar cells.

8. Limitations of MXenes in polymer nanocomposites for various applications

There is no doubt that MXenes when added to polymers can improve the overall properties of the resulting nanocomposites. However, their practical implementation across diverse applications is hindered by inherent limitations such as MXene oxidation susceptibility, brittleness of polymer at higher MXene concentrations, color change due to MXene, and poor dispersion of MXenes in many solvents. These challenges are particularly critical when MXenes are combined with polymers for specific applications, where uniform distribution and long-term stability are essential. The limitations of MXenes in polymer nanocomposites for various applications are as follows:

(1) Energy storage: oxidation degradation in MXenes affects their conductivity and electrochemical characteristics, reducing the overall energy storage performance. Higher MXene concentration may lead to brittleness of the nanocomposite, which can limit mechanical flexibility, impacting stability during cyclic stability studies. Poor dispersion in polymers may also result in non-uniform coatings, lowering the specific capacitance and energy density.

(2) Sensors: oxidation of MXenes can reduce sensitivity and selectivity due to reduced conductivity. MXene concentrations beyond optimized range may impact the mechanical durability of sensors, thereby limiting their sensitivity and flexibility. Poor MXene dispersion in polymers may result in non-uniform sensing layers, affecting the reliability and repeatability of sensors.

(3) 3D/4D printing: the brittleness of MXene–polymer composites restricts their flexibility and printability, posing challenges for fabricating complex structures. MXene oxidation during post-processing can further compromise the mechanical strength and structural stability of these nanocomposites. Poor dispersion of MXenes within polymer matrices impairs resolution and uniformity, which can limit the controlled precision and performance of printed architectures.

(4) EMI shielding: when MXenes are incorporated into polymers, oxidation-induced degradation, mechanical brittleness, and poor dispersion can negatively impact EMI shielding performance. Oxidation at the MXene–polymer interface can reduce conductivity, lowering shielding effectiveness. Despite polymer flexibility, MXenes may still contribute to brittleness, weakening the composite under stress. Poor dispersion of MXenes leads to uneven conductivity, resulting in inhomogeneous shielding layers and reduced EMI performance. Proper dispersion and oxidation control are crucial for maximizing the effectiveness of polymer–MXene composites in EMI shielding applications.

(5) Anti-corrosion applications: in anti-corrosion applications, oxidized MXenes can degrade their protective barriers, reducing efficiency. Poor dispersion of MXenes can cause uneven coatings, leading to defects and corrosion pathways. High concentrations of MXenes can lead to fragility that can result in cracks, compromising the protective performance. Effective dispersion and oxidation control are crucial for maintaining the integrity of MXene-based coatings.

(6) Flexible electronics: in MXene–polymer composites for flexible electronics, the overconcentration of MXenes in polymers may lead to brittleness of MXenes, which limits flexibility, affecting stretchability and durability. Oxidation-induced color changes alter optical properties, restricting their use in transparent or visual devices. Poor dispersion of MXenes within the polymer matrix leads to reduced conductivity and structural inconsistencies, which degrade performance. Effective dispersion and oxidation control are crucial for enhancing the properties of MXene-based polymer composites in flexible electronic applications.

(7) Antimicrobial applications: when MXenes are mixed with polymers for antimicrobial applications, their susceptibility to oxidation degradation may reduce antibacterial efficacy over time. Poor dispersion in the polymer matrix leads to uneven distribution, compromising the uniformity of the antimicrobial effect. Proper dispersion and oxidation control are crucial to maintaining the long-term effectiveness of MXene–polymer-based antimicrobial composites.

(8) Drug delivery and photothermal therapy: when MXenes are added to polymers for drug delivery and photothermal therapy, their oxidation sensitivity reduces photothermal efficiency and chemical stability, affecting target delivery precision. Limited biocompatibility requires surface modifications, which may alter the structural integrity of MXenes. Dispersion challenges of MXenes in the polymer matrix hinder uniform drug loading and controlled release, impacting therapeutic effectiveness. Proper surface modification and dispersion control are essential to optimize the performance of MXene-based drug delivery and photothermal therapy systems.

(9) Water desalination and purification membranes: when MXenes are added to polymers for water desalination and purification membranes, MXene oxidation can impact ion selectivity and permeation performance, limiting their reliability and durability. The higher concentration of MXenes may lead to brittleness of the membranes under operational conditions. Limited solvent compatibility results in poor dispersion within the polymer matrix, reducing uniform pore formation and compromising membrane performance. Effective dispersion, oxidation control, and solvent compatibility are crucial for enhancing the long-term performance of MXene-based water desalination and purification membranes.

(10) Solar cells: MXene oxidation lowers conductivity and stability, affecting solar cell efficiency. High concentrations cause agglomeration, disrupting charge transport, while poor solvent compatibility results in non-uniform films, compromising light absorption and carrier mobility. Enhanced dispersion, oxidation resistance, and solvent compatibility are crucial for improving solar cell performance.

9. Challenges and opportunities in MXene–polymer nanocomposites

9.1 Challenges

Synthesis of MXene–polymer nanocomposites poses several challenges, which can impact the final properties and performance of the materials.

(1) Uniform dispersion of MXenes in the polymer matrix: as MXenes tend to agglomerate due to their high surface energy, it can ultimately lead to poor interfacial interactions and reduced mechanical properties of the nanocomposite.

(2) Stability: dispersion stability is another issue that needs to be addressed. MXene–polymer nanocomposites can be sensitive to environmental factors as MXenes are prone to oxidation, leading to potential degradation or loss of functionality over time.

(3) Interface compatibility: achieving strong interactions and uniform dispersion of MXene nanosheets within polymer matrices is crucial for optimizing the properties of nanocomposites. Surface functionalization for proper interaction is itself a challenging task.

(4) Scalability and reproducibility: large-scale synthesis of MXene–polymer nanocomposites with consistent properties remains challenging, hindering widespread commercial applications. Processing technique selection for uniform MXenes dispersion is necessary for high-quality nanocomposites. High-cost instruments may be required for large-scale mixing.

(5) Mechanical properties: optimizing the ratio of MXenes and polymers is crucial for any property. MXene–polymer nanocomposites may face limitations in achieving high mechanical strength and toughness, especially in certain applications that demand robust materials if optimization is not suitable for that application.

9.2 Opportunities

Once perfect compatibility between MXenes and polymers is achieved, MXene–polymer nanocomposites may offer enhanced mechanical, thermal, electrical, and optical properties in versatile materials, making them compatible with diverse applications.

(1) Multifunctionality: the unique properties of MXene–polymer hybrids open up opportunities for developing new nanocomposites with multiple functionalities, enabling versatile applications.

(2) Biomedical applications: MXene–polymer hybrids, due to their biocompatibility and antibacterial properties, hold promise in drug delivery systems, tissue engineering, and medical implants.

(3) Energy-related applications: MXene–polymer nanocomposites, due to their porous structures, can be employed in energy storage devices to enhance performance and stability.

(4) Environmental applications: MXene-based nanocomposites have potential in environmental remediation, sensing, and water purification membranes owing to their better adsorption and catalytic traits.

(5) New-age technology integration: the combination of cutting-edge technologies, such as nanocomposite fabrication, the Internet of Things (IoT), and artificial intelligence (AI), holds tremendous potential in designing and developing future smart materials with enhanced properties and functionalities.

(6) Hence, MXene–polymer nanocomposites offer exciting prospects for addressing various challenges and capitalizing on their unique properties to explore novel applications in diverse industries. However, further research is needed to overcome existing limitations and fully unlock their potential for practical utilization.

10. Future perspectives

The future of MXene–polymer nanocomposites is exceptionally promising, with vast potential across multiple domains. MXenes offer numerous beneficial properties, but these advantages are contingent on preventing oxidation. By addressing this challenge, the full spectrum of MXene's capabilities can be harnessed by integrating these with polymers, paving the way for groundbreaking applications and advancements in various fields. Ongoing advancements in MXene synthesis, functionalization, and nanocomposite fabrication are likely to yield innovative materials with enhanced properties such as lightweight structures, improved mechanical strength, superior electrical conductivity, and increased thermal stability. These developments could revolutionize industries from aerospace to electronics. Additionally, MXene-based nanocomposites show great promise in sustainable technologies, potentially leading to more efficient and eco-friendly solutions in energy storage, water purification, and environmental remediation. In the biomedical field, the biocompatibility and antibacterial properties of MXene–polymers hold potential for breakthroughs in drug delivery systems, tissue engineering scaffolds, and bioactive coatings for implants. The tunable properties of these nanocomposites also pave the way for the creation of smart materials capable of responding to external stimuli, which could transform applications in sensors, actuators, and adaptive coatings. Moreover, the integration of multiple functionalities within a single MXene–polymer material opens exciting possibilities for multifunctional devices that perform various tasks simultaneously. Combining MXene–polymers with other nanomaterials, such as graphene, metal nanoparticles, or quantum dots, may lead to new synergistic effects and advanced functionalities. Furthermore, the intersection of nanocomposite fabrication technologies with artificial intelligence and the Internet of Things holds great promise for enhancing the design and deployment of advanced smart materials. As research and interdisciplinary collaboration continue, MXene–polymer nanocomposites are set to address global challenges and drive significant innovations across a range of industries.

11. Conclusions

In conclusion, this comprehensive review emphasizes the synthesis methods and diverse applications of MXene–polymer nanocomposites while keeping in mind the serious issue

of MXene oxidation. The various fabrication techniques, such as solution blending, *in situ* polymerization, LBL assembly, and electrospinning, offer opportunities to tailor the properties of these nanocomposites for specific applications. MXenes can be easily hybridized with various polymers such as PVA, PDMS, PPy, PEDOT:PSS, polyaniline, polypropylene, polyurethane, and many biopolymers. MXene–polymer nanocomposites exhibit conductivity, stability, flexibility, biocompatibility, and ion diffusion, leading to enhanced performance and durability in various devices. The incorporation of polymers in MXene-based sensors enhances sensitivity, selectivity, flexibility, and response time, enabling more accurate and efficient detection of target analytes. MXene–polymer composites provide EMI shielding effectiveness, lightweight, and flexible characteristics, making them suitable for applications in the electronics, telecommunications, and aerospace industries. The combination of MXenes with polymers offers flexibility, stretchability, and improved mechanical properties, enabling the development of flexible electronic devices. MXene–polymer composites induce higher porosity in the nanocomposite, which can increase the charge storage capacity. MXene–polymer composites offer enhanced photothermal conversion efficiency, controlled drug delivery, enabling effective cancer treatment, and wound healing. MXene–polymer composites provide enhanced adsorption capacity, selective adsorption, improved stability, membrane performance, antifouling properties, scalability, and environmental compatibility, making them effective materials for water purification and desalination processes. These advantages highlight the potential of MXene–polymer composites in addressing various challenges and advancing technological applications. The unique properties and synergistic effects resulting from the combination of MXenes and polymers create exciting opportunities in various fields, enabling the development of efficient, sustainable, and functional materials and devices. This advancement ensures that MXene oxidation will not hinder the progress toward innovative solutions.

Data availability

No new data were created in this review. All data referenced are from previously published sources and are available in the respective cited articles.

Author contributions

Sunil Kumar – original draft, conceptualization, and data curation; Syed Muhammad Zain Mehdi – original draft, data curation, and editing; Manish Taunk – original draft and editing; Sanjeev Kumar – review and editing; Amit Aherwar – review and editing; Sudhanshu Singh – review and editing; Tej Singh – review and editing.

Conflicts of interest

The authors declare that there is no conflict of interest.

Acknowledgements

During the preparation of this work, the author(s) used ChatGPT to improve the grammar. After using this tool/service, the author(s) reviewed and edited the content as needed and take(s) full responsibility for the content of the publication.

References

1 (*a*) S. Y. Zhao, Y. Y. Zhang, J. Yang and S. Kitipornchai, Folded graphene reinforced nanocomposites with superior strength and toughness: A molecular dynamics study, *J. Mater. Sci. Technol.*, 2022, **120**, 196–204, DOI: 10.1016/j.jmst.2021.12.042; (*b*) Y. Zhang, B. Zhu, X. Cai, X. M. Yuan, S. Y. Zhao, J. W. Yu, K. Qiao and R. M. Qin, Rapid *In Situ* Polymerization of Polyacrylonitrile/Graphene Oxide Nanocomposites as Precursors for High-Strength Carbon Nanofibers, *ACS Appl. Mater. Interfaces*, 2021, **13**(14), 16846–16858, DOI: 10.1021/acsami.1c02643; (*c*) M. L. Yan, W. C. Jiao, G. M. Ding, Z. M. Chu, Y. F. Huang and R. G. Wang, High strength and toughness epoxy nanocomposites reinforced with graphene oxide-nanocellulose micro/nanoscale structures, *Appl. Surf. Sci.*, 2019, **497**, 143802, DOI: 10.1016/j.apsusc.2019.143802; (*d*) O. Jankovsky, M. Lojka, A. M. Lauermannova, F. Antoncik, M. Pavlikova, M. Zaleska, Z. Pavlik, A. Pivak and D. Sedmidubsky, Towards novel building materials: High-strength nanocomposites based on graphene, graphite oxide and magnesium oxychloride, *Appl. Mater. Today*, 2020, **20**, 100766, DOI: 10.1016/j.apmt.2020.100766; (*e*) X. Fan, F. C. Wang, Q. Gao, Y. Zhang, F. Huang, R. L. Xiao, J. B. Qin, H. Zhang, X. T. Shi and G. C. Zhang, Nature inspired hierarchical structures in nano-cellular epoxy/graphene-Fe3O4 nanocomposites with ultra-efficient EMI and robust mechanical strength, *J. Mater. Sci. Technol.*, 2022, **103**, 177–185, DOI: 10.1016/j.jmst.2021.06.030.

2 (*a*) A. Ryu, H. Yim, S. Yoo, J. Park, D. G. Lee, J. Y. Lee, H. C. Song, S. H. Baek, S. Nahm and J. W. Choi, Layer-Controlled Perovskite 2D Nanosheet Interlayer for the Energy Storage Performance of Nanocomposites, *Small*, 2023, DOI: 10.1002/smll.202300526; (*b*) F. H. Likhi, M. Singh, S. V. Chavan, T. M. Cao, M. Shanbedi and A. Karim, Effects of Film Confinement on Dielectric and Electrical Properties of Graphene Oxide and Reduced Graphene Oxide-Based Polymer Nanocomposites: Implications for Energy Storage, *ACS Appl. Nano Mater.*, 2023, **6**(13), 11699–11714, DOI: 10.1021/acsanm.3c01674; (*c*) C. I. Idumah, Phosphorene polymeric nanocomposites for electrochemical energy storage applications, *J. Energy Storage*, 2023, **69**, 107940, DOI: 10.1016/j.est.2023.107940; (*d*) S. Bera, M. Singh, R. Thantirige, S. K. Tiwary, B. T. Shook, E. Nieves, D. Raghavan, A. Karim and N. R. Pradhan, 2D-Nanofiller-Based Polymer Nanocomposites for Capacitive Energy Storage Applications, *Small Sci.*, 2023, **3**(7), DOI: 10.1002/smsc.202300016; (*e*) Prateek, V. K. Thakur and

R. K. Gupta, Recent Progress on Ferroelectric Polymer-Based Nanocomposites for High Energy Density Capacitors: Synthesis, Dielectric Properties, and Future Aspects, *Chem. Rev.*, 2016, **116**(7), 4260–4317, DOI: 10.1021/acs.chemrev.5b00495; (*f*) K. Mishra, N. Devi, S. S. Siwal, Q. B. Zhang, W. F. Alsanie, F. Scarpa and V. K. Thakur, Ionic Liquid-Based Polymer Nanocomposites for Sensors, Energy, Biomedicine, and Environmental Applications: Roadmap to the Future, *Adv. Sci.*, 2022, **9**(26), 2202187, DOI: 10.1002/advs.202202187; (*g*) E. E. Elemike, J. Adeyemi, D. C. Onwudiwe, L. Wei and A. O. Oyedeji, The future of energy materials: A case of MXenes-carbon dots nanocomposites, *J. Energy Storage*, 2022, **50**, 104711, DOI: 10.1016/j.est.2022.104711.

3 (*a*) N. Jouault, F. Dalmas, S. Said, E. Di Cola, R. Schweins, J. Jestin and F. Boue, Direct Measurement of Polymer Chain Conformation in Well-Controlled Model Nanocomposites by Combining SANS and SAXS, *Macromolecules*, 2010, **43**(23), 9881–9891, DOI: 10.1021/ma101682t; (*b*) F. Faupel, V. Zaporojtchenko, T. Strunskus and M. Elbahri, Metal–polymer Nanocomposites for Functional Applications, *Adv. Eng. Mater.*, 2010, **12**(12), 1177–1190, DOI: 10.1002/adem.201000231; (*c*) Y. W. Su, W. H. Lin, Y. J. Hsu and K. H. Wei, Conjugated Polymer/Nanocrystal Nanocomposites for Renewable Energy Applications in Photovoltaics and Photocatalysis, *Small*, 2014, **10**(22), 4427–4442, DOI: 10.1002/smll.201401508; (*d*) Y. Imai, D. Shimamoto and Y. Hotta, Effect of wet jet milling of carbon nanotube on electrical properties of polymer nanocomposites, *Mater. Chem. Phys.*, 2014, **148**(3), 1178–1183, DOI: 10.1016/j.matchemphys.2014.09.044; (*e*) C. A. Grabowski, H. Koerner, J. S. Meth, A. Dang, C. M. Hui, K. Matyjaszewski, M. R. Bockstaller, M. F. Durstock and R. A. Vaia, Performance of Dielectric Nanocomposites: Matrix-Free, Hairy Nanoparticle Assemblies and Amorphous Polymer-Nanoparticle Blends, *ACS Appl. Mater. Interfaces*, 2014, **6**(23), 21500–21509, DOI: 10.1021/am506521r; (*f*) L. Chen, D. H. Du, K. Sun, J. H. Hou and J. Y. Ouyang, Improved Efficiency and Stability of Polymer Solar Cells Utilizing Two-Dimensional Reduced Graphene Oxide: Graphene Oxide Nanocomposites as Hole-Collection Material, *ACS Appl. Mater. Interfaces*, 2014, **6**(24), 22334–22342, DOI: 10.1021/am506326y.

4 (*a*) S. J. Zhang, W. Lin, C. P. Wong, D. G. Bucknall and S. Kumar, Nanocomposites of Carbon Nanotube Fibers Prepared by Polymer Crystallization, *ACS Appl. Mater. Interfaces*, 2010, **2**(6), 1642–1647, DOI: 10.1021/am1001663; (*b*) A. L. Flory, T. Ramanathan and L. C. Brinson, Physical Aging of Single Wall Carbon Nanotube Polymer Nanocomposites: Effect of Functionalization of the Nanotube on the Enthalpy Relaxation, *Macromolecules*, 2010, **43**(9), 4247–4252, DOI: 10.1021/ma901670m; (*c*) H. M. Duong, N. Yamamoto, K. Bui, D. V. Papavassiliou, S. Maruyama and B. L. Wardle, Morphology Effects on Nonisotropic Thermal Conduction of Aligned Single-Walled and Multi-Walled Carbon Nanotubes in Polymer Nanocomposites, *J. Phys. Chem. C*, 2010, **114**(19), 8851–8860, DOI: 10.1021/jp102138c; (*d*) U. Basuli, T. K. Chaki, S. Chattopadhyay and S. Sabharwal, Thermal and Mechanical Properties of Polymer-Nanocomposites Based on Ethylene Methyl Acrylate and Multiwalled Carbon Nanotube, *Polym. Compos.*, 2010, **31**(7), 1168–1178, DOI: 10.1002/pc.20903; (*e*) K. W. Putz, O. C. Compton, M. J. Palmeri, S. T. Nguyen and L. C. Brinson, High-Nanofiller-Content Graphene Oxide–polymer Nanocomposites *via* Vacuum-Assisted Self-Assembly, *Adv. Funct. Mater.*, 2010, **20**(19), 3322–3329, DOI: 10.1002/adfm.201000723; (*f*) G. L. Li, G. Liu, M. Li, D. Wan, K. G. Neoh and E. T. Kang, Organo- and Water-Dispersible Graphene Oxide–polymer Nanosheets for Organic Electronic Memory and Gold Nanocomposites, *J. Phys. Chem. C*, 2010, **114**(29), 12742–12748, DOI: 10.1021/jp102640s; (*g*) H. Kim, A. A. Abdala and C. W. Macosko, Graphene/Polymer Nanocomposites, *Macromolecules*, 2010, **43**(16), 6515–6530, DOI: 10.1021/ma100572e; (*h*) Y. Zare and H. Garmabi, Predictions of Takayanagi model for tensile modulus of polymer/CNT nanocomposites by properties of nanoparticles and filler network, *Colloid Polym. Sci.*, 2017, **295**(6), 1039–1047, DOI: 10.1007/s00396-017-4092-y; (*i*) L. L. Ren, H. Li, Z. L. Xie, D. Ai, Y. Zhou, Y. Liu, S. Y. Zhang, L. J. Yang, X. T. Zhao, Z. R. Peng, *et al.*, High-Temperature High-Energy-Density Dielectric Polymer Nanocomposites Utilizing Inorganic Core-Shell Nanostructured Nanofillers, *Adv. Energy Mater.*, 2021, **11**(28), 2101297, DOI: 10.1002/aenm.202101297; (*j*) Y. Danlee, F. Mederos-Henry, S. Hermans, C. Bailly and I. Huynen, Ranking Broadband Microwave Absorption Performance of Multilayered Polymer Nanocomposites Containing Carbon and Metallic Nanofillers, *Front. Mater.*, 2020, **7**, 214, DOI: 10.3389/fmats.2020.00214.

5 (*a*) Y. Xie, Y. Dall'Agnese, M. Naguib, Y. Gogotsi, M. W. Barsoum, H. L. L. Zhuang and P. R. C. Kent, Prediction and Characterization of MXene Nanosheet Anodes for Non-Lithium-Ion Batteries, *ACS Nano*, 2014, **8**(9), 9606–9615, DOI: 10.1021/nn503921j; (*b*) C. Y. Shi, M. Beidaghi, M. Naguib, O. Mashtalir, Y. Gogotsi and S. J. L. Billinge, Structure of Nanocrystalline Ti3C2 MXene Using Atomic Pair Distribution Function, *Phys. Rev. Lett.*, 2014, **112**(12), 125501, DOI: 10.1103/PhysRevLett.112.125501; (*c*) M. Ghidiu, M. Naguib, C. Shi, O. Mashtalir, L. M. Pan, B. Zhang, J. Yang, Y. Gogotsi, S. J. L. Billinge and M. W. Barsoum, Synthesis and characterization of two-dimensional Nb4C3 (MXene), *Chem. Commun.*, 2014, **50**(67), 9517–9520, DOI: 10.1039/c4cc03366c; (*d*) D. Q. Er, J. W. Li, M. Naguib, Y. Gogotsi and V. B. Shenoy, Ti3C2 MXene as a High Capacity Electrode Material for Metal (Li, Na, K, Ca) Ion Batteries, *ACS Appl. Mater. Interfaces*, 2014, **6**(14), 11173–11179, DOI: 10.1021/am501144q; (*e*) Y. Gogotsi and B. Anasori, The Rise of MXenes, *ACS Nano*, 2019, **13**(8), 8491–8494, DOI: 10.1021/acsnano.9b06394.

6 (*a*) M. Naguib, M. Kurtoglu, V. Presser, J. Lu, J. J. Niu, M. Heon, L. Hultman, Y. Gogotsi and M. W. Barsoum,

Two-Dimensional Nanocrystals Produced by Exfoliation of Ti3AlC2, *Adv. Mater.*, 2011, **23**(37), 4248–4253, DOI: 10.1002/adma.201102306; (*b*) X. Wang, C. Garnero, G. Rochard, D. Magne, S. Morisset, S. Hurand, P. Chartier, J. Rousseau, T. Cabioc'h, C. Coutanceau, *et al.*, A new etching environment (FeF3/HCl) for the synthesis of two-dimensional titanium carbide MXenes: a route towards selective reactivity *vs.* water, *J. Mater. Chem. A*, 2017, **5**(41), 22012–22023, DOI: 10.1039/c7ta01082f; (*c*) C. D. Wang, H. W. Shou, S. M. Chen, S. Q. Wei, Y. X. Lin, P. J. Zhang, Z. F. Liu, K. F. Zhu, X. Guo, X. J. Wu, *et al.*, HCl-Based Hydrothermal Etching Strategy toward Fluoride-Free MXenes, *Adv. Mater.*, 2021, **33**(27), 2101015, DOI: 10.1002/adma.202101015; (*d*) M. S. Mohseni-Salehi, E. Taheri-Nassaj, A. Babaei, A. S. Ghazvini and M. Soleimanzade, Effect of temperature and atmosphere on V2AlC etching for V2CTx MXenes synthesis used as anode for Li-ion storage systems, *J. Energy Storage*, 2023, **66**, 107462, DOI: 10.1016/j.est.2023.107462; (*e*) S. Kumar, D. W. Kang, H. Hong, M. A. Rehman, Y. J. Lee, N. S. Lee and Y. H. Seo, Effect of Ti3C2Tx MXenes etched at elevated temperatures using concentrated acid on binder-free supercapacitors, *RSC Adv.*, 2020, **10**(68), 41837–41845, DOI: 10.1039/d0ra05376g.

7 (*a*) Y. Gogotsi and Q. Huang, MXenes: Two-Dimensional Building Blocks for Future Materials and Devices, *ACS Nano*, 2021, **15**(4), 5775–5780, DOI: 10.1021/acsnano.1c03161; (*b*) D. B. Lioi, G. Neher, J. E. Heckler, T. Back, F. Mehmood, D. Nepal, R. Pachter, R. Vaia and W. J. Kennedy, Electron-Withdrawing Effect of Native Terminal Groups on the Lattice Structure of Ti3C2TX MXenes Studied by Resonance Raman Scattering: Implications for Embedding MXenes in Electronic Composites, *ACS Appl. Nano Mater.*, 2019, **2**(10), 6087–6091, DOI: 10.1021/acsanm.9b01194; (*c*) S. Athavale, S. A. Micci-Barreca, K. Arole, V. Kotasthane, J. L. Lutkenhaus, M. Radovic and M. J. Green, Effect of terminal groups on the degradation stability of Ti3C2Tz MXenes, *Nanoscale*, 2023, 12567–12573, DOI: 10.1039/d3nr02386a.

8 A. S. Zeraati, S. A. Mirkhani, P. C. Sun, M. Naguib, P. V. Braun and U. Sundararaj, Improved synthesis of Ti3C2Tx MXenes resulting in exceptional electrical conductivity, high synthesis yield, and enhanced capacitance, *Nanoscale*, 2021, **13**(6), 3572–3580, DOI: 10.1039/d0nr06671k.

9 A. Lipatov, A. Goad, M. J. Loes, N. S. Vorobeva, J. Abourahma, Y. Gogotsi and A. Sinitskii, High electrical conductivity and breakdown current density of individual monolayer Ti3C2Tx MXene flakes, *Matter*, 2021, **4**(4), 1413–1427, DOI: 10.1016/j.matt.2021.01.021.

10 (*a*) B. P. Zhang, P. W. Wong, J. X. Guo, Y. S. Zhou, Y. Wang, J. W. Sun, M. N. Jiang, Z. K. Wang and A. K. An, Transforming Ti3C2Tx MXene's intrinsic hydrophilicity into superhydrophobicity for efficient photothermal membrane desalination, *Nat. Commun.*, 2022, **13**(1), 3315, DOI: 10.1038/s41467-022-31028-6; (*b*) Y. X. Guan, M. M. Zhang, J. Qin, X. X. Ma, C. Li and J. L. Tang, Hydrophilicity-Dependent Distinct Frictional Behaviors of Different Modified MXene Nanosheets, *J. Phys. Chem. C*, 2020, **124**(25), 13664–13671, DOI: 10.1021/acs.jpcc.0c01551.

11 X. L. Li, Z. D. Huang, C. E. Shuck, G. J. Liang, Y. Gogotsi and C. Y. Zhi, MXene chemistry, electrochemistry and energy storage applications, *Nat. Rev. Chem*, 2022, **6**(6), 389–404, DOI: 10.1038/s41570-022-00384-8.

12 K. Maleski, C. E. Ren, M. Q. Zhao, B. Anasori and Y. Gogotsi, Size-Dependent Physical and Electrochemical Properties of Two-Dimensional MXene Flakes, *ACS Appl. Mater. Interfaces*, 2018, **10**(29), 24491–24498, DOI: 10.1021/acsami.8b04662.

13 Y. J. Zhang, W. Y. Xia, Y. B. Wu and P. H. Zhang, Prediction of MXene based 2D tunable band gap semiconductors: GW quasiparticle calculations, *Nanoscale*, 2019, **11**(9), 3993–4000, DOI: 10.1039/c9nr01160a.

14 C. Q. Hu, Z. J. Du, Z. M. Wei, L. Li and G. Z. Shen, Functionalized Ti3C2Tx MXene with layer-dependent band gap for flexible NIR photodetectors, *Appl. Phys. Rev.*, 2023, **10**(2), 021402, DOI: 10.1063/5.0140861.

15 (*a*) X. D. Liu, Y. Liu, S. L. Dong, X. F. Zhang and S. D. Hou, Synthesis of ultra-high specific surface area aerogels with nitrogen-enriched Ti3C2Tx nanosheets as high-performance supercapacitor electrodes, *J. Mater. Chem. C*, 2022, **10**(40), 14929–14938, DOI: 10.1039/d2tc01987f; (*b*) C. E. Ren, M. Q. Zhao, T. Makaryan, J. Halim, M. Boota, S. Kota, B. Anasori, M. W. Barsoum and Y. Gogotsi, Porous Two-Dimensional Transition Metal Carbide (MXene) Flakes for High-Performance Li-Ion Storage, *Chemelectrochem*, 2016, **3**(5), 689–693, DOI: 10.1002/celc.201600059.

16 Z. Ling, C. E. Ren, M. Q. Zhao, J. Yang, J. M. Giammarco, J. S. Qiu, M. W. Barsoum and Y. Gogotsi, Flexible and conductive MXene films and nanocomposites with high capacitance, *Proc. Natl. Acad. Sci.*, 2014, **111**(47), 16676–16681, DOI: 10.1073/pnas.1414215111.

17 W. Y. Zhang, H. X. Jin and J. X. Zhang, Nb2CTx MXene as High-Performance Energy Storage Material with Na, K, and Liquid K-Na Alloy Anodes, *Langmuir*, 2021, **37**(3), 1102–1109, DOI: 10.1021/acs.langmuir.0c02957.

18 Y. Dall'Agnese, P. L. Taberna, Y. Gogotsi and P. Simon, Two-Dimensional Vanadium Carbide (MXene) as Positive Electrode for Sodium-Ion Capacitors, *J. Phys. Chem. Lett.*, 2015, **6**(12), 2305–2309, DOI: 10.1021/acs.jpclett.5b00868.

19 (*a*) D. Liu, R. W. Wang, W. Chang, L. Zhang, B. Q. Peng, H. D. Li, S. Q. Liu, M. Yan and C. S. Guo, Ti3C2 MXene as an excellent anode material for high-performance microbial fuel cells, *J. Mater. Chem. A*, 2018, **6**(42), 20887–20895, DOI: 10.1039/c8ta07305h; (*b*) M. M. Fei, R. Z. Lin, Y. M. Deng, H. X. Xian, R. J. Bian, X. L. Zhang, J. G. Cheng, C. X. Xu and D. Y. Cai, Polybenzimidazole/Mxene composite membranes for intermediate temperature polymer electrolyte membrane fuel cells, *Nanotechnology*, 2018, **29**(3), 035403, DOI: 10.1088/1361-6528/aa9ab0.

20 (*a*) P. D. Kolubah, H. O. Mohamed, M. Ayach, A. R. Hari, H. N. Alshareef, P. Saikaly, K. J. Chae and P. Castano, W2N-MXene composite anode catalyst for efficient microbial fuel cells using domestic wastewater, *Chem. Eng. J.*, 2023, **461**, 141821, DOI: 10.1016/j.cej.2023.141821; (*b*) D. M. Jiang, C. Y. Zhu, Y. He, C. C. Xing, K. Xie, Y. Xu and Y. Q. Wang, Polyaniline-MXene-coated carbon cloth as an anode for microbial fuel cells, *J. Solid State Electrochem.*, 2022, **26**(11), 2435–2443, DOI: 10.1007/s10008-022-05255-2; (*c*) J. F. Chen, Y. W. Zhang, Y. Q. Wu, J. Y. Wang, Y. Y. Zhao, M. K. Wang, J. Q. Yang, J. Y. Liu, R. J. Wang, Y. W. Yang, *et al.*, Enhanced bioelectrochemical performance by NiCoAl-LDH/MXene hybrid as cathode catalyst for microbial fuel cell, *Int. J. Hydrogen Energy*, 2023, **48**(15), 6056–6066, DOI: 10.1016/j.ijhydene.2022.11.173.

21 (*a*) J. X. Chen, Z. L. Li, F. L. Ni, W. X. Ouyang and X. S. Fang, Bio-inspired transparent MXene electrodes for flexible UV photodetectors, *Mater. Horiz.*, 2020, **7**(7), 1828–1833, DOI: 10.1039/d0mh00394h; (*b*) H. Xu, A. B. Ren, J. Wu and Z. M. Wang, Recent Advances in 2D MXenes for Photodetection, *Adv. Funct. Mater.*, 2020, **30**(24), 2000907, DOI: 10.1002/adfm.202000907.

22 (*a*) L. J. Yao, X. Tian, X. X. Cui, R. J. Zhao, X. C. Xiao and Y. D. Wang, Partially oxidized Ti3C2Tx MXene-sensitive material-based ammonia gas sensor with high-sensing performances for room temperature application, *J. Mater. Sci.:Mater. Electron.*, 2021, **32**(23), 27837–27848, DOI: 10.1007/s10854-021-07166-w; (*b*) Y. Y. Pei, X. L. Zhang, Z. Y. Hui, J. Y. Zhou, X. Huang, G. Z. Sun and W. Huang, Ti3C2TX MXene for Sensing Applications: Recent Progress, Design Principles, and Future Perspectives, *ACS Nano*, 2021, **15**(3), 3996–4017, DOI: 10.1021/acsnano.1c00248; (*c*) L. Lorencova, T. Bertok, J. Filip, M. Jerigova, D. Velic, P. Kasak, K. A. Mahmoud and J. Tkac, Highly stable Ti3C2Tx (MXene)/Pt nanoparticles-modified glassy carbon electrode for H2O2 and small molecules sensing applications, *Sensor. Actuator. B Chem.*, 2018, **263**, 360–368, DOI: 10.1016/j.snb.2018.02.124.

23 (*a*) C. F. Zhang, L. McKeon, M. P. Kremer, S. H. Park, O. Ronan, A. Seral-Ascaso, S. Barwich, C. O. Coileain, N. McEvoy, H. C. Nerl, *et al.*, Additive-free MXene inks and direct printing of micro-supercapacitors, *Nat. Commun.*, 2019, **10**, 1795, DOI: 10.1038/s41467-019-09398-1; (*b*) T. Z. Guo, D. Zhou, S. G. Deng, M. Jafarpour, J. Avaro, A. Neels, J. Heier and C. F. Zhang, Rational Design of Ti3C2Tx MXene Inks for Conductive, Transparent Films, *ACS Nano*, 2023, **17**(4), 3737–3749, DOI: 10.1021/acsnano.2c11180; (*c*) Y. Z. Shao, L. S. Wei, X. Y. Wu, C. M. Jiang, Y. Yao, B. Peng, H. Chen, J. T. Huangfu, Y. B. Ying, C. A. F. O. Zhang, *et al.*, Room-temperature high-precision printing of flexible wireless electronics based on MXene inks, *Nat. Commun.*, 2022, **13**(1), 3223, DOI: 10.1038/s41467-022-30648-2.

24 M. Aakyiir, B. Tanner, P. L. Yap, H. Rastin, T. T. Tung, D. Losic, Q. S. Meng and J. Ma, 3D printing interface-modified PDMS/MXene nanocomposites for stretchable conductors, *J. Mater. Sci. Technol.*, 2022, **117**, 174–182, DOI: 10.1016/j.jmst.2021.11.048.

25 (*a*) J. Orangi, F. Hamade, V. A. Davis and M. Beidaghi, 3D Printing of Additive-Free 2D Ti3C2Tx (MXene) Ink for Fabrication of Micro-Supercapacitors with Ultra-High Energy Densities, *ACS Nano*, 2020, **14**(1), 640–650, DOI: 10.1021/acsnano.9b07325; (*b*) S. P. Zhang, S. S. Rana, T. Bhatta, G. B. Pradhan, S. Sharma, H. Y. S. Song, S. Jeong and J. Y. Park, 3D printed smart glove with pyramidal MXene/Ecoflex composite-based toroidal triboelectric nanogenerators for wearable human-machine interaction applications, *Nano Energy*, 2023, **106**, 108110, DOI: 10.1016/j.nanoen.2022.108110; (*c*) M. M. Yuan, L. B. Wang, X. Q. Liu, X. Y. Du, G. B. Zhang, Y. K. Chang, Q. X. Xia, Q. K. Hu and A. G. Zhou, 3D printing quasi-solid-state micro-supercapacitors with ultrahigh areal energy density based on high concentration MXene sediment, *Chem. Eng. J.*, 2023, **451**, 138686, DOI: 10.1016/j.cej.2022.138686.

26 L. Li, J. Meng, X. R. Bao, Y. P. Huang, X. P. Yan, H. L. Qian, C. Zhang and T. X. Liu, Direct-Ink-Write 3D Printing of Programmable Micro-Supercapacitors from MXene-Regulating Conducting Polymer Inks, *Adv. Energy Mater.*, 2023, **13**(9), 2203683, DOI: 10.1002/aenm.202203683.

27 (*a*) V. T. Nguyen, B. K. Min, S. K. Kim, Y. Yi and C. G. Choi, A flexible and high-performance electrochromic smart window produced by WO3/Ti3C2Tx MXene hybrids, *J. Mater. Chem. C*, 2021, **9**(9), 3183–3192, DOI: 10.1039/d0tc05547f; (*b*) Y. Y. Li, Y. Q. Wang, J. Lu, W. W. Wang and D. Wang, Synergistically photothermal Au Nanoprisms@MXene enable adaptive solar modulation of HA-PNIPAM hydrogels for smart window br, *Chem. Eng. J.*, 2023, **457**, 141299, DOI: 10.1016/j.cej.2023.141299; (*c*) Y. Y. Li, Y. Q. Wang, J. Lu, W. W. Wang and D. Wang, Synergistically photothermal Au Nanoprisms@MXene enable adaptive solar modulation of HA-PNIPAM hydrogels for smart window, *Chem. Eng. J.*, 2023, **462**, 142119, DOI: 10.1016/j.cej.2023.142119; (*d*) S. Kumar, H. M. Park, V. H. Nguyen, M. Kim, N. Nasir, M. Kumar and Y. Seo, Application dependent stability of Ti3C2Tx MXene in PDLC-based smart-windows, *Ceram. Int.*, 2022, **48**(23), 35092–35099, DOI: 10.1016/j.ceramint.2022.08.099; (*e*) S. Kumar, D. Kang, V. Nguyen, N. Nasir, H. Hong, M. Kim, D. C. Nguyen, Y. J. Lee, N. Lee and Y. Seo, Application of Titanium-Carbide MXene-Based Transparent Conducting Electrodes in Flexible Smart Windows, *ACS Appl. Mater. Interfaces*, 2021, **13**(34), 40976–40985, DOI: 10.1021/acsami.1c12100.

28 (*a*) Y. Dai, X. Y. Wu, L. L. Li, Y. Zhang, Z. M. Deng, Z. Z. Yu and H. B. Zhang, 3D printing of resilient, lightweight and conductive MXene/reduced graphene oxide architectures for broadband electromagnetic interference shielding, *J. Mater. Chem. A*, 2022, **10**(21), 11375–11385, DOI: 10.1039/d2ta01388f; (*b*) M. K. Han, C. E. Shuck, R. Rakhmanov, D. Parchment, B. Anasori, C. M. Koo, G. Friedman and Y. Gogotsi, Beyond Ti3C2Tx: MXenes for Electromagnetic

Interference Shielding, *ACS Nano*, 2020, **14**(4), 5008–5016, DOI: 10.1021/acsnano.0c01312.

29 F. Shahzad, M. Alhabeb, C. B. Hatter, B. Anasori, S. M. Hong, C. M. Koo and Y. Gogotsi, Electromagnetic interference shielding with 2D transition metal carbides (MXenes), *Science*, 2016, **353**(6304), 1137–1140, DOI: 10.1126/science.aag2421.

30 (*a*) S. Lai, J. Jeon, S. K. Jang, J. Xu, Y. J. Choi, J. H. Park, E. Hwang and S. Lee, Surface group modification and carrier transport properties of layered transition metal carbides (Ti2CTx, T: -OH, -F and -O) (vol 7, pg 19390, 2015), *Nanoscale*, 2016, **8**(2), 1216, DOI: 10.1039/c5nr90214b; (*b*) R. B. Rakhi, B. Ahmed, M. N. Hedhili, D. H. Anjum and H. N. Alshareef, Effect of Postetch Annealing Gas Composition on the Structural and Electrochemical Properties of Ti2CTx MXene Electrodes for Supercapacitor Applications, *Chem. Mater.*, 2015, **27**(15), 5314–5323, DOI: 10.1021/acs.chemmater.5b01623.

31 J. X. Zhao, H. Y. Lu, X. J. Wei, Y. Y. Gao, Y. Z. Song and B. A. Xu, Direct writing additive-free V2CTx MXene architectures enables Zn-ion hybrid capacitor with ultrahigh energy density, *J. Energy Storage*, 2023, **66**, 107481, DOI: 10.1016/j.est.2023.107481.

32 S. P. Selvam and S. B. Cho, Silver chalcogenide loaded V2CTx MXene-molecularly imprinted polymer-based novel ratiometric sensor for the early predictive cancer marker: L-Fucose, *Chem. Eng. J.*, 2023, **469**, 144016, DOI: 10.1016/j.cej.2023.144016.

33 (*a*) J. Halim, K. M. Cook, M. Naguib, P. Eklund, Y. Gogotsi, J. Rosen and M. W. Barsoum, X-ray photoelectron spectroscopy of select multi-layered transition metal carbides (MXenes), *Appl. Surf. Sci.*, 2016, **362**, 406–417, DOI: 10.1016/j.apsusc.2015.11.089; (*b*) Y. F. Yan, H. Han, Y. J. Dai, H. Zhu, W. H. Liu, X. Tang, W. Gan and H. Li, Nb2CTx MXene Nanosheets for Dye Adsorption, *ACS Appl. Nano Mater.*, 2021, **4**(11), 11763–11769, DOI: 10.1021/acsanm.1c02339.

34 (*a*) Y. K. Zhang, G. F. Zhang, S. Zhao, A. L. Gao, J. Cui and Y. H. Yan, Three-Dimensional MXene-Based Functional Materials for Water Treatment: Preparation, Functional Tailoring, and Applications, *Ind. Eng. Chem. Res.*, 2023, **62**(19), 7297–7335, DOI: 10.1021/acs.iecr.3c00306; (*b*) M. Li, X. G. Dai, M. N. Wang and H. Bai, Bioinspired Macroporous Materials of MXene Nanosheets: Ice-Templated Assembly and Multifunctional Applications, *Small Methods*, 2023, 2300213, DOI: 10.1002/smtd.202300213; (*c*) H. Korkmaz, U. C. Hasar and O. M. Ramahi, Thin-film MXene-based metamaterial absorber design for solar cell applications, *Opt. Quant. Electron.*, 2023, **55**(6), 530, DOI: 10.1007/s11082-023-04810-z; (*d*) A. C. Khot, T. D. Dongale, K. A. Nirmal, J. K. Deepthi, S. S. Sutar and T. G. Kim, 2D Ti3C2Tx MXene-derived self-assembled 3D TiO2nanoflowers for nonvolatile memory and synaptic learning applications, *J. Mater. Sci. Technol.*, 2023, **150**, 1–10, DOI: 10.1016/j.jmst.2023.01.003.

35 A. Szuplewska, D. Kulpińska, A. Dybko, A. M. Jastrzębska, T. Wojciechowski, A. Rozmysłowska, M. Chudy, I. Grabowska-Jadach, W. Ziemkowska, Z. Brzózka, *et al.*, 2D Ti2C (MXene) as a novel highly efficient and selective agent for photothermal therapy, *Mater. Sci. Eng. C*, 2019, **98**, 874–886, DOI: 10.1016/j.msec.2019.01.021.

36 M. Tian, W. Gan and E.-S. Oh, MXene Clay (Ti2C)-Containing *In Situ* Polymerized Hollow Core–Shell Binder for Silicon-Based Anodes in Lithium-Ion Batteries, *ACS Omega*, 2023, **8**(51), 49302–49310, DOI: 10.1021/acsomega.3c07752.

37 Y. Wu, J. Li, G. Sui, D.-F. Chai, Y. Li, D. Guo, D. Chu and K. Liang, Interface and doping engineering of V2C-MXene-based electrocatalysts for enhanced electrocatalysis of overall water splitting, *Carbon Energy*, 2024, **6**(10), e583, DOI: 10.1002/cey2.583.

38 M. Jenitha, D. Durgalakshmi, S. Balakumar and R. A. Rakkesh, Vanadium-based MXenes: synthesis, structural insights, and electrochemical properties for Zn-ion battery applications: a beginner's guide, *Emerg. Mater.*, 2024, DOI: 10.1007/s42247-024-00916-6.

39 D. Ponnalagar, D.-R. Hang, S. E. Islam, C.-T. Liang and M. M. C. Chou, Recent progress in two-dimensional Nb2C MXene for applications in energy storage and conversion, *Mater. Des.*, 2023, **231**, 112046, DOI: 10.1016/j.matdes.2023.112046.

40 J. Palisaitis, I. Persson, J. Halim, J. Rosen and P. O. Å. Persson, On the Structural Stability of MXene and the Role of Transition Metal Adatoms, *Nanoscale*, 2018, **10**(23), 10850–10855, DOI: 10.1039/C8NR01986J.

41 L. Yang, J. Du, J. Deng, N. H. M. Sulaiman, X. Feng, C. Liu and X. Zhou, Defective Nb2C MXene Cocatalyst on TiO2 Microsphere for Enhanced Photocatalytic CO2 Conversion to Methane, *Small*, 2024, **20**(19), 2307007, DOI: 10.1002/smll.202307007.

42 (*a*) Y.-W. Cheng, J.-H. Dai, Y.-M. Zhang and Y. Song, Two-Dimensional, Ordered, Double Transition Metal Carbides (MXenes): A New Family of Promising Catalysts for the Hydrogen Evolution Reaction, *J. Phys. Chem. C*, 2018, **122**(49), 28113–28122, DOI: 10.1021/acs.jpcc.8b08914; (*b*) M. He, Y. Zhou, Q. Luo and J. Yang, Platinum monolayer dispersed on MXenes for electrocatalyzed hydrogen evolution: a first-principles study, *Nanoscale*, 2024, **16**(33), 15670–15676, DOI: 10.1039/D4NR01864H.

43 Y. Gao, Y. Cao, H. Zhuo, X. Sun, Y. Gu, G. Zhuang, S. Deng, X. Zhong, Z. Wei, X. Li, *et al.*, Mo2TiC2 MXene: A Promising Catalyst for Electrocatalytic Ammonia Synthesis, *Catal. Today*, 2020, **339**, 120–126, DOI: 10.1016/j.cattod.2018.12.029.

44 S. Hua, B. Huang, Z. Le and Q. Huang, Mo-based Mo2Ti2C3 MXene as photothermal nanoagents to eradicating methicillin-resistant Staphylococcus aureus with photothermal therapy, *Mater. Des.*, 2023, **231**, 112033, DOI: 10.1016/j.matdes.2023.112033.

45 M. Saraf, B. Chacon, S. Ippolito, R. W. Lord, M. Anayee, R. Wang, A. Inman, C. E. Shuck and Y. Gogotsi, Enhancing Charge Storage of Mo2Ti2C3 MXene by Partial

Oxidation, *Adv. Funct. Mater.*, 2024, **34**(1), 2306815, DOI: 10.1002/adfm.202306815.

46 (*a*) J. Yoon, S. Kim, K. H. Park, S. Lee, S. J. Kim, H. Lee, T. Oh and C. M. Koo, Biocompatible and Oxidation-Resistant Ti3C2Tx MXene with Halogen-Free Surface Terminations, *Small Methods*, 2023, 2201579, DOI: 10.1002/smtd.202201579; (*b*) Q. Fan, M. J. Yi, C. X. Chai, W. W. Li, P. Qi, J. H. Wang and J. C. Hao, Oxidation stability enhanced MXene-based porous materials derived from water-in-ionic liquid Pickering emulsions for wearable piezoresistive sensor and oil/water separation applications, *J. Colloid Interface Sci.*, 2022, **618**, 311–321, DOI: 10.1016/j.jcis.2022.03.073; (*c*) T. Habib, X. F. Zhao, S. A. Shah, Y. X. Chen, W. M. Sun, H. An, J. L. Lutkenhaus, M. Radovic and M. J. Green, Oxidation stability of Ti3C2Tx MXene nanosheets in solvents and composite films, *npj 2D Mater. Appl.*, 2019, **3**, 8, DOI: 10.1038/s41699-019-0089-3.

47 C. F. J. Zhang, S. Pinilla, N. McEyoy, C. P. Cullen, B. Anasori, E. Long, S. H. Park, A. Seral-Ascaso, A. Shmeliov, D. Krishnan, *et al.*, Oxidation Stability of Colloidal Two-Dimensional Titanium Carbides (MXenes), *Chem. Mater.*, 2017, **29**(11), 4848–4856, DOI: 10.1021/acs.chemmater.7b00745.

48 J. Kim, Y. Yoon, S. K. Kim, S. Park, W. Song, S. Myung, H. K. Jung, S. S. Lee, D. H. Yoon and K. S. An, Chemically Stabilized and Functionalized 2D-MXene with Deep Eutectic Solvents as Versatile Dispersion Medium, *Adv. Funct. Mater.*, 2021, **31**(13), 2008722, DOI: 10.1002/adfm.202008722.

49 X. F. Zhao, H. X. Cao, B. J. Coleman, Z. Y. Tan, I. J. Echols, E. B. Pentzer, J. L. Lutkenhaus, M. Radovic and M. J. Green, The Role of Antioxidant Structure in Mitigating Oxidation in Ti3C2Tx and Ti2CTx MXenes, *Adv. Mater. Interfaces*, 2022, **9**(20), 2200480, DOI: 10.1002/admi.202200480.

50 S. Lee, E. H. Kim, S. Yu, H. Kim, C. Park, S. W. Lee, H. Han, W. Jin, K. Lee, C. E. Lee, *et al.*, Polymer-Laminated Ti3C2Tx MXene Electrodes for Transparent and Flexible Field-Driven Electronics, *ACS Nano*, 2021, **15**(5), 8940–8952, DOI: 10.1021/acsnano.1c01621.

51 (*a*) A. A. Shamsabadi, A. P. Isfahani, S. K. Salestan, A. Rahimpour, B. Ghalei, E. Sivaniah and M. Soroush, Pushing Rubbery Polymer Membranes To Be Economic for CO2 Separation: Embedment with Ti3C2Tx MXene Nanosheets, *ACS Appl. Mater. Interfaces*, 2020, **12**(3), 3984–3992, DOI: 10.1021/acsami.9b19960; (*b*) I. Amin, H. van den Brekel, K. Nemani, E. Batyrev, A. de Vooys, H. van der Weijde, B. Anasori and N. R. Shiju, Ti3C2Tx MXene Polymer Composites for Anticorrosion: An Overview and Perspective, *ACS Appl. Mater. Interfaces*, 2022, 43749–43758, DOI: 10.1021/acsami.2c11953.

52 V. Natu, J. L. Hart, M. Sokol, H. Chiang, M. L. Taheri and M. W. Barsoum, Edge Capping of 2D-MXene Sheets with Polyanionic Salts To Mitigate Oxidation in Aqueous Colloidal Suspensions, *Angew. Chem. Int. Ed.*, 2019, **58**(36), 12655–12660, DOI: 10.1002/anie.201906138.

53 C. W. Wu, B. Unnikrishnan, I. W. P. Chen, S. G. Harroun, H. T. Chang and C. C. Huang, Excellent oxidation resistive MXene aqueous ink for micro-supercapacitor application, *Energy Storage Mater.*, 2020, **25**, 563–571, DOI: 10.1016/j.ensm.2019.09.026.

54 Y. Q. Shi, C. Liu, Z. P. Duan, B. Yu, M. H. Liu and P. A. Song, Interface engineering of MXene towards super-tough and strong polymer nanocomposites with high ductility and excellent fire safety, *Chem. Eng. J.*, 2020, **399**, 125829, DOI: 10.1016/j.cej.2020.125829.

55 (*a*) M. F. Liu, Y. L. Zhuo, A. Sarycheva, Y. Gogotsi, M. A. Bissett, R. J. Young and I. A. Kinloch, Deformation of and Interfacial Stress Transfer in Ti3C2 MXene–polymer Composites, *ACS Appl. Mater. Interfaces*, 2022, **14**(8), 10681–10690, DOI: 10.1021/acsami.1c21611; (*b*) S. J. Wan, X. Li, Y. L. Wang, Y. Chen, X. Xie, R. Yang, A. P. Tomsia, L. Jiang and Q. F. Cheng, Strong sequentially bridged MXene sheets, *Proc. Natl. Acad. Sci.*, 2020, **117**(44), 27154–27161, DOI: 10.1073/pnas.2009432117.

56 R. A. Soomro, P. Zhang, B. M. Fan, Y. Wei and B. Xu, Progression in the Oxidation Stability of MXenes, *Nano–Micro Lett.*, 2023, **15**(1), 108, DOI: 10.1007/s40820-023-01069-7.

57 M. Mozafari and M. Soroush, Surface functionalization of MXenes, *Mater. Adv.*, 2021, **2**(22), 7277–7307, DOI: 10.1039/D1MA00625H.

58 Z. H. Fu, N. Wang, D. Legut, C. Si, Q. F. Zhang, S. Y. Du, T. C. Germann, J. S. Francisco and R. F. Zhang, Rational Design of Flexible Two-Dimensional MXenes with Multiple Functionalities, *Chem. Rev.*, 2019, **119**(23), 11980–12031, DOI: 10.1021/acs.chemrev.9b00348.

59 X. S. Zhang, X. F. Wang, Z. W. Lei, L. L. Wang, M. W. Tian, S. F. Zhu, H. Xiao, X. N. Tang and L. J. Qu, Flexible MXene-Decorated Fabric with Interwoven Conductive Networks for Integrated Joule Heating, Electromagnetic Interference Shielding, and Strain Sensing Performances, *ACS Appl. Mater. Interfaces*, 2020, **12**(12), 14459–14467, DOI: 10.1021/acsami.0c01182.

60 L. Li, X. Y. Fu, S. Chen, S. Uzun, A. S. Levitt, C. E. Shuck, W. Han and Y. Gogotsi, Hydrophobic and Stable MXene–polymer Pressure Sensors for Wearable Electronics, *ACS Appl. Mater. Interfaces*, 2020, **12**(13), 15362–15369, DOI: 10.1021/acsami.0c00255.

61 K. Chen, Y. P. Hu, F. Wang, M. X. Liu, P. Liu, C. Li, Y. S. Yu, X. F. Xiao and Q. Feng, Ultra-stretchable, adhesive, and self-healing MXene/polyampholytes hydrogel as flexible and wearable epidermal sensors, *Colloids Surf., A*, 2022, **645**, 128897, DOI: 10.1016/j.colsurfa.2022.128897.

62 Y. L. Cui, J. Zhu, H. Tong and R. Zou, Advanced perspectives on MXene composite nanomaterials: Types synthetic methods, thermal energy utilization and 3D-printed techniques, *Iscience*, 2023, **26**(1), 105824, DOI: 10.1016/j.isci.2022.105824.

63 T. Li, T. H. Chen, X. C. Shen, H. H. Shi, E. Jabari and H. E. Naguib, A binder jet 3D printed MXene composite for strain sensing and energy storage application,

Nanoscale Adv., 2022, **4**(3), 916–925, DOI: 10.1039/d1na00698c.

64 H. D. Liu, C. F. Du, L. L. Liao, H. J. Zhang, H. Q. Zhou, W. C. Zhou, T. N. Ren, Z. C. Sun, Y. F. Lu, Z. T. Nie, *et al.*, Approaching intrinsic dynamics of MXenes hybrid hydrogel for 3D printed multimodal intelligent devices with ultrahigh superelasticity and temperature sensitivity, *Nat. Commun.*, 2022, **13**(1), 3420, DOI: 10.1038/s41467-022-31051-7.

65 (*a*) G. J. Adekoya, O. C. Adekoya, R. E. Sadiku, Y. Hamam and S. S. Ray, Applications of MXene-Containing Polypyrrole Nanocomposites in Electrochemical Energy Storage and Conversion, *ACS Omega*, 2022, 39498–39519, DOI: 10.1021/acsomega.2c02706; (*b*) S.-M. Liu, M.-X. Chen, Y. Xie, D.-H. Liu, J.-F. Zheng, X. Xiong, H. Jiang, L.-C. Wang, H. Luo and K. Han, Nb2CTx MXene boosting PEO polymer electrolyte for all-solid-state Li-S batteries: two birds with one stone strategy to enhance Li+ conductivity and polysulfide adsorptivity, *Rare Met.*, 2023, **42**(8), 2562–2576, DOI: 10.1007/s12598-022-02260-2.

66 H. Yan, W. Li, H. Li, X. Q. Fan and M. H. Zhu, Ti3C2 MXene nanosheets toward high-performance corrosion inhibitor for epoxy coating, *Prog. Org. Coat.*, 2019, **135**, 156–167, DOI: 10.1016/j.porgcoat.2019.06.013.

67 X. He, J. Wu, X. Huang, Y. Chen, L. Zhang and X. Sheng, Three-in-one polymer nanocomposite coating *via* constructing tannic acid functionalized MXene/BP hybrids with superior corrosion resistance, friction resistance, and flame-retardancy, *Chem. Eng. Sci.*, 2024, **283**, 119429, DOI: 10.1016/j.ces.2023.119429.

68 L. Li, X. Y. Liu, J. F. Wang, Y. Y. Yang, Y. X. Cao and W. J. Wang, New application of MXene in polymer composites toward remarkable anti-dripping performance for flame retardancy, *Composites, Part A*, 2019, **127**, 105649, DOI: 10.1016/j.compositesa.2019.105649.

69 Y. Jin, Y. Y. Fan, X. X. Meng, J. Y. Li, C. Li, J. Sunarso, N. T. Yang, B. Meng and W. M. Zhang, Modeling of hydrated cations transport through 2D MXene (Ti3C2Tx) membranes for water purification, *J. Membr. Sci.*, 2021, **631**, 119346, DOI: 10.1016/j.memsci.2021.119346.

70 J. X. Hu, Y. Q. Zhan, G. Y. Zhang, Q. Y. Feng, W. Yang, Y. H. Chiao, S. R. Zhang and A. Sun, Durable and super-hydrophilic/underwater super-oleophobic two-dimensional MXene composite lamellar membrane with photocatalytic self-cleaning property for efficient oil/water separation in harsh environments, *J. Membr. Sci.*, 2021, **637**, 119627, DOI: 10.1016/j.memsci.2021.119627.

71 (*a*) C. E. Ren, K. B. Hatzell, M. Alhabeb, Z. Ling, K. A. Mahmoud and Y. Gogotsi, Charge- and Size-Selective Ion Sieving Through Ti3C2Tx MXene Membranes, *J. Phys. Chem. Lett.*, 2015, **6**(20), 4026–4031, DOI: 10.1021/acs.jpclett.5b01895; (*b*) R. L. Han, X. F. Ma, Y. L. Xie, D. Teng and S. H. Zhang, Preparation of a new 2D MXene/PES composite membrane with excellent hydrophilicity and high flux, *RSC Adv.*, 2017, **7**(89), 56204–56210, DOI: 10.1039/c7ra10318b.

72 (*a*) B. Deng, H. Lian, B. Xue, R. Song, S. Chen, Z. Wang, T. Xu, H. Dong and S. Wang, Niobium-Carbide MXene Modified Hybrid Hole Transport Layer Enabling High-Performance Organic Solar Cells Over 19%, *Small*, 2023, **19**(23), 2207505, DOI: 10.1002/smll.202207505; (*b*) J. P. F. Assunção, H. G. Lemos, J. H. H. Rossato, G. L. Nogueira, J. V. M. Lima, S. L. Fernandes, R. K. Nishihora, R. V. Fernandes, S. A. Lourenço, D. Bagnis, *et al.*, Interface passivation with Ti3C2Tx-MXene doped PMMA film for highly efficient and stable inverted perovskite solar cells, *J. Mater. Chem. C*, 2024, **12**(2), 562–574, DOI: 10.1039/D3TC03810F.

73 Q. Gu, J. Wang, R. Peng, W. Song, L. Xie, R. Zhou and Z. Ge, Nonfullerene Organic Solar Cells with 18.17% Efficiency Obtained Using a V2C/PEDOT:PSS Composite Hole-Transport Layer, *ACS Appl. Energy Mater.*, 2023, **6**(3), 1982–1988, DOI: 10.1021/acsaem.2c03883.

74 K. Rasool, M. Helal, A. Ali, C. E. Ren, Y. Gogotsi and K. A. Mahmoud, Antibacterial Activity of Ti3C2Tx MXene, *ACS Nano*, 2016, **10**(3), 3674–3684, DOI: 10.1021/acsnano.6b00181.

75 M. A. K. Purbayanto, M. Jakubczak, D. Bury, V. G. Nair, M. Birowska, D. Moszczynska and A. Jastrzebska, Tunable Antibacterial Activity of a Polypropylene Fabric Coated with Bristling Ti3C2Tx MXene Flakes Coupling the Nanoblade Effect with ROS Generation, *ACS Appl. Nano Mater.*, 2022, **5**(4), 5373–5386, DOI: 10.1021/acsanm.2c00365.

76 Y. J. Gao, Y. H. Dong, S. T. Yang, A. C. Mo, X. Zeng, Q. M. Chen and Q. Peng, Size-dependent photothermal antibacterial activity of Ti3C2Tx MXene nanosheets against methicillin-resistant Staphylococcus aureus, *J. Colloid Interface Sci.*, 2022, **617**, 533–541, DOI: 10.1016/j.jcis.2022.03.032.

77 Y. Pan, Y. T. Hang, X. H. Zhao, G. P. Liu and W. Q. Jin, Optimizing separation performance and interfacial adhesion of PDMS/PVDF composite membranes for butanol recovery from aqueous solution, *J. Membr. Sci.*, 2019, **579**, 210–218, DOI: 10.1016/j.memsci.2019.03.008.

78 X. Y. Shi, M. H. Gao, W. W. Hu, D. Luo, S. Z. Hu, T. Huang, N. Zhang and Y. Wang, Largely enhanced adsorption performance and stability of MXene through in-situ depositing polypyrrole nanoparticles, *Sep. Purif. Technol.*, 2022, **287**, 120596, DOI: 10.1016/j.seppur.2022.120596.

79 P. K. Sharma, S. K. Pradhan, M. Pramanik, M. V. Limaye and S. B. Singh, MXene Based Electrospun Polymer Electrolyte fibers: Fabrication and Enhanced Ionic Conductivity, *Chemistryselect*, 2022, **7**(40), e202201986, DOI: 10.1002/slct.202201986.

80 E. A. Mayerberger, O. Urbanek, R. M. McDaniel, R. M. Street, M. W. Barsoum and C. L. Schauer, Preparation and characterization of polymer-Ti3C2Tx (MXene) composite nanofibers produced *via* electrospinning, *J. Appl. Polym. Sci.*, 2017, **134**(37), 45295, DOI: 10.1002/App.45295.

81 M. Boota, B. Anasori, C. Voigt, M. Q. Zhao, M. W. Barsoum and Y. Gogotsi, Pseudocapacitive Electrodes Produced by

Oxidant-Free Polymerization of Pyrrole between the Layers of 2D Titanium Carbide (MXene), *Adv. Mater.*, 2016, **28**(7), 1517–1522, DOI: 10.1002/adma.201504705.

82 Q. W. Wang, H. B. Zhang, J. Liu, S. Zhao, X. Xie, L. X. Liu, R. Yang, N. Koratkar and Z. Z. Yu, Multifunctional and Water-Resistant MXene-Decorated Polyester Textiles with Outstanding Electromagnetic Interference Shielding and Joule Heating Performances, *Adv. Funct. Mater.*, 2019, **29**(7), 1806819, DOI: 10.1002/adfm.201806819.

83 P. Yi, H. H. Zou, Y. H. Yu, X. F. Li, Z. Y. Li, G. Deng, C. Y. Chen, M. Fang, J. Z. He, X. Sun, *et al.*, MXene-Reinforced Liquid Metal/Polymer Fibers *via* Interface Engineering for Wearable Multifunctional Textiles, *ACS Nano*, 2022, DOI: 10.1021/acsnano.2c04863.

84 T. Z. Zhou, Y. Z. Yu, B. He, Z. Wang, T. Xiong, Z. X. Wang, Y. T. Liu, J. W. Xin, M. Qi, H. Z. Zhang, *et al.*, Ultra-compact MXene fibers by continuous and controllable synergy of interfacial interactions and thermal drawing-induced stresses, *Nat. Commun.*, 2022, **13**(1), 4564, DOI: 10.1038/s41467-022-32361-6.

85 (*a*) K. H. Tan, L. Samylingam, N. Aslfattahi, R. Saidur and K. Kadirgama, Optical and conductivity studies of polyvinyl alcohol-MXene (PVA-MXene) nanocomposite thin films for electronic applications, *Opt. Laser Technol.*, 2021, **136**, 106772, DOI: 10.1016/j.optlastec.2020.106772; (*b*) W. J. Yu, Y. Li, B. J. Xin and Z. Lu, MXene/PVA Fiber-based Supercapacitor with Stretchability for Wearable Energy Storage, *Fibers Polym.*, 2022, **23**(11), 2994–3001, DOI: 10.1007/s12221-022-4389-4; (*c*) Y. Yi, M. Chiao, K. A. Mahmoud and B. Wang, An MXene-doped PVA/PVP hydrogel-based strain sensor applicable in liquid environment, *Smart Mater. Struct.*, 2023, **32**(2), 025010, DOI: 10.1088/1361-665X/acafbc; (*d*) L. M. Li, X. F. Ji and K. Chen, Conductive, self-healing, and antibacterial Ag/MXene-PVA hydrogel as wearable skin-like sensors, *J. Biomater. Appl.*, 2023, **37**(7), 1169–1181, DOI: 10.1177/08853282221131137; (*e*) C. X. Li, A. Zheng, J. Y. Zhou, W. W. Huang, Y. Zhang, J. X. Han, L. Y. Cao and D. Y. Yang, A self-adhesive, self-healing and antibacterial hydrogel based on PVA/MXene-Ag/sucrose for fast-response, high-sensitivity and ultra-durable strain sensors, *New J. Chem.*, 2023, **47**(14), 6621–6630, DOI: 10.1039/d3nj00586k; (*f*) R. Haataja, S. Myllymaki, O. Laitinen, H. Jantunen and H. Liimatainen, Controlling the cell and surface architecture of cellulose nanofiber/PVA/Ti3C2TX MXene hybrid cryogels for optimized permittivity and EMI shielding performance, *Mater. Des.*, 2023, **228**, 111855, DOI: 10.1016/j.matdes.2023.111855.

86 (*a*) D. Z. Wang, Y. Lin, D. W. Hu, P. K. Jiang and X. Y. Huang, Multifunctional 3D-MXene/PDMS nanocomposites for electrical, thermal and triboelectric applications, *Composites, Part A*, 2020, **130**, 105754, DOI: 10.1016/j.compositesa.2019.105754; (*b*) W. G. Lu, B. Mustafa, Z. Y. Wang, F. Z. Lian and G. L. Yu, PDMS-Encapsulated MXene@Polyester Fabric Strain Sensor for Multifunctional Sensing Applications, *Nanomaterials*, 2022, **12**(5), 871, DOI: 10.3390/nano12050871; (*c*) H. B. Liu, R. L. Fu, X. Q. Su, B. Y. Wu, H. Wang, Y. Xu and X. H. Liu, Electrical insulating MXene/PDMS/BN composite with enhanced thermal conductivity for electromagnetic shielding application, *Compos. Commun.*, 2021, **23**, 100593, DOI: 10.1016/j.coco.2020.100593.

87 (*a*) O. Faruk and B. Adak, Recent advances in PEDOT:PSS integrated graphene and MXene-based composites for electrochemical supercapacitor applications, *Synth. Met.*, 2023, **297**, 117384, DOI: 10.1016/j.synthmet.2023.117384; (*b*) S. Chetana, S. Upadhyay, N. C. Joshi, N. Kumar, P. Choudhary, N. Sharma and V. N. Thakur, A facile supercritical fluid synthesis of cobalt sulfide integrated with MXene and PANI/PEDOT nanocomposites as electrode material for supercapacitor applications, *Flatchem*, 2023, **37**, 100456, DOI: 10.1016/j.flatc.2022.100456; (*c*) M. Y. Zhang, W. K. Yang, Z. Q. Wang, H. Liu, R. Yin, C. T. Liu and C. Y. Shen, Highly compressible and thermal insulative conductive MXene/PEDOT:PSS@melamine foam for promising wearable piezoresistive sensor, *Appl. Phys. Lett.*, 2023, **122**(4), 043507, DOI: 10.1063/5.0137571; (*d*) X. Z. Jin, Z. Y. Yang, C. H. Huang, J. H. Yang and Y. Wang, PEDOT:PSS/MXene/PEG composites with remarkable thermal management performance and excellent HF-band & X-band electromagnetic interference shielding efficiency for electronic packaging, *Chem. Eng. J.*, 2022, **448**, 137599, DOI: 10.1016/j.cej.2022.137599.

88 T. Cheng, X. L. Yang, S. Yang, L. Li, Z. T. Liu, J. Qu, C. F. Meng, X. C. Li, Y. Z. Zhang and W. Y. Lai, Flexible Transparent Bifunctional Capacitive Sensors with Superior Areal Capacitance and Sensing Capability based on PEDOT:PSS/MXene/Ag Grid Hybrid Electrodes, *Adv. Funct. Mater.*, 2023, **33**(5), 2210997, DOI: 10.1002/adfm.202210997.

89 (*a*) Z. W. He, H. M. Xie, H. Q. Wu, J. H. Chen, S. Y. Ma, X. Duan, A. Q. Chen and Z. Kong, Recent Advances in MXene/Polyaniline-Based Composites for Electrochemical Devices and Electromagnetic Interference Shielding Applications, *ACS Omega*, 2021, **6**(35), 22468–22477, DOI: 10.1021/acsomega.1c02996; (*b*) M. Elancheziyan, M. Eswaran, C. E. Shuck, S. Senthilkumar, S. Elumalai, R. Dhanusuraman and V. K. Ponnusamy, Facile synthesis of polyaniline/titanium carbide (MXene) nanosheets/palladium nanocomposite for efficient electrocatalytic oxidation of methanol for fuel cell application, *Fuel*, 2021, **303**, 121329, DOI: 10.1016/j.fuel.2021.121329.

90 (*a*) C. Q. Yang, D. Z. Zhang, D. Y. Wang, H. X. Luan, X. Y. Chen and W. Y. Yan, In Situ Polymerized MXene/Polypyrrole/Hydroxyethyl Cellulose- Based Flexible Strain Sensor Enabled by Machine Learning for Handwriting Recognition, *ACS Appl. Mater. Interfaces*, 2023, **15**(4), 5811–5821, DOI: 10.1021/acsami.2c18989; (*b*) L. Wang, H. Wu, X. Zhai, J. Shi, Q. Q. Zhou, H. Li and J. M. Wan, Ti3C2Tx MXene/dopamine-modified polypyrrole flexible composite electrodes with application in energy storage devices, *J. Alloys Compd.*, 2023, **946**, 169347, DOI: 10.1016/j.jallcom.2023.169347; (*c*) W. L. Luo, Y. Sun, Y. Q. Han,

J. X. Ding, T. X. Li, C. P. Hou and Y. Ma, Flexible Ti3C2Tx MXene/polypyrrole composite films for high-performance all-solid asymmetric supercapacitors, *Electrochim. Acta*, 2023, **441**, 141818, DOI: 10.1016/j.electacta.2023.141818; (*d*) Z. L. Liu, R. Zhang, H. L. Xiong, L. L. Zhang, J. Z. Li, L. Q. Wang and Z. A. Qiao, Swelling-Induced Structural Transformation Strategy: Controllable Synthesis of 2D Porous Polypyrrole/MXene Heterostructures with Tunable Pore Structures, *Adv. Mater. Interfaces*, 2023, **10**(11), 2202501, DOI: 10.1002/admi.202202501.

91 Z. T. Wu, T. X. Shang, Y. Q. Deng, Y. Tao and Q. H. Yang, The Assembly of MXenes from 2D to 3D, *Adv. Sci.*, 2020, **7**(7), 1903077, DOI: 10.1002/advs.201903077.

92 S. He, X. Sun, H. Zhang, C. Yuan, Y. Wei and J. Li, Preparation Strategies and Applications of MXene–polymer Composites: A Review, *Macromol. Rapid Commun.*, 2021, **42**(19), 2100324, DOI: 10.1002/marc.202100324.

93 H. Riazi, S. K. Nemani, M. C. Grady, B. Anasori and M. Soroush, Ti3C2 MXene–polymer nanocomposites and their applications, *J. Mater. Chem. A*, 2021, **9**(13), 8051–8098, DOI: 10.1039/D0TA08023C.

94 K. Gong, K. Zhou, X. Qian, C. Shi and B. Yu, MXene as emerging nanofillers for high-performance polymer composites: A review, *Composites, Part B*, 2021, **217**, 108867, DOI: 10.1016/j.compositesb.2021.108867.

95 (*a*) X. Chen, Y. Zhao, L. Li, Y. Wang, J. Wang, J. Xiong, S. Du, P. Zhang, X. Shi and J. Yu, MXene/Polymer Nanocomposites: Preparation, Properties, and Applications, *Polym. Rev.*, 2021, **61**(1), 80–115, DOI: 10.1080/15583724.2020.1729179; (*b*) M. Carey and M. W. Barsoum, MXene polymer nanocomposites: a review, *Mater. Today Adv.*, 2021, **9**, 100120, DOI: 10.1016/j.mtadv.2020.100120; (*c*) H. Aghamohammadi, N. Amousa and R. Eslami-Farsani, Recent advances in developing the MXene/polymer nanocomposites with multiple properties: A review study, *Synth. Met.*, 2021, **273**, 116695, DOI: 10.1016/j.synthmet.2020.116695.

96 M. Naguib, M. Kurtoglu, V. Presser, J. Lu, J. Niu, M. Heon, L. Hultman, Y. Gogotsi and M. W. Barsoum, Two-Dimensional Nanocrystals Produced by Exfoliation of Ti3AlC2, *Adv. Mater.*, 2011, **23**(37), 4248–4253.

97 T. A. Oyehan, B. A. Salami, A. A. Abdulrasheed, H. U. Hambali, A. Gbadamosi, E. Valsami-Jones and T. A. Saleh, MXenes: Synthesis, properties, and applications for sustainable energy and environment, *Appl. Mater. Today*, 2023, **35**, 101993, DOI: 10.1016/j.apmt.2023.101993.

98 C. E. Shuck, M. Han, K. Maleski, K. Hantanasirisakul, S. J. Kim, J. Choi, W. E. B. Reil and Y. Gogotsi, Effect of Ti3AlC2 MAX Phase on Structure and Properties of Resultant Ti3C2Tx MXene, *ACS Appl. Nano Mater.*, 2019, **2**(6), 3368–3376, DOI: 10.1021/acsanm.9b00286.

99 V. Natu, R. Pai, M. Sokol, M. Carey, V. Kalra and M. W. Barsoum, 2D Ti3C2Tz MXene Synthesized by Water-free Etching of Ti3AlC2 in Polar Organic Solvents, *Chem*, 2020, **6**(3), 616–630, DOI: 10.1016/j.chempr.2020.01.019.

100 S. Yang, P. Zhang, F. Wang, A. G. Ricciardulli, M. R. Lohe, P. W. M. Blom and X. Feng, Fluoride-Free Synthesis of Two-Dimensional Titanium Carbide (MXene) Using A Binary Aqueous System, *Angew. Chem., Int. Ed.*, 2018, **57**(47), 15491–15495, DOI: 10.1002/anie.201809662.

101 L. Liu, M. Orbay, S. Luo, S. Duluard, H. Shao, J. Harmel, P. Rozier, P.-L. Taberna and P. Simon, Exfoliation and Delamination of Ti3C2Tx MXene Prepared *via* Molten Salt Etching Route, *ACS Nano*, 2022, **16**(1), 111–118.

102 T. Li, L. Yao, Q. Liu, J. Gu, R. Luo, J. Li, X. Yan, W. Wang, P. Liu, B. Chen, *et al.*, Fluorine-Free Synthesis of High-Purity Ti3C2T (T=OH, O) *via* Alkali Treatment, *Angew. Chem., Int. Ed.*, 2018, **57**(21), 6115–6119, DOI: 10.1002/anie.201800887.

103 D. Wang, C. Zhou, A. S. Filatov, W. Cho, F. Lagunas, M. Wang, S. Vaikuntanathan, C. Liu, R. F. Klie and D. V. Talapin, Direct synthesis and chemical vapor deposition of 2D carbide and nitride MXenes, *Science*, 2023, **379**(6638), 1242–1247, DOI: 10.1126/science.add9204.

104 J. Halim, S. Kota, M. R. Lukatskaya, M. Naguib, M.-Q. Zhao, E. J. Moon, J. Pitock, J. Nanda, S. J. May, Y. Gogotsi, *et al.*, Synthesis and Characterization of 2D Molybdenum Carbide (MXene), *Adv. Funct. Mater.*, 2016, **26**(18), 3118–3127, DOI: 10.1002/adfm.201505328.

105 E. Rems, M. Anayee, E. Fajardo, R. L. Lord, D. Bugallo, Y. Gogotsi and Y.-J. Hu, Computationally Guided Synthesis of MXenes by Dry Selective Extraction, *Adv. Mater.*, 2023, **35**(45), 2305200, DOI: 10.1002/adma.202305200.

106 X. Xiao, H. Yu, H. Jin, M. Wu, Y. Fang, J. Sun, Z. Hu, T. Li, J. Wu, L. Huang, *et al.*, Salt-Templated Synthesis of 2D Metallic MoN and Other Nitrides, *ACS Nano*, 2017, **11**(2), 2180–2186, DOI: 10.1021/acsnano.6b08534.

107 H. Ding, Y. Li, M. Li, K. Chen, K. Liang, G. Chen, J. Lu, J. Palisaitis, P. O. Å. Persson, P. Eklund, *et al.*, Chemical scissor–mediated structural editing of layered transition metal carbides, *Science*, 2023, **379**(6637), 1130–1135, DOI: 10.1126/science.add5901.

108 S. Kumar, N. Kumari and Y. Seo, MXenes: Versatile 2D materials with tailored surface chemistry and diverse applications, *J. Energy Chem.*, 2024, **90**, 253–293, DOI: 10.1016/j.jechem.2023.11.031.

109 (*a*) T. Schultz, N. C. Frey, K. Hantanasirisakul, S. Park, S. J. May, V. B. Shenoy, Y. Gogotsi and N. Koch, Surface Termination Dependent Work Function and Electronic Properties of Ti3C2Tx MXene, *Chem. Mater.*, 2019, **31**(17), 6590–6597, DOI: 10.1021/acs.chemmater.9b00414; (*b*) N. M. Caffrey, Effect of mixed surface terminations on the structural and electrochemical properties of two-dimensional Ti3C2T2 and V2CT2 MXenes multilayers, *Nanoscale*, 2018, **10**(28), 13520–13530, DOI: 10.1039/C8NR03221A.

110 T. M. Su, X. H. Ma, J. H. Tong, H. B. Ji, Z. Z. Qin and Z. L. Wu, Surface engineering of MXenes for energy and

environmental applications, *J. Mater. Chem. A*, 2022, **10**(19), 10265–10296, DOI: **10.1039/d2ta01140a**.

111 A. V. Mohammadi, J. Rosen and Y. Gogotsi, The world of two-dimensional carbides and nitrides (MXenes), *Science*, 2021, **372**(6547), 1165, DOI: **10.1126/science.abf1581**.

112 (*a*) Y. D. Zhu, X. Y. Ma, L. P. Li, Q. J. Yang, F. Jin, Z. N. Chen, C. P. Wu, H. B. Shi, Z. Q. Feng, S. K. Yin, *et al.*, Surface Functional Modification by Ti3C2Tx MXene on PLLA Nanofibers for Optimizing Neural Stem Cell Engineering, *Adv. Healthcare Mater.*, 2023, 2300731, DOI: **10.1002/adhm.202300731**; (*b*) J. B. Zhang, S. Tang, N. Ding, P. Ma and Z. T. Zhang, Surface-modified Ti3C2 MXene nanosheets for mesenchymal stem cell osteogenic differentiation *via* photothermal conversion, *Nanoscale Adv.*, 2023, **5**(11), 2921–2932, DOI: **10.1039/d3na00187c**; (*c*) W. K. Yuan, L. L. Zhu, Y. J. Zheng, W. Y. Guo, Y. L. Min and J. C. Fan, Surface Engineering with Interfacial Poly(glutamic acid)/MXene/Aramid Nanofibers Protective Layer for Dendrite-Free Zinc Anodes, *Energy Fuel.*, 2023, **37**(11), 8031–8041, DOI: **10.1021/acs.energyfuels.3c01058**; (*d*) M. A. Tokmedash, N. Nagpal, P. Y. Chen, J. S. VanEpps and J. H. Min, Stretchable, Nano-Crumpled MXene Multilayers Impart Long-Term Antibacterial Surface Properties, *Adv. Mater. Interfaces*, 2023, **10**(16), DOI: **10.1002/admi.202202350**; (*e*) V. Sharma, S. Sardana, R. Dhiman and A. Mahajan, Surface engineered MXene with multi-electroactive sites for developing durable and efficient water-splitting electrolyzer, *Appl. Phys. Lett.*, 2023, **122**(19), 191601, DOI: **10.1063/5.0142311**; (*f*) T. Schultz, P. Barmann, E. Longhi, R. Meena, Y. Geerts, Y. Gogotsi, S. Barlow, S. R. Marder, T. Petit and N. Koch, Work function and energy level alignment tuning at Ti3C2Tx MXene surfaces and interfaces using (metal-)organic donor/acceptor molecules, *Phys. Rev. Mater.*, 2023, **7**(4), 045002, DOI: **10.1103/PhysRevMaterials.7.045002**; (*g*) M. N. Mustafa, M. A. A. M. Abdah, A. Numan, Y. Sulaiman, R. Walvekar and M. Khalid, Development of high-performance MXene/nickel cobalt phosphate nanocomposite for electrochromic energy storage system using response surface methodology, *J. Energy Storage*, 2023, **68**, 107880, DOI: **10.1016/j.est.2023.107880**; (*h*) J. L. Guo, Z. L. Shang, Y. Sun, C. H. Li, J. Y. Xia, Y. X. Zou, K. Du, G. Q. Liu, F. Zhou and W. M. Liu, Surface-modified Ti3C2Tx MXene as anti-wear and extreme pressure additive for PFPE supramolecular gel, *Tribol. Int.*, 2023, **186**, 108611, DOI: **10.1016/j.triboint.2023.108611**; (*i*) H. X. Di, D. Zhao, X. B. Hui, Z. X. Wang, L. W. Yin, Z. Qian, E. Y. Guo and C. X. Wang, Surface Ti vacancy passivation of Ti3C2O2 MXene *via* transition metal atoms as high-performance potassium-ion batteries anodes, *Appl. Surf. Sci.*, 2023, **630**, 157504, DOI: **10.1016/j.apsusc.2023.157504**; (*j*) H. Bark, G. Thangavel, R. J. Liu, D. H. C. Chua and P. S. Lee, Effective Surface Modification of 2D MXene toward Thermal Energy Conversion and Management, *Small Methods*, 2023, 2300077, DOI: **10.1002/smtd.202300077**; (*k*) N. Almarzooqi, S. H. Y. Hong, P. Verma, A. Shaheen, A. Schiffer and F. AlMarzooqi, Photothermal Surface Heating Membrane Distillation Using 3D-Printed Ti3C2TX MXene-Based Nanocomposite Spacers, *ACS Appl. Mater. Interfaces*, 2023, **15**(17), 20998–21007, DOI: **10.1021/acsami.3c00830**.

113 S. Kumar, S. M. Z. Mehdi, M. Ali, S. R. Choi, S. Yoo, M. Kim, M. Suleman, T. Singh and Y. Seo, Supercapacitors with enhanced energy storage and hydrogen evolution reaction performance *via* sequential alkali-modified MXenes, *J. Mater. Chem. C*, 2024, **12**(46), 18732–18745.

114 (*a*) K. Arole, J. W. Blivin, S. Saha, D. E. Holta, X. Zhao, A. Sarmah, H. Cao, M. Radovic, J. L. Lutkenhaus and M. J. Green, Water-dispersible Ti3C2Tz MXene nanosheets by molten salt etching, *iScience*, 2021, **24**(12), 103403, DOI: **10.1016/j.isci.2021.103403**; (*b*) L. Y. Liu, M. Orbay, S. Luo, S. Duluard, H. Shao, J. Harmel, P. Rozier, P. L. Taberna and P. Simon, Exfoliation and Delamination of Ti CTMXene Prepared Molten Salt Etching Route, *ACS Nano*, 2022, **16**(1), 111–118, DOI: **10.1021/acsnano.1c08498**.

115 M. Li, J. Lu, K. Luo, Y. B. Li, K. K. Chang, K. Chen, J. Zhou, J. Rosen, L. Hultman, P. Eklund, *et al.*, Element Replacement Approach by Reaction with Lewis Acidic Molten Salts to Synthesize Nanolaminated MAX Phases and MXenes, *J. Am. Chem. Soc.*, 2019, **141**(11), 4730–4737, DOI: **10.1021/jacs.9b00574**.

116 V. Natu and M. W. Barsoum, MXene Surface Terminations: A Perspective, *J. Phys. Chem. C*, 2023, **127**(41), 20197–20206, DOI: **10.1021/acs.jpcc.3c04324**.

117 V. Natu and M. W. Barsoum, MXene Surface Terminations: A Perspective, *J. Phys. Chem. C*, 2023, **127**, 20197–20206, DOI: **10.1021/acs.jpcc.3c04324**.

118 I. Persson, L. A. Naslund, J. Halim, M. W. Barsoum, V. Darakchieva, J. Palisaitis, J. Rosen and P. O. A. Persson, On the organization and thermal behavior of functional groups on Ti3C2 MXene surfaces in vacuum, *2d Mater*, 2018, **5**(1), 015002, DOI: **10.1088/2053-1583/aa89cd**.

119 K. W. Xiong, P. H. Wang, G. Yang, Z. F. Liu, H. J. Zhang, S. W. Jin and X. Xu, Functional Group Effects on the Photoelectronic Properties of MXene (Sc2CT2, T = O, F, OH) and Their Possible Photocatalytic Activities, *Sci. Rep.*, 2017, **7**, 15095, DOI: **10.1038/s41598-017-15233-8**.

120 M. Hassan, A. Ali, K. Rasool and K. Mahmoud, Ion conduction in polyvinylidene fluoride (PVDF)/MXene nanolayers membrane for water treatment applications, *ACS National Meeting Book of Abstracts*, 2016, vol. 251.

121 D. Y. Qu, Y. Y. Jian, L. H. Guo, C. Su, N. Tang, X. M. Zhang, W. W. Hu, Z. Wang, Z. H. Zhao, P. Zhong, *et al.*, An Organic Solvent-Assisted Intercalation and Collection (OAIC) for Ti3C2Tx MXene with Controllable Sizes and Improved Yield, *Nano–Micro Lett.*, 2021, **13**(1), 188, DOI: **10.1007/s40820-021-00705-4**.

122 X. Li, X. Yin, M. Han, C. Song, X. Sun, H. Xu, L. Cheng and L. Zhang, A controllable heterogeneous structure and electromagnetic wave absorption properties of Ti2CTx

MXene, *J. Mater. Chem. C*, 2017, **5**(30), 7621–7628, DOI: 10.1039/C7TC01991B.

123 S. Doo, A. Chae, D. Kim, T. Oh, T. Y. Ko, S. J. Kim, D.-Y. Koh and C. M. Koo, Mechanism and Kinetics of Oxidation Reaction of Aqueous Ti3C2Tx Suspensions at Different pHs and Temperatures, *ACS Appl. Mater. Interfaces*, 2021, **13**(19), 22855–22865, DOI: 10.1021/acsami.1c04663.

124 V. Natu, J. L. Hart, M. Sokol, H. Chiang, M. L. Taheri and M. W. Barsoum, Edge Capping of 2D-MXene Sheets with Polyanionic Salts To Mitigate Oxidation in Aqueous Colloidal Suspensions, *Angew. Chem., Int. Ed.*, 2019, **58**(36), 12655–12660, DOI: 10.1002/anie.201906138.

125 C. J. Zhang, S. Pinilla, N. McEvoy, C. P. Cullen, B. Anasori, E. Long, S.-H. Park, A. Seral-Ascaso, A. Shmeliov, D. Krishnan, *et al.*, Oxidation Stability of Colloidal Two-Dimensional Titanium Carbides (MXenes), *Chem. Mater.*, 2017, **29**(11), 4848–4856, DOI: 10.1021/acs.chemmater.7b00745.

126 S. Huang and V. N. Mochalin, Hydrolysis of 2D Transition-Metal Carbides (MXenes) in Colloidal Solutions, *Inorg. Chem.*, 2019, **58**(3), 1958–1966, DOI: 10.1021/acs.inorgchem.8b02890.

127 F. J. Xia, J. C. Lao, R. H. Yu, X. H. Sang, J. Y. Luo, Y. Li and J. S. Wu, Ambient oxidation of Ti3C2 MXene initialized by atomic defects, *Nanoscale*, 2019, **11**(48), 23330–23337, DOI: 10.1039/c9nr07236e.

128 X. H. Sang, Y. Xie, M. W. Lin, M. Alhabeb, K. L. Van Aken, Y. Gogotsi, P. R. C. Kent, K. Xiao and R. R. Unocic, Atomic Defects in Monolayer Titanium Carbide (Ti3C2Tx) MXene, *ACS Nano*, 2016, **10**(10), 9193–9200, DOI: 10.1021/acsnano.6b05240.

129 (*a*) R. Ibragimova, P. Rinke and H.-P. Komsa, Native Vacancy Defects in MXenes at Etching Conditions, *Chem. Mater.*, 2022, **34**(7), 2896–2906, DOI: 10.1021/acs.chemmater.1c03179; (*b*) R. Khaledialidusti, A. K. Mishra and A. Barnoush, Atomic defects in monolayer ordered double transition metal carbide (Mo2TiC2Tx) MXene and CO2 adsorption, *J. Mater. Chem. C*, 2020, **8**(14), 4771–4779, DOI: 10.1039/C9TC06046D.

130 (*a*) S. Doo, A. Chae, D. Kim, T. Oh, T. Y. Ko, S. J. Kim, D. Y. Koh and C. M. Koo, Mechanism and Kinetics of Oxidation Reaction of Aqueous Ti3C2Tx Suspensions at Different pHs and Temperatures, *ACS Appl. Mater. Interfaces*, 2021, **13**(19), 22855–22865, DOI: 10.1021/acsami.1c04663; (*b*) D. Kim, T. Y. Ko, H. Kim, G. H. Lee, S. Cho and C. M. Koo, Nonpolar Organic Dispersion of 2D Ti3C2Tx MXene Flakes *via* Simultaneous Interfacial Chemical Grafting and Phase Transfer Method, *ACS Nano*, 2019, **13**(12), 13818–13828, DOI: 10.1021/acsnano.9b04088.

131 J. B. Li, R. Z. Qin, L. Yan, Z. Chi, Z. H. Yu, N. T. Li, M. J. Hu, H. L. Chen and G. C. Shan, Plasmonic Light Illumination Creates a Channel To Achieve Fast Degradation of Ti3C2TX Nanosheets, *Inorg. Chem.*, 2019, **58**(11), 7285–7294, DOI: 10.1021/acs.inorgchem.9b00329.

132 X. Zhao, A. Vashisth, J. W. Blivin, Z. Tan, D. E. Holta, V. Kotasthane, S. A. Shah, T. Habib, S. Liu, J. L. Lutkenhaus, *et al.*, pH, Nanosheet Concentration, and Antioxidant Affect the Oxidation of Ti3C2Tx and Ti2CTx MXene Dispersions, *Adv. Mater. Interfaces*, 2020, **7**(20), 2000845, DOI: 10.1002/admi.202000845.

133 S. Kumar, H. M. Park, T. Singh, M. Kumar and Y. Seo, Long-Term Stability Studies and Applications of $Ti_3C_2T_x$ MXene, *Int. J. Energy Res.*, 2023, **2023**, 5275439, DOI: 10.1155/2023/5275439.

134 S. H. Huang and V. N. Mochalin, Hydrolysis of 2D Transition-Metal Carbides (MXenes) in Colloidal Solutions, *Inorg. Chem.*, 2019, **58**(3), 1958–1966, DOI: 10.1021/acs.inorgchem.8b02890.

135 X. Li, N. Xue, Q. Yao, L. Han, X. Zhao, B. Li, T. He and X. Tao, Obtaining Ambient-Stable MXene Ti3C2T through Avoidance of Surface Oxidation Active Sites, *Adv. Mater. Interfaces*, 2022, **9**(24), 2200991, DOI: 10.1002/admi.202200991.

136 S. Chertopalov and V. N. Mochalin, Environment-Sensitive Photoresponse of Spontaneously Partially Oxidized Ti3C2 MXene Thin Films, *ACS Nano*, 2018, **12**(6), 6109–6116, DOI: 10.1021/acsnano.8b02379.

137 M. A. Hope, A. C. Forse, K. J. Griffith, M. R. Lukatskaya, M. Ghidiu, Y. Gogotsi and C. P. Grey, NMR reveals the surface functionalisation of Ti3C2 MXene, *Phys. Chem. Chem. Phys.*, 2016, **18**(7), 5099–5102, DOI: 10.1039/c6cp00330c.

138 (*a*) V. Kamysbayev, A. S. Filatov, H. Hu, X. Rui, F. Lagunas, D. Wang, R. F. Klie and D. V. Talapin, Covalent surface modifications and superconductivity of two-dimensional metal carbide MXenes, *Science*, 2020, **369**(6506), 979–983, DOI: 10.1126/science.aba8311; (*b*) J. Yoon, S. Kim, K. H. Park, S. Lee, S. J. Kim, H. Lee, T. Oh and C. M. Koo, Biocompatible and Oxidation-Resistant Ti3C2Tx MXene with Halogen-Free Surface Terminations, *Small Methods*, 2023, **7**(8), 2201579, DOI: 10.1002/smtd.202201579; (*c*) A. Dash, R. Vaßen, O. Guillon and J. Gonzalez-Julian, Molten salt shielded synthesis of oxidation prone materials in air, *Nat. Mater.*, 2019, **18**(5), 465–470, DOI: 10.1038/s41563-019-0328-1.

139 L. H. Karlsson, J. Birch, J. Halim, M. W. Barsoum and P. O. A. Persson, Atomically Resolved Structural and Chemical Investigation of Single MXene Sheets, *Nano Lett.*, 2015, **15**(8), 4955–4960, DOI: 10.1021/acs.nanolett.5b00737.

140 Y. Zheng, W. Chen, Y. Sun, C. Huang, Z. Wang and D. Zhou, High conductivity and stability of polystyrene/MXene composites with orientation-3D network binary structure, *J. Colloid Interface Sci.*, 2021, **595**, 151–158.

141 S. Lee, E. H. Kim, S. Yu, H. Kim, C. Park, S. W. Lee, H. Han, W. Jin, K. Lee and C. E. Lee, Polymer-laminated Ti3C2TX MXene electrodes for transparent and flexible field-driven electronics, *ACS Nano*, 2021, **15**(5), 8940–8952.

142 Z. Hao, S. Zhang, S. Yang, X. Li, Y. Gao, J. Peng, L. Li, L. Bao and X. Li, Bridged Ti3C2Tx MXene film with superior oxidation resistance and structural stability for high-performance flexible supercapacitors, *ACS Appl. Energy Mater.*, 2022, **5**(3), 2898–2908.

143 Z. Xu, X. Ding, S. Li, F. Huang, B. Wang, S. Wang, X. Zhang, F. Liu and H. Zhang, Oxidation-resistant MXene-based melamine foam with ultralow-percolation thresholds for electromagnetic-infrared compatible shielding, *ACS Appl. Mater. Interfaces*, 2022, **14**(35), 40396–40407.

144 A. Chae, G. Murali, S. Y. Lee, J. Gwak, S. J. Kim, Y. J. Jeong, H. Kang, S. Park, A. S. Lee and D. Y. Koh, Highly oxidation-resistant and self-healable MXene-based hydrogels for wearable strain sensor, *Adv. Funct. Mater.*, 2023, **33**(24), 2213382.

145 I. Amin, H. v. d. Brekel, K. Nemani, E. Batyrev, A. de Vooys, H. van der Weijde, B. Anasori and N. R. Shiju, Ti3C2Tx MXene polymer composites for anticorrosion: an overview and perspective, *ACS Appl. Mater. Interfaces*, 2022, **14**(38), 43749–43758.

146 K. Zhao, J. W. Lee, Z. G. Yu, W. Jiang, J. W. Oh, G. Kim, H. Han, Y. Kim, K. Lee and S. Lee, Humidity-tolerant moisture-driven energy generator with MXene aerogel–organohydrogel bilayer, *ACS Nano*, 2023, **17**(6), 5472–5485.

147 L.-X. Liu, W. Chen, H.-B. Zhang, L. Ye, Z. Wang, Y. Zhang, P. Min and Z.-Z. Yu, Super-tough and environmentally stable aramid. Nanofiber@ MXene coaxial fibers with outstanding electromagnetic interference shielding efficiency, *Nano–Micro Lett.*, 2022, **14**(1), 111.

148 G. S. Lee, T. Yun, H. Kim, I. H. Kim, J. Choi, S. H. Lee, H. J. Lee, H. S. Hwang, J. G. Kim and D.-w. Kim, Mussel inspired highly aligned Ti3C2Tx MXene film with synergistic enhancement of mechanical strength and ambient stability, *ACS Nano*, 2020, **14**(9), 11722–11732.

149 N. Liu, Q. Li, H. Wan, L. Chang, H. Wang, J. Fang, T. Ding, Q. Wen, L. Zhou and X. Xiao, High-temperature stability in air of Ti3C2Tx MXene-based composite with extracted bentonite, *Nat. Commun.*, 2022, **13**(1), 5551.

150 H.-W. Zhang, L.-Y. Yang, M.-L. Huang, M.-H. Cheng, Z.-S. Feng, F. Meng, Z. Lin and Y. Wang, Flexible MXene/sodium alginate composite fabric with high structural stability and oxidation resistance for electromagnetic interference shielding, *Nano Res.*, 2024, 1–10.

151 T. Habib, X. Zhao, S. A. Shah, Y. Chen, W. Sun, H. An, J. L. Lutkenhaus, M. Radovic and M. J. Green, Oxidation stability of Ti3C2Tx MXene nanosheets in solvents and composite films, *npj 2D Mater. Appl.*, 2019, **3**(1), 8, DOI: **10.1038/s41699-019-0089-3**.

152 S. Kumar, H. M. Park, M. Kim, N. Nasir, M. Kumar and Y. Seo, Application dependent stability of Ti3C2Tx MXene in PDLC-based smart-windows, *Ceram. Int.*, 2022, **48**(23), 35092–35099.

153 (*a*) Y. Zheng, W. Chen, Z. Wang and Q. Wang, Polystyrene/rGO composites with orientation-3d network binary structure and its surprising conductivity, *Macromolecules*, 2018, **51**(20), 7993–8000; (*b*) L. Yang, Z. Wang, Y. Ji, J. Wang and G. Xue, Highly ordered 3D graphene-based polymer composite materials fabricated by "particle-constructing" method and their outstanding conductivity, *Macromolecules*, 2014, **47**(5), 1749–1756.

154 M. Alhabeb, K. Maleski, B. Anasori, P. Lelyukh, L. Clark, S. Sin and Y. Gogotsi, Guidelines for synthesis and processing of two-dimensional titanium carbide (Ti3C2Tx MXene), *Chem. Mater.*, 2017, **29**(18), 7633–7644.

155 V. Natu, J. L. Hart, M. Sokol, H. Chiang, M. L. Taheri and M. W. Barsoum, Edge capping of 2D-MXene sheets with polyanionic salts to mitigate oxidation in aqueous colloidal suspensions, *Angew. Chem.*, 2019, **131**(36), 12785–12790.

156 F. Wu, Y. Ye, R. Chen, T. Zhao, J. Qian, X. Zhang, L. Li, Q. Huang, X. Bai and Y. Cui, Gluing Carbon Black and Sulfur at Nanoscale: A Polydopamine-Based'Nano-Binder'for Double-Shelled Sulfur Cathodes, *Adv. Energy Mater.*, 2017, **7**(3), 1601591.

157 I. H. Kim, T. Yun, J. E. Kim, H. Yu, S. P. Sasikala, K. E. Lee, S. H. Koo, H. Hwang, H. J. Jung and J. Y. Park, Mussel-Inspired Defect Engineering of Graphene Liquid Crystalline Fibers for Synergistic Enhancement of Mechanical Strength and Electrical Conductivity, *Adv. Mater.*, 2018, **30**(40), 1803267.

158 W. Tian, A. VahidMohammadi, Z. Wang, L. Ouyang, M. Beidaghi and M. M. Hamedi, Layer-by-layer self-assembly of pillared two-dimensional multilayers, *Nat. Commun.*, 2019, **10**(1), 2558.

159 M. Dong, Y. Hu, X. Yu, M. Liu, E. Bilotti, H. Zhang and D. G. Papageorgiou, Probing Interfacial Interactions in Ternary Nanocomposites of Ti3C2Tx MXene Nanoplatelets, Multiwalled Carbon Nanotubes, and Poly(vinyl alcohol) toward Synergistic Reinforcement, *ACS Appl. Polym. Mater.*, 2024, **6**(1), 207–217, DOI: **10.1021/acsapm.3c01816**.

160 Y. Zhan, X. Zheng, B. Nan, M. Lu, J. Shi and K. Wu, Flexible MXene/aramid nanofiber nanocomposite film with high thermal conductivity and flame retardancy, *Eur. Polym. J.*, 2023, **186**, 111847, DOI: **10.1016/j.eurpolymj.2023.111847**.

161 N. Li, X. Wang, Y. Liu, Y. Li, J. Li, Z. Qin and T. Jiao, Ultrastretchable, Self-Adhesive and conductive MXene nanocomposite hydrogel for body-surface temperature distinguishing and electrophysiological signal monitoring, *Chem. Eng. J.*, 2024, **483**, 149303, DOI: **10.1016/j.cej.2024.149303**.

162 N. Bisht, S. Jaiswal, J. Vishwakarma, S. K. Gupta, R. J. Yeo, S. K. R. S. Sankaranarayanan, C. Dhand and N. Dwivedi, MXene enhanced Shape Memory Polymer Composites: The rise of MXenes as fillers for stimuli-responsive materials, *Chem. Eng. J.*, 2024, **498**, 155154, DOI: **10.1016/j.cej.2024.155154**.

163 Z. Ling, C. E. Ren, M.-Q. Zhao, J. Yang, J. M. Giammarco, J. Qiu, M. W. Barsoum and Y. Gogotsi, Flexible and conductive MXene films and nanocomposites with high capacitance, *Proc. Natl. Acad. Sci. U. S. A.*, 2014, **111**(47), 16676–16681.

164 S. Wan, X. Li, Y. Wang, Y. Chen, X. Xie, R. Yang, A. P. Tomsia, L. Jiang and Q. Cheng, Strong sequentially bridged MXene sheets, *Proc. Natl. Acad. Sci. U. S. A.*, 2020, **117**(44), 27154–27161, DOI: **10.1073/pnas.2009432117**.

165 L. Wang, H. Qiu, P. Song, Y. Zhang, Y. Lu, C. Liang, J. Kong, L. Chen and J. Gu, 3D Ti3C2Tx MXene/C hybrid foam/epoxy nanocomposites with superior electromagnetic

interference shielding performances and robust mechanical properties, *Composites, Part A*, 2019, **123**, 293–300.

166 J. Liu, H.-B. Zhang, X. Xie, R. Yang, Z. Liu, Y. Liu and Z.-Z. Yu, Multifunctional, Superelastic, and Lightweight MXene/Polyimide Aerogels, *Small*, 2018, **14**(45), 1802479, DOI: 10.1002/smll.201802479.

167 J.-Q. Luo, S. Zhao, H.-B. Zhang, Z. Deng, L. Li and Z.-Z. Yu, Flexible, stretchable and electrically conductive MXene/natural rubber nanocomposite films for efficient electromagnetic interference shielding, *Compos. Sci. Technol.*, 2019, **182**, 107754.

168 H. Zhang, L. Wang, A. Zhou, C. Shen, Y. Dai, F. Liu, J. Chen, P. Li and Q. Hu, Effects of 2-D transition metal carbide Ti2CTx on properties of epoxy composites, *RSC Adv.*, 2016, **6**(90), 87341–87352.

169 R. Liu, M. Miao, Y. Li, J. Zhang, S. Cao and X. Feng, Ultrathin biomimetic polymeric Ti3C2Tx MXene composite films for electromagnetic interference shielding, *ACS Appl. Mater. Interfaces*, 2018, **10**(51), 44787–44795.

170 Y. Pan, L. Fu, Q. Zhou, Z. Wen, C. T. Lin, J. Yu, W. Wang and H. Zhao, Flammability, thermal stability and mechanical properties of polyvinyl alcohol nanocomposites reinforced with delaminated Ti3C2Tx (MXene), *Polym. Compos.*, 2020, **41**(1), 210–218.

171 W. Zhi, S. Xiang, R. Bian, R. Lin, K. Wu, T. Wang and D. Cai, Study of MXene-filled polyurethane nanocomposites prepared *via* an emulsion method, *Compos. Sci. Technol.*, 2018, **168**, 404–411.

172 X. Sheng, Y. Zhao, L. Zhang and X. Lu, Properties of two-dimensional Ti3C2 MXene/thermoplastic polyurethane nanocomposites with effective reinforcement *via* melt blending, *Compos. Sci. Technol.*, 2019, **181**, 107710.

173 S. Mazhar, A. A. Qarni, Y. U. Haq, Z. U. Haq and I. Murtaza, Promising PVC/MXene based flexible thin film nanocomposites with excellent dielectric, thermal and mechanical properties, *Ceram. Int.*, 2020, **46**(8), 12593–12605.

174 S. Liu, L. Wang, X. Wang, L. Liu, A. Zhou and X. Cao, Preparation, mechanical and thermal characteristics of d-Ti3C2/PVA film, *Mater. Today Commun.*, 2020, **22**, 100799.

175 C. B. Hatter, J. Shah, B. Anasori and Y. Gogotsi, Micromechanical response of two-dimensional transition metal carbonitride (MXene) reinforced epoxy composites, *Composites, Part B*, 2020, **182**, 107603.

176 L. Wang, L. Chen, P. Song, C. Liang, Y. Lu, H. Qiu, Y. Zhang, J. Kong and J. Gu, Fabrication on the annealed Ti3C2Tx MXene/Epoxy nanocomposites for electromagnetic interference shielding application, *Composites, Part B*, 2019, **171**, 111–118.

177 Y. Shi, C. Liu, L. Liu, L. Fu, B. Yu, Y. Lv, F. Yang and P. Song, Strengthening, toughing and thermally stable ultra-thin MXene nanosheets/polypropylene nanocomposites *via* nanoconfinement, *Chem. Eng. J.*, 2019, **378**, 122267.

178 A. Shayesteh Zeraati, S. A. Mirkhani, P. Sun, M. Naguib, P. V. Braun and U. Sundararaj, Improved synthesis of Ti3C2Tx MXenes resulting in exceptional electrical conductivity, high synthesis yield, and enhanced capacitance, *Nanoscale*, 2021, **13**(6), 3572–3580, DOI: 10.1039/D0NR06671K.

179 M. Naguib, T. Saito, S. Lai, M. S. Rager, T. Aytug, M. Parans Paranthaman, M.-Q. Zhao and Y. Gogotsi, Ti3C2Tx (MXene)–polyacrylamide nanocomposite films, *RSC Adv.*, 2016, **6**(76), 72069–72073, DOI: 10.1039/C6RA10384G.

180 Z. Hadi, J. K. Yeganeh, Y. Zare, M. T. Munir and K. Y. Rhee, Predicting of electrical conductivity for Polymer-MXene nanocomposites, *J. Mater. Res. Technol.*, 2024, **28**, 4229–4238, DOI: 10.1016/j.jmrt.2024.01.014.

181 Y. Yu, P. Yi, W. Xu, X. Sun, G. Deng, X. Liu, J. Shui and R. Yu, Environmentally Tough and Stretchable MXene Organohydrogel with Exceptionally Enhanced Electromagnetic Interference Shielding Performances, *Nano–Micro Lett.*, 2022, **14**(1), 77, DOI: 10.1007/s40820-022-00819-3.

182 W.-T. Cao, F.-F. Chen, Y.-J. Zhu, Y.-G. Zhang, Y.-Y. Jiang, M.-G. Ma and F. Chen, Binary Strengthening and Toughening of MXene/Cellulose Nanofiber Composite Paper with Nacre-Inspired Structure and Superior Electromagnetic Interference Shielding Properties, *ACS Nano*, 2018, **12**(5), 4583–4593, DOI: 10.1021/acsnano.8b00997.

183 D. Wang, Y. Lin, D. Hu, P. Jiang and X. Huang, Multifunctional 3D-MXene/PDMS nanocomposites for electrical, thermal and triboelectric applications, *Composites, Part A*, 2020, **130**, 105754.

184 E. A. Mayerberger, O. Urbanek, R. M. McDaniel, R. M. Street, M. W. Barsoum and C. L. Schauer, Preparation and characterization of polymer-Ti3C2Tx (MXene) composite nanofibers produced *via* electrospinning, *J. Appl. Polym. Sci.*, 2017, **134**(37), 45295.

185 M. Naguib, T. Saito, S. Lai, M. S. Rager, T. Aytug, M. P. Paranthaman, M.-Q. Zhao and Y. Gogotsi, Ti3C2Tx (MXene)–polyacrylamide nanocomposite films, *RSC Adv.*, 2016, **6**(76), 72069–72073.

186 P. Sobolčiak, A. Ali, M. K. Hassan, M. I. Helal, A. Tanvir, A. Popelka, M. A. Al-Maadeed, I. Krupa and K. A. Mahmoud, 2D Ti3C2Tx (MXene)-reinforced polyvinyl alcohol (PVA) nanofibers with enhanced mechanical and electrical properties, *PLoS One*, 2017, **12**(8), e0183705.

187 R. Sun, H. B. Zhang, J. Liu, X. Xie, R. Yang, Y. Li, S. Hong and Z. Z. Yu, Highly conductive transition metal carbide/carbonitride (MXene)@ polystyrene nanocomposites fabricated by electrostatic assembly for highly efficient electromagnetic interference shielding, *Adv. Funct. Mater.*, 2017, **27**(45), 1702807.

188 S. Tu, Q. Jiang, X. Zhang and H. N. Alshareef, Large dielectric constant enhancement in MXene percolative polymer composites, *ACS Nano*, 2018, **12**(4), 3369–3377.

189 C. Han, H. Zhang, Q. Chen, T. Li, L. Kong, H. Zhao and L. He, A directional piezoelectric sensor based on anisotropic PVDF/MXene hybrid foam enabled by unidirectional freezing, *Chem. Eng. J.*, 2022, **450**, 138280, DOI: 10.1016/j.cej.2022.138280.

190 M. Safarkhani, B. F. Far, Y. Huh and N. Rabiee, Thermally Conductive MXene, *ACS Biomater. Sci. Eng.*, 2023, **9**(12), 6516–6530, DOI: **10.1021/acsbiomaterials.3c01420**.

191 R. Liu and W. Li, High-Thermal-Stability and High-Thermal-Conductivity Ti3C2Tx MXene/Poly(vinyl alcohol) (PVA) Composites, *ACS Omega*, 2018, **3**(3), 2609–2617, DOI: **10.1021/acsomega.7b02001**.

192 Y. Cao, Q. Deng, Z. Liu, D. Shen, T. Wang, Q. Huang, S. Du, N. Jiang, C.-T. Lin and J. Yu, Enhanced thermal properties of poly(vinylidene fluoride) composites with ultrathin nanosheets of MXene, *RSC Adv.*, 2017, **7**(33), 20494–20501, DOI: **10.1039/C7RA00184C**.

193 C. Ji, Y. Wang, Z. Ye, L. Tan, D. Mao, W. Zhao, X. Zeng, C. Yan, R. Sun, D. J. Kang, *et al.*, Ice-Templated MXene/Ag–Epoxy Nanocomposites as High-Performance Thermal Management Materials, *ACS Appl. Mater. Interfaces*, 2020, **12**(21), 24298–24307, DOI: **10.1021/acsami.9b22744**.

194 M. Wang, Y. Liu, H. Zhang, Y. Wu and L. Pan, Thermal conductivities of Ti3C2Tx MXenes and their interfacial thermal performance in MXene/epoxy composites – a molecular dynamics simulation, *Int. J. Heat Mass Transfer*, 2022, **194**, 123027, DOI: **10.1016/j.ijheatmasstransfer.2022.123027**.

195 H. Gholivand, S. Fuladi, Z. Hemmat, A. Salehi-Khojin and F. Khalili-Araghi, Effect of surface termination on the lattice thermal conductivity of monolayer Ti3C2Tz MXenes, *J. Appl. Phys.*, 2019, **126**(6), 065101, DOI: **10.1063/1.5094294**.

196 Y. Cao, Q. Deng, Z. Liu, D. Shen, T. Wang, Q. Huang, S. Du, N. Jiang, C.-T. Lin and J. Yu, Enhanced thermal properties of poly (vinylidene fluoride) composites with ultrathin nanosheets of MXene, *RSC Adv.*, 2017, **7**(33), 20494–20501.

197 R. Liu and W. Li, High-thermal-stability and high-thermal-conductivity Ti3C2Tx MXene/poly (vinyl alcohol)(PVA) composites, *ACS Omega*, 2018, **3**(3), 2609–2617.

198 C. Yan, C. Ji, X. Zeng, R. Sun and C.-P. Wong, Interconnecting the promising MXenes *via* Ag nanowire in epoxy nanocomposites for high-performance thermal management applications, in *2018 19th International Conference on Electronic Packaging Technology (ICEPT)*, IEEE, 2018, pp. 510–512.

199 R. Kang, Z. Zhang, L. Guo, J. Cui, Y. Chen, X. Hou, B. Wang, C.-T. Lin, N. Jiang and J. Yu, Enhanced thermal conductivity of epoxy composites filled with 2D transition metal carbides (MXenes) with ultralow loading, *Sci. Rep.*, 2019, **9**(1), 9135.

200 Z. Y. Huang, S. J. Wang, S. Kota, Q. W. Pan, M. W. Barsoum and C. Y. Li, Structure and crystallization behavior of poly(ethylene oxide)/Ti3C2Tx MXene nanocomposites, *Polymer*, 2016, **102**, 119–126, DOI: **10.1016/j.polymer.2016.09.011**.

201 M. Carey, Z. Hinton, V. Natu, R. Pai, M. Sokol, N. J. Alvarez, V. Kalra and M. W. Barsoum, Dispersion and Stabilization of Alkylated 2D MXene in Nonpolar Solvents and Their Pseudocapacitive Behavior, *Cell Rep. Phys. Sci.*, 2020, **1**(4), 100042, DOI: **10.1016/j.xcrp.2020.100042**.

202 L. F. Wei, J. Z. Ma, W. B. Zhang, Z. Y. Pan, Z. L. Ma, S. L. Kang and Q. Q. Fan, Enhanced Antistatic and Self-Heatable Wearable Coating with Self-Tiered Structure Caused by Amphiphilic MXene in Waterborne Polymer, *Langmuir*, 2020, **36**(23), 6580–6588, DOI: **10.1021/acs.langmuir.9b03943**.

203 (*a*) S. Srivatsa, P. Packo, L. Mishnaevsky, T. Uhl and K. Grabowski, Deformation of Bioinspired MXene-Based Polymer Composites with Brick and Mortar Structures: A Computational Analysis, *Materials*, 2020, **13**(22), 5189, DOI: **10.3390/ma13225189**; (*b*) H. W. Mao, C. Gu, S. Q. Yan, Q. Xin, S. Cheng, P. Tan, X. J. Wang, F. Xiu, X. Q. Liu, J. Q. Liu, *et al.*, MXene Quantum Dot/Polymer Hybrid Structures with Tunable Electrical Conductance and Resistive Switching for Nonvolatile Memory Devices, *Adv. Electron. Mater.*, 2020, **6**(1), 1900493, DOI: **10.1002/aelm.201900493**; (*c*) X. Jin, W. S. Zhang, S. Y. Liu, T. P. Zhang, Z. H. Song, W. L. Shao, R. Y. Mao, M. Yao, X. G. Jian and F. Y. Hu, Highly stable Ti3C2Tx MXene-based sandwich-like structure *via* interfacial self-assembly of nitrogen-rich polymer network for superior sodium-ion storage performance, *Chem. Eng. J.*, 2023, **451**, 138763, DOI: **10.1016/j.cej.2022.138763**; (*d*) F. C. Sun, X. Z. Wang, D. C. Wu, M. El-Khouly, T. A. Zheng, B. Zhang and Y. Chen, Conjugated Polymer-Functionalized 2D MXene Nanosheets for Nonvolatile Memory Devices with High Environmental Stability, *ACS Appl. Nano Mater.*, 2023, **6**(9), 7186–7195, DOI: **10.1021/acsanm.3c00220**.

204 C. T. Lan, H. Jia, M. H. Qiu and S. H. Fu, Ultrathin MXene/Polymer Coatings with an Alternating Structure on Fabrics for Enhanced Electromagnetic Interference Shielding and Fire-Resistant Protective Performances, *ACS Appl. Mater. Interfaces*, 2021, **13**(32), 38761–38772, DOI: **10.1021/acsami.1c11638**.

205 Y. W. Cao, Y. C. Jia, X. D. Meng, X. Y. Fan, J. Zhang, J. Zhou, D. Matoga, C. W. Bielawski and J. X. Geng, Covalently grafting conjugated porous polymers to MXene offers a two-dimensional sandwich-structured electrocatalytic sulfur host for lithium-sulfur batteries, *Chem. Eng. J.*, 2022, **446**, 137365, DOI: **10.1016/j.cej.2022.137365**.

206 Q. Y. Guan, H. J. Yan and Y. Q. Cai, Strongly Modulated Exfoliation and Functionalization of MXenes with Rationally Designed Groups in Polymer: A Theoretical Study, *Chem. Mater.*, 2022, **34**(21), 9414–9424, DOI: **10.1021/acs.chemmater.2c01721**.

207 P. Zhang, X. J. Yang, P. Li, Y. Y. Zhao and Q. J. Niu, Fabrication of novel MXene (Ti3C2)/polyacrylamide nanocomposite hydrogels with enhanced mechanical and drug release properties, *Soft Matter*, 2020, **16**(1), 162–169, DOI: **10.1039/c9sm01985e**.

208 J. T. Lee, B. C. Wyatt, G. A. Davis, A. N. Masterson, A. L. Pagan, A. Shah, B. Anasori and R. Sardar, Covalent Surface Modification of Ti3C2Tx MXene with Chemically Active Polymeric Ligands Producing Highly Conductive and Ordered Microstructure Films, *ACS Nano*, 2021, **15**(12), 19600–19612, DOI: **10.1021/acsnano.1c06670**.

209 Q. Q. Guo, X. X. Zhang, F. Y. Zhao, Q. C. Song, G. H. Su, Y. X. Tan, Q. C. Tao, T. Zhou, Y. M. Yu, Z. H. Zhou, *et al.*, Protein-Inspired Self-Healable Ti3C2 MXenes/Rubber-Based Supramolecular Elastomer for Intelligent Sensing, *ACS Nano*, 2020, **14**(3), 2788–2797, DOI: **10.1021/acsnano.9b09802**.

210 (*a*) S. B. Tu, Q. Jiang, J. W. Zhang, X. He, M. N. Hedhili, X. X. Zhang and H. N. Alshareef, Enhancement of Dielectric Permittivity of Ti3C2Tx, MXene/Polymer Composites by Controlling Flake Size and Surface Termination, *ACS Appl. Mater. Interfaces*, 2019, **11**(30), 27358–27362, DOI: **10.1021/acsami.9b09137**; (*b*) C. I. Idumah, Influence of surfaces and interfaces on MXene and MXene hybrid polymeric nanoarchitectures, properties, and applications, *J. Mater. Sci.*, 2022, **57**(31), 14579–14619, DOI: **10.1007/s10853-022-07526-9**.

211 C. Y. Jiao, Z. M. Deng, P. Min, J. J. Lai, Q. Q. Gou, R. Gao, Z. Z. Yu and H. B. Zhang, Photothermal healable, stretchable, and conductive MXene composite films for efficient electromagnetic interference shielding, *Carbon*, 2022, **198**, 179–187, DOI: **10.1016/j.carbon.2022.07.017**.

212 W. Eom, H. Shin, R. B. Ambade, S. H. Lee, K. H. Lee, D. J. Kang and T. H. Han, Large-scale wet-spinning of highly electroconductive MXene fibers, *Nat. Commun.*, 2020, **11**(1), 2825, DOI: **10.1038/s41467-020-16671-1**.

213 W. Q. Tian, A. VahidMohammadi, Z. Wang, L. Q. Ouyang, M. Beidaghi and M. M. Hamedi, Layer-by-layer self-assembly of pillared two-dimensional multilayers, *Nat. Commun.*, 2019, **10**, 2558, DOI: **10.1038/s41467-019-10631-0**.

214 X. Y. Wu, B. Y. Han, H. B. Zhang, X. Xie, T. X. Tu, Y. Zhang, Y. Dai, R. Yang and Z. Z. Yu, Compressible, durable and conductive polydimethylsiloxane-coated MXene foams for high-performance electromagnetic interference shielding, *Chem. Eng. J.*, 2020, **381**, 122622, DOI: **10.1016/j.cej.2019.122622**.

215 Y. Pan, M. He, J. Wu, H. Qi and Y. Cheng, One-step synthesis of MXene-functionalized PEDOT:PSS conductive polymer hydrogels for wearable and noninvasive monitoring of sweat glucose, *Sens. Actuators, B*, 2024, **401**, 135055, DOI: **10.1016/j.snb.2023.135055**.

216 (*a*) J. J. Yin, F. K. Zhan, T. F. Jiao, H. Z. Deng, G. D. Zou, Z. H. Bai, Q. R. Zhang and Q. M. Peng, Highly efficient catalytic performances of nitro compounds *via* hierarchical PdNPs-loaded MXene/polymer nanocomposites synthesized through electrospinning strategy for wastewater treatment, *Chin. Chem. Lett.*, 2020, **31**(4), 992–995, DOI: **10.1016/j.cclet.2019.08.047**; (*b*) X. X. Huang, R. Wang, T. F. Jiao, G. D. Zou, F. K. Zhan, J. J. Yin, L. X. Zhang, J. X. Zhou and Q. M. Peng, Facile Preparation of Hierarchical AgNP-Loaded MXene/Fe3O4/Polymer Nanocomposites by Electrospinning with Enhanced Catalytic Performance for Wastewater Treatment, *ACS Omega*, 2019, **4**(1), 1897–1906, DOI: **10.1021/acsomega.8b03615**.

217 C. M. Jiang, C. Wu, X. J. Li, Y. Yao, L. Y. Lan, F. N. Zhao, Z. Z. Ye, Y. B. Ying and J. F. Ping, All-electrospun flexible triboelectric nanogenerator based on metallic MXene nanosheets, *Nano Energy*, 2019, **59**, 268–276, DOI: **10.1016/j.nanoen.2019.02.052**.

218 J. Yun, I. Echols, P. Flouda, S. Y. Wang, A. Easley, X. F. Zhao, Z. Y. Tan, E. Prehn, G. Zi, M. Radovic, *et al.*, Layer-by-Layer Assembly of Polyaniline Nanofibers and MXene Thin-Film Electrodes for Electrochemical Energy Storage, *ACS Appl. Mater. Interfaces*, 2019, **11**(51), 47929–47938, DOI: **10.1021/acsami.9b16692**.

219 H. Zhang, L. B. Wang, A. G. Zhou, C. J. Shen, Y. H. Dai, F. F. Liu, J. F. Chen, P. Li and Q. K. Hu, Effects of 2-D transition metal carbide Ti2CTx on properties of epoxy composites, *RSC Adv.*, 2016, **6**(90), 87341–87352, DOI: **10.1039/c6ra14560d**.

220 S. S. Zhang, T. T. Tu, T. Y. Li, Y. Cai, Z. Y. Wang, Y. Zhou, D. Wang, L. Fang, X. S. Ye and B. Liang, 3D MXene/PEDOT:PSS Composite Aerogel with a Controllable Patterning Property for Highly Sensitive Wearable Physical Monitoring and Robotic Tactile Sensing, *ACS Appl. Mater. Interfaces*, 2022, **14**(20), 23877–23887, DOI: **10.1021/acsami.2c03350**.

221 Y. C. Chen, Y. F. Lin, C. T. Liu, Y. C. Liu, M. H. Lin, G. Y. Lan, Y. S. Cheng, H. L. Yu, C. C. Huang, H. T. Chang, *et al.*, Facilitation of Osteogenic Differentiation of hASCs on PEDOT:PSS/MXene Composite Sponge with Electrical Stimulation, *ACS Appl. Polym. Mater.*, 2023, **5**(7), 4753–4766, DOI: **10.1021/acsapm.3c00146**.

222 K. Liu, H. S. Du, W. Liu, M. Zhang, Y. X. Wang, H. Y. Liu, X. Y. Zhang, T. Xu and C. L. Si, Strong, flexible, and highly conductive cellulose nanofibril/PEDOT:PSS/MXene nanocomposite films for efficient electromagnetic interference shielding, *Nanoscale*, 2022, **14**(40), 14902–14912, DOI: **10.1039/d2nr00468b**.

223 G. J. Chang, L. J. Zeng, L. Xie, B. Xue and Q. Zheng, Ultrathin multifunctional electromagnetic interference shielding MXene/AgNWs/PEDOT:PSS coatings with superior electro/photo-thermal transition ability and water repellency, *Chem. Eng. J.*, 2023, **470**, 144033, DOI: **10.1016/j.cej.2023.144033**.

224 Q. Gu, J. Wang, R. X. Peng, W. Song, R. Zhou and Z. Y. Ge, Nonfullerene Organic Solar Cells with 18.17% Efficiency Obtained Using a V2C/PEDOT:PSS Composite Hole-Transport Layer, *ACS Appl. Energy Mater.*, 2023, DOI: **10.1021/acsaem.2c03883**.

225 B. Z. Deng, H. Lian, B. T. Xue, R. C. Song, S. Chen, Z. H. Wang, T. Xu, H. L. Dong and S. H. Wang, Niobium-Carbide MXene Modified Hybrid Hole Transport Layer Enabling High-Performance Organic Solar Cells Over 19%, *Small*, 2023, **19**(23), DOI: **10.1002/smll.202207505**.

226 V. T. Nguyen, B. K. Min, Y. Yi, S. J. Kim and C. G. Choi, MXene(Ti3C2TX)/graphene/PDMS composites for multifunctional broadband electromagnetic interference shielding skins, *Chem. Eng. J.*, 2020, **393**, 124608, DOI: **10.1016/j.cej.2020.124608**.

227 W. B. Zhu, H. S. Luo, Z. H. Tang, H. Zhang, T. Fan, Y. Y. Wang, P. Huang, Y. Q. Li and S. Y. Fu, Ti3C2Tx

MXene/Bamboo Fiber/PDMS Pressure Sensor with Simultaneous Ultrawide Linear Sensing Range, Superb Environmental Stability, and Excellent Biocompatibility, *ACS Sustain. Chem. Eng.*, 2022, **10**(11), 3546–3556, DOI: 10.1021/acssuschemeng.1c07994.

228 X. M. Xu, H. Wu, X. He, M. K. Hota, Z. X. Liu, S. F. Zhuo, H. Kim, X. X. Zhang and H. N. Alshareef, Iontronics Using V2CTx MXene-Derived Metal-Organic Framework Solid Electrolytes, *ACS Nano*, 2020, **14**(8), 9840–9847, DOI: 10.1021/acsnano.0c02497.

229 V. T. Nguyen, Q. D. Nguyen, B. K. Min, Y. Yi and C. G. Choi, Ti3C2Tx MXene/carbon nanotubes/waterborne polyurethane based composite ink for electromagnetic interference shielding and sheet heater applications, *Chem. Eng. J.*, 2022, **430**, 133171, DOI: 10.1016/j.cej.2021.133171.

230 J. Y. Jing, Z. L. Ma, R. C. Jiang, Y. Zhang and L. Shao, Flexible Polyurethane@Ti3C2Tx/Silver Nanowires Composite Films with Cocontinuous Segregated Structures for Superior Electromagnetic Interference Shielding and Joule Heating, *Adv. Eng. Mater.*, 2023, **25**(11), 2201938, DOI: 10.1002/adem.202201938.

231 C. C. Zhao, M. Zhou and H. B. Yu, High water and oxygen reactivity inducing excellent anti-corrosive performance in waterborne Ti2CTx/epoxy composite coating, *Appl. Surf. Sci.*, 2022, **586**, 152880, DOI: 10.1016/j.apsusc.2022.152880.

232 W. Y. Liang and I. Zhitomirsky, MXene-polypyrrole electrodes for asymmetric supercapacitors, *Electrochim. Acta*, 2022, **406**, 139843, DOI: 10.1016/j.electacta.2022.139843.

233 G. Y. Liu, J. H. Zou, Q. Y. Tang, X. Y. Yang, Y. W. Zhang, Q. Zhang, W. Huang, P. Chen, J. J. Shao and X. C. Dong, Surface Modified Ti3C2 MXene Nanosheets for Tumor Targeting Photothermal/Photodynamic/Chemo Synergistic Therapy, *ACS Appl. Mater. Interfaces*, 2017, **9**(46), 40077–40086, DOI: 10.1021/acsami.7b13421.

234 E. A. Mayerberger, R. M. Street, R. M. McDaniel, M. W. Barsoum and C. L. Schauer, Antibacterial properties of electrospun Ti3C2Tz (MXene)/chitosan nanofibers, *RSC Adv.*, 2018, **8**(62), 35386–35394, DOI: 10.1039/c8ra06274a.

235 T. Yousaf, A. Areeb, M. Murtaza, A. Munir, Y. Khan and A. Waseem, Silane-Grafted MXene (Ti3C2TX) Membranes for Enhanced Water Purification Performance, *ACS Omega*, 2022, **7**(23), 19502–19512, DOI: 10.1021/acsomega.2c01143.

236 C. Likitaporn, M. Okhawilai, P. Kasemsiri, J. Q. Qin, P. Potiyaraj and H. Uyama, High electrolyte uptake of MXene integrated membrane separators for Zn-ion batteries, *Sci. Rep.*, 2022, **12**(1), 19915, DOI: 10.1038/s41598-022-24578-8.

237 G. Basara, M. Saeidi-Javash, X. Ren, G. Bahcecioglu, B. C. Wyatt, B. Anasori, Y. L. Zhang and P. Zorlutuna, Electrically conductive 3D printed Ti(3)C(2)Tx MXene-PEG composite constructs for cardiac tissue engineering, *Acta Biomater.*, 2022, **139**, 179–189, DOI: 10.1016/j.actbio.2020.12.033.

238 C. G. Jiang, W. Y. Xie and D. F. Wu, Balancing the Overall Performance of Poly(vinyl alcohol)/MXene Composite Organohydrogels for Flexible Strain Sensors, *ACS Appl. Polym. Mater.*, 2023, **5**(1), 370–380, DOI: 10.1021/acsapm.2c01546370.

239 J. H. Liu, X. J. Meng, F. Dong, S. Y. Ren, B. Wang and F. Tan, Highly Stretchable and Sensitive Ti3C2TX MXene/Sodium Alginate/Acrylamide Hydrogel for Flexible Electronic Sensors, *ACS Appl. Polym. Mater.*, 2022, 8216–8226, DOI: 10.1021/acsapm.2c01169.

240 T. T. Tang, S. C. Wang, Y. Jiang, Z. G. Xu, Y. Chen, T. S. Peng, F. Khan, J. B. Feng, P. G. Song and Y. Zhao, Flexible and flame-retarding phosphorylated MXene/polypropylene composites for efficient electromagnetic interference shielding, *J. Mater. Sci. Technol.*, 2022, **111**, 66–75, DOI: 10.1016/j.jmst.2021.08.091.

241 Y. K. Zhang, C. Chen, Z. F. Chen, T. T. Zhang, Y. L. Wang, S. Y. Cao and J. Ma, Superior Anticorrosion Performance of Well-Dispersed MXene- Polymer Composite Coatings Enabled by Covalent Modification and Ambient Electron-Beam Curing, *ACS Appl. Mater. Interfaces*, 2023, **15**(8), 11099–11110, DOI: 10.1021/acsami.2c22184.

242 (*a*) Y. Qian, J. Zhong and J. P. Ou, Improvement in alkali-resistance of basalt fiber-reinforced polymer by Ti3C2TX (MXene) modified matrix, *Polym. Compos.*, 2023, **44**(4), 2581–2591, DOI: 10.1002/pc.27265; (*b*) K. Hou, Y. F. Yang, H. Zhou, X. M. Chen and S. B. Ge, Enhanced Yield of Large-Sized Ti3C2Tx MXene Polymers Nanosheets *via* Cyclic Ultrasonic-Centrifugal Separation, *Polymers*, 2023, **15**(6), 1330, DOI: 10.3390/polym15061330.

243 T. M. Kim, B. Ryplida, G. B. Lee and S. Y. Park, Cancer cells targeting H2O2-responsive MXene-integrated hyaluronic acid polymer dots coated sensor, *J. Ind. Eng. Chem.*, 2023, **120**, 188–194, DOI: 10.1016/j.jiec.2022.12.025.

244 Y. Zhou, Y. B. Zou, Z. Y. Peng, C. Y. Yu and W. B. Zhong, Arbitrary deformable and high-strength electroactive polymer/MXene anti-exfoliative composite films assembled into high performance, flexible all-solid-state supercapacitors, *Nanoscale*, 2020, **12**(40), 20797–20810, DOI: 10.1039/d0nr04980h.

245 Q. H. Deng, Y. F. Feng, W. Li, X. Q. Xu, C. Peng and Q. Wu, Strong interface effect induced high-k property in polymer based ternary composites filled with 2D layered Ti3C2 MXene nanosheets, *J. Mater. Sci.:Mater. Electron.*, 2019, **30**(10), 9106–9113, DOI: 10.1007/s10854-019-01239-7.

246 (*a*) X. H. Zheng, J. K. Shen, Q. L. Hu, W. Q. Nie, Z. Q. Wang, L. H. Zou and C. L. Li, Vapor phase polymerized conducting polymer/MXene textiles for wearable electronics, *Nanoscale*, 2021, **13**(3), 1832–1841, DOI: 10.1039/d0nr07433k; (*b*) S. Sharma, A. Chhetry, S. Ko and J. Y. Park, Highly Sensitive and Stable Pressure Sensor Based on Polymer-Mxene Composite Nanofiber Mat for Wearable Health Monitoring, *Proc. – IEEE Micro Electro.*, 2020, 810–813; (*c*) K. N. Kim, S. Y. Kim, S. H. Choi, M. Lee, W. Song, J. Lim, S. S. Lee and S. Myung, All-Printed Wearable Triboelectric Nanogenerator with Ultra-Charged Electron Accumulation Polymers Based on MXene Nanoflakes, *Adv. Electron.*

Mater., 2022, **8**(12), 2200819, DOI: **10.1002/aelm.202200819**.

247 (*a*) R. N. Zhang, Q. Liu, Z. Z. Wang, X. D. Yang and Y. X. Guo, Conductive polymer doped two-dimensional MXene materials: opening the channel of magnesium ion transport, *RSC Adv.*, 2022, **12**(7), 4329–4335, DOI: **10.1039/d1ra08690a**; (*b*) D. Parajuli, N. Murali, K. C. Devendra, B. Karki, K. Samatha, A. A. Kim, M. Park and B. Pant, Advancements in MXene–polymer Nanocomposites in Energy Storage and Biomedical Applications, *Polymers*, 2022, **14**(16), 3433, DOI: **10.3390/polym14163433**.

248 Z. H. Zhou, W. Panatdasirisuk, T. S. Mathis, B. Anasori, C. H. Lu, X. X. Zhang, Z. W. Liao, Y. Gogotsi and S. Yang, Layer-by-layer assembly of MXene and carbon nanotubes on electrospun polymer films for flexible energy storage, *Nanoscale*, 2018, **10**(13), 6005–6013, DOI: **10.1039/c8nr00313k**.

249 (*a*) Y. Q. Liu, D. R. Xu, Y. Ding, X. X. Lv, T. T. Huang, B. L. Yuan, L. Jiang, X. Y. Sun, Y. Q. Yao and J. Tang, A conductive polyacrylamide hydrogel enabled by dispersion-enhanced MXene@chitosan assembly for highly stretchable and sensitive wearable skin, *J. Mater. Chem. B*, 2021, **9**(42), 8862–8870, DOI: **10.1039/d1tb01798e**; (*b*) K. Maleski, V. N. Mochalin and Y. Gogotsi, Dispersions of Two-Dimensional Titanium Carbide MXene in Organic Solvents, *Chem. Mater.*, 2017, **29**(4), 1632–1640, DOI: **10.1021/acs.chemmater.6b04830**.

250 K. Li, X. H. Wang, S. Li, P. Urbankowski, J. M. Li, Y. X. Xu and Y. Gogotsi, An Ultrafast Conducting Polymer@MXene Positive Electrode with High Volumetric Capacitance for Advanced Asymmetric Supercapacitors, *Small*, 2020, **16**(4), 1906851, DOI: **10.1002/smll.201906851**.

251 (*a*) W. Z. Bao, L. Liu, C. Y. Wang, S. Choi, D. Wang and G. X. Wang, Facile Synthesis of Crumpled Nitrogen-Doped MXene Nanosheets as a New Sulfur Host for Lithium-Sulfur Batteries, *Adv. Energy Mater.*, 2018, **8**(13), 1702485, DOI: **10.1002/aenm.201702485**; (*b*) S. M. Z. Mehdi, H. Ghulam Abbas, M. Ali, S. B. H. Rizvi, S. R. Choi, J. C. Goak, Y. Seo, S. Kumar and N. Lee, Enhanced Electrochemical Performance and Theoretical Insights of Ni-Intercalated Ti3C2Tx MXene, *Energy Environ. Mater.*, 2025, e12876.

252 J. K. Harris and E. L. Ratcliff, Ion diffusion coefficients in poly(3-alkylthiophenes) for energy conversion and biosensing: role of side-chain length and microstructure, *J. Mater. Chem. C*, 2020, **8**(38), 13319–13327, DOI: **10.1039/d0tc03690k**.

253 C. Chen, M. Boota, X. Q. Xie, M. Q. Zhao, B. Anasori, C. E. Ren, L. Miao, J. J. Jiang and Y. Gogotsi, Charge transfer induced polymerization of EDOT confined between 2D titanium carbide layers, *J. Mater. Chem. A*, 2017, **5**(11), 5260–5265, DOI: **10.1039/c7ta00149e**.

254 H. Xue, P.-H. Huang, M. Göthelid, A. Strömberg, F. Niklaus and J. Li, Ultrahigh-Rate On-Paper PEDOT:PSS-Ti2C Microsupercapacitors with Large Areal Capacitance, *Adv. Funct. Mater.*, 2024, **34**(49), 2409210, DOI: **10.1002/adfm.202409210**.

255 Y. Yao, W. Feng, M. Chen, X. Zhong, X. Wu, H. Zhang and Y. Yu, Boosting the Electrochemical Performance of Li–S Batteries with a Dual Polysulfides Confinement Strategy, *Small*, 2018, **14**(42), 1802516, DOI: **10.1002/smll.201802516**.

256 L. Q. Qin, Q. Z. Tao, X. J. Liu, M. Fahlman, J. Halim, P. O. A. Perssona, J. Rosen and F. L. Zhang, Polymer-MXene composite films formed by MXene-facilitated electrochemical polymerization for flexible solid-state microsupercapacitors, *Nano Energy*, 2019, **60**, 734–742, DOI: **10.1016/j.nanoen.2019.04.002**.

257 (*a*) S. M. Liu, M. X. Chen, Y. Xie, D. H. Liu, J. F. Zheng, X. Xiong, H. Jiang, L. C. Wang, H. Luo and K. Han, Nb2CTx MXene boosting PEO polymer electrolyte for all-solid-state Li-S batteries: two birds with one stone strategy to enhance Li+ conductivity and polysulfide adsorptivity, *Rare Met.*, 2023, **42**, 2562–2576, DOI: **10.1007/s12598-022-02260-2**; (*b*) Y. X. Zhang, F. Wu, Y. X. Huang, S. J. Li, C. Li, Z. H. Wang and M. Xie, A novel gel polymer electrolyte doped with MXene enables dendrite-free cycling for high-performance sodium metal batteries, *J. Mater. Chem. A*, 2022, **10**(21), 11553–11561, DOI: **10.1039/d2ta00452f**; (*c*) H. S. Xu, H. Zhang, Y. F. Wang, C. Tang, T. Y. Xiao, Z. Xu, H. Li, F. G. Xu and Y. Y. Mai, Two-dimensional sandwich-like MXene-conductive polymer nanocomposite with in-plane cylindrical mesopores for long cycling lithium-sulfur batteries, *2d Mater*, 2023, **10**(2), 024006, DOI: **10.1088/2053-1583/acbec4**; (*d*) Q. W. Pan, Y. W. Zheng, S. Kota, W. C. Huang, S. J. Wang, H. Qi, S. Kim, Y. F. Tu, M. W. Barsoum and C. Y. Li, 2D MXene-containing polymer electrolytes for all-solid-state lithium metal batteries, *Nanoscale Adv.*, 2019, **1**(1), 395–402, DOI: **10.1039/c8na00206a**.

258 C. K. Liu, Y. Tian, Y. L. An, Q. L. Yang, S. L. Xiong, J. K. Feng and Y. T. Qian, Robust and flexible polymer/MXene-derived two dimensional TiO2 hybrid gel electrolyte for dendrite-free solid-state zinc-ion batteries, *Chem. Eng. J.*, 2022, **430**, 132748, DOI: **10.1016/j.cej.2021.132748**.

259 X. Li, Y. L. Lu, Z. H. Shi, G. Liu, G. Xu, Z. J. An, H. Xing, Q. M. Chen, R. P. S. Han and Q. J. Liu, Onion-inspired MXene/chitosan-quercetin multilayers: Enhanced response to H2O molecules for wearable human physiological monitoring, *Sensor. Actuator. B Chem.*, 2021, **329**, 129209, DOI: **10.1016/j.snb.2020.129209**.

260 J. Zhou, S. H. H. Shokouh, H. P. Komsa, L. Rieppo, L. F. Cui, Z. P. Lv and K. Kordas, MXene–polymer Hybrid for High-Performance Gas Sensor Prepared by Microwave-Assisted In-Situ Intercalation, *Adv. Mater. Sci. Technol.*, 2022, **7**(9), 2101565, DOI: **10.1002/admt.202101565**.

261 S. Sharma, A. Chhetry, M. Sharifuzzaman, H. Yoon and J. Y. Park, Wearable capacitive pressure sensor based on MXene composite nanofibrous scaffolds for reliable human physiological signal acquisition, *ACS Appl. Mater. Interfaces*, 2020, **12**(19), 22212–22224.

262 K. Wang, Z. Lou, L. L. Wang, L. J. Zhao, S. F. Zhao, D. Y. Wang, W. Han, K. Jiang and G. Z. Shen, Bioinspired Interlocked Structure-Induced High Deformability for

Two-Dimensional Titanium Carbide (MXene)/Natural Microcapsule-Based Flexible Pressure Sensors, *ACS Nano*, 2019, **13**(8), 9139–9147, DOI: 10.1021/acsnano.9b03454.

263 R. Z. Qin, M. J. Hu, X. Li, T. Liang, H. Y. Tan, J. Z. Liu and G. C. Shan, A new strategy for the fabrication of a flexible and highly sensitive capacitive pressure sensor, *Microsyst. Nanoeng.*, 2021, **7**(1), 100, DOI: 10.1038/s41378-021-00327-1.

264 H. Riazi, G. Taghizadeh and M. Soroush, MXene-Based Nanocomposite Sensors, *ACS Omega*, 2021, **6**(17), 11103–11112, DOI: 10.1021/acsomega.0c05828.

265 L. Jin, C. L. Wu, K. Wei, L. F. He, H. Gao, H. X. Zhang, K. Zhang, A. M. Asiri, K. A. Alamry, L. Yang, *et al.*, Polymeric Ti3C2Tx MXene Composites for Room Temperature Ammonia Sensing, *ACS Appl. Nano Mater.*, 2020, **3**(12), 12071–12079, DOI: 10.1021/acsanm.0c02577.

266 G. Ge, Y. Z. Zhang, W. L. Zhang, W. Yuan, J. K. El-Demellawi, P. Zhang, E. Di Fabrizio, X. C. Dong and H. N. Alshareef, Ti3C2Tx MXene-Activated Fast Gelation of Stretchable and Self-Healing Hydrogels: A Molecular Approach, *ACS Nano*, 2021, **15**(2), 2698–2706, DOI: 10.1021/acsnano.0c07998.

267 X. B. Li, L. Z. He, Y. F. Li, M. Y. Chao, M. K. Li, P. B. Wan and L. Q. Zhang, Healable, Degradable, and Conductive MXene Nanocomposite Hydrogel for Multifunctional Epidermal Sensors, *ACS Nano*, 2021, **15**(4), 7765–7773, DOI: 10.1021/acsnano.1c01751.

268 (*a*) Y. M. Shao, Y. Zhu, R. Zheng, P. Wang, Z. Z. Zhao and J. An, Highly sensitive and selective surface molecularly imprinted polymer electrochemical sensor prepared by Au and MXene modified glassy carbon electrode for efficient detection of tetrabromobisphenol A in water, *Adv. Compos. Hybrid Mater.*, 2022, **5**(4), 3104–3116, DOI: 10.1007/s42114-022-00562-8; (*b*) Z. Q. Peng, X. D. Zhang, C. M. Zhao, C. S. Gan and C. H. Zhu, Hydrophobic and stable MXene/reduced graphene oxide/polymer hybrid materials pressure sensors with an ultrahigh sensitive and rapid response speed pressure sensor for health monitoring, *Mater. Chem. Phys.*, 2021, **271**, 124729, DOI: 10.1016/j.matchemphys.2021.124729; (*c*) L. G. Gong, X. X. Qi, K. Yu, J. Q. Gao, B. B. Zhou and G. Y. Yang, Covalent conductive polymer chain and organic ligand ethylenediamine modified MXene-like-{AlW12O40} compounds for fully symmetric supercapacitors, electrochemical sensors and photocatalysis mechanisms, *J. Mater. Chem. A*, 2020, **8**(11), 5709–5720, DOI: 10.1039/c9ta14103k.

269 M. H. Tran, R. Brilmayer, L. Liu, H. Zhuang, C. Hess, A. Andrieu-Brunsen and C. S. Birkel, Synthesis of a smart hybrid MXene with switchable conductivity for temperature sensing, *ACS Appl. Nano Mater.*, 2020, **3**(5), 4069–4076.

270 Y. Zhang, K. Chen, Y. Li, J. Lan, B. Yan, L. Shi and R. Ran, High-strength, self-healable, temperature-sensitive, MXene-containing composite hydrogel as a smart compression sensor, *ACS Appl. Mater. Interfaces*, 2019, **11**(50), 47350–47357.

271 I. J. Echols, H. An, X. Zhao, E. M. Prehn, Z. Tan, M. Radovic, M. J. Green and J. L. Lutkenhaus, pH-Response of polycation/Ti3C2Tx MXene layer-by-layer assemblies for use as resistive sensors, *Mol. Syst. Des. Eng.*, 2020, **5**(1), 366–375.

272 S. Sharma, A. Chhetry, S. Zhang, H. Yoon, M. Sharifuzzaman, X. Hui and J. Y. Park, *ACS Nano*, 2021, **15**, 4380.

273 L. Li, X. Fu, S. Chen, S. Uzun, A. S. Levitt, C. E. Shuck, W. Han and Y. Gogotsi, Hydrophobic and stable MXene–polymer pressure sensors for wearable electronics, *ACS Appl. Mater. Interfaces*, 2020, **12**(13), 15362–15369.

274 X. Shi, H. Wang, X. Xie, Q. Xue, J. Zhang, S. Kang, C. Wang, J. Liang and Y. Chen, Bioinspired ultrasensitive and stretchable MXene-based strain sensor *via* nacre-mimetic microscale "brick-and-mortar" architecture, *ACS Nano*, 2018, **13**(1), 649–659.

275 Y. Lu, X. Qu, W. Zhao, Y. Ren, W. Si, W. Wang, Q. Wang, W. Huang and X. Dong, Highly stretchable, elastic, and sensitive MXene-based hydrogel for flexible strain and pressure sensors, *Research*, 2020, **2020**, 2038560.

276 X. Li, L. He, Y. Li, M. Chao, M. Li, P. Wan and L. Zhang, Healable, degradable, and conductive MXene nanocomposite hydrogel for multifunctional epidermal sensors, *ACS Nano*, 2021, **15**(4), 7765–7773.

277 Q. Wang, X. Pan, C. Lin, H. Gao, S. Cao, Y. Ni and X. Ma, Modified Ti3C2TX (MXene) nanosheet-catalyzed self-assembled, anti-aggregated, ultra-stretchable, conductive hydrogels for wearable bioelectronics, *Chem. Eng. J.*, 2020, **401**, 126129.

278 (*a*) J. Q. Luo, S. Zhao, H. B. Zhang, Z. M. Deng, L. L. Li and Z. Z. Yu, Flexible, stretchable and electrically conductive MXene/natural rubber nanocomposite films for efficient electromagnetic interference shielding, *Compos. Sci. Technol.*, 2019, **182**, 107754, DOI: 10.1016/j.compscitech.2019.107754; (*b*) H. T. Yang, J. L. Li, X. Xiao, J. H. Wang, Y. F. Li, K. R. Li, Z. P. Li, H. C. Yang, Q. Wang, J. Yang, *et al.*, Topographic design in wearable MXene sensors with in-sensor machine learning for full-body avatar reconstruction, *Nat. Commun.*, 2022, **13**(1), 5311, DOI: 10.1038/s41467-022-33021-5; (*c*) J. L. Sun, Y. Chang, L. Dong, K. K. Zhang, Q. L. Hua, J. H. Zang, Q. S. Chen, Y. Y. Shang, C. F. Pan and C. X. Shan, MXene enhanced self-powered alternating current electroluminescence devices for patterned flexible displays, *Nano Energy*, 2021, **86**, 106077, DOI: 10.1016/j.nanoen.2021.106077.

279 Y. J. Wan, X. M. Li, P. L. Zhu, R. Sun, C. P. Wong and W. H. Liao, Lightweight, flexible MXene/polymer film with simultaneously excellent mechanical property and high-performance electromagnetic interference shielding, *Composites, Part A*, 2020, **130**, 105764, DOI: 10.1016/j.compositesa.2020.105764.

280 R. Han, L. Zheng, G. Li, G. Chen, S. Ma, S. Cai and Y. Li, Self-poled poly (vinylidene fluoride)/MXene piezoelectric energy harvester with boosted power generation ability and the roles of crystalline orientation and polarized

interfaces, *ACS Appl. Mater. Interfaces*, 2021, **13**(39), 46738–46748.

281 Q. Zhao, L. Yang, Y. Ma, H. Huang, H. He, H. Ji, Z. Wang and J. Qiu, Highly sensitive, reliable and flexible pressure sensor based on piezoelectric PVDF hybrid film using MXene nanosheet reinforcement, *J. Alloys Compd.*, 2021, **886**, 161069.

282 L. J. Zhao, L. L. Wang, Y. Q. Zheng, S. F. Zhao, W. Wei, D. W. Zhang, X. Y. Fu, K. Jiang, G. Z. Shen and W. Han, Highly-stable polymer-crosslinked 2D MXene-based flexible biocompatible electronic skins for *in vivo* biomonitoring, *Nano Energy*, 2021, **84**, 105921, DOI: 10.1016/j.nanoen.2021.105921.

283 (*a*) X. M. Wu, B. Huang, R. Y. Lv, Q. G. Wang and Y. Wang, Highly flexible and low capacitance loss supercapacitor electrode based on hybridizing decentralized conjugated polymer chains with MXene, *Chem. Eng. J.*, 2019, **378**, 122246, DOI: 10.1016/j.cej.2019.122246; (*b*) K. Raagulan, R. Braveenth, B. M. Kim, K. J. Lim, S. B. Lee, M. Kim and K. Y. Chai, An effective utilization of MXene and its effect on electromagnetic interference shielding: flexible, free-standing and thermally conductive composite from MXene-PAT-poly(p-aminophenol)-polyaniline co–polymer, *RSC Adv.*, 2020, **10**(3), 1613–1633, DOI: 10.1039/c9ra09522e; (*c*) N. Kong, K. Lv, W. T. Chen, J. Guan, P. F. Zhao, J. L. Tao and J. Z. Zhang, Natural Polymer Template for Low-Cost Producing HighPerformance Ti3C2Tx MXene Electrodes for Flexible Supercapacitors, *ACS Appl. Mater. Interfaces*, 2022, **14**(51), 56877–56885, DOI: 10.1021/acsami.2c18559; (*d*) G. S. Gund, J. H. Park, R. Harpalsinh, M. Kota, J. H. Shin, T. I. Kim, Y. Gogotsi and H. S. Park, MXene/Polymer Hybrid Materials for Flexible AC-Filtering Electrochemical Capacitors, *Joule*, 2019, **3**(1), 164–176, DOI: 10.1016/j.joule.2018.10.017.

284 J. Yun, J. Park, M. Ryoo, N. Kitchamsetti, T. S. Goh and D. Kim, Piezo-triboelectric hybridized nanogenerator embedding MXene based bifunctional conductive filler in polymer matrix for boosting electrical power, *Nano Energy*, 2023, **105**, 108018.

285 S. Wang, H.-Q. Shao, Y. Liu, C.-Y. Tang, X. Zhao, K. Ke, R.-Y. Bao, M.-B. Yang and W. Yang, Boosting piezoelectric response of PVDF–TrFE *via* MXene for self-powered linear pressure sensor, *Compos. Sci. Technol.*, 2021, **202**, 108600.

286 M. Guo, J. Jiang, J. Qian, C. Liu, J. Ma, C. W. Nan and Y. Shen, Flexible robust and high-density FeRAM from array of organic ferroelectric nano-lamellae by self-assembly, *Advanced Science*, 2019, **6**(6), 1801931.

287 P. Martins, A. Lopes and S. Lanceros-Mendez, Electroactive phases of poly (vinylidene fluoride): Determination, processing and applications, *Prog. Polym. Sci.*, 2014, **39**(4), 683–706.

288 F. Mokhtari, K. A. S. Usman, J. Zhang, R. Komljenovic, Z. a. Simon, B. Dharmasiri, A. Rezk, P. C. Sherrell, L. C. Henderson and R. J. Varley, Enhanced Acoustoelectric Energy Harvesting with Ti3C2Tx MXene in an All-Fiber Nanogenerator, *ACS Appl. Mater. Interfaces*, 2025, **17**(2), 3214–3228.

289 S. S. Rana, M. T. Rahman, M. Salauddin, S. Sharma, P. Maharjan, T. Bhatta, H. Cho, C. Park and J. Y. Park, Electrospun PVDF–TrFE/MXene nanofiber mat-based triboelectric nanogenerator for smart home appliances, *ACS Appl. Mater. Interfaces*, 2021, **13**(4), 4955–4967.

290 L. Kou, R. Haque, R. Sadri, R. Z. Auliya, M. Kaur, E. P. Roberts, W. C. Gan, M. A. S. Mohammad Haniff, C. F. Dee and P. C. Ooi, Enhanced Piezoelectric Nanogenerator Based on Tridoped Graphene and Ti3CNTx MXene Quasi-3D Heterostructure, *Ind. Eng. Chem. Res.*, 2024, **63**(36), 15853–15868.

291 Y. Kim, X. Wu, C. Lee and J. H. Oh, Characterization of PI/PVDF–TrFE composite nanofiber-based triboelectric nanogenerators depending on the type of the electrospinning system, *ACS Appl. Mater. Interfaces*, 2021, **13**(31), 36967–36975.

292 G. Min, A. Pullanchiyodan, A. S. Dahiya, E. S. Hosseini, Y. Xu, D. M. Mulvihill and R. Dahiya, Ferroelectric-assisted high-performance triboelectric nanogenerators based on electrospun P (VDF–TrFE) composite nanofibers with barium titanate nanofillers, *Nano Energy*, 2021, **90**, 106600.

293 D. Wang, D. Zhang, P. Li, Z. Yang, Q. Mi and L. Yu, Electrospinning of flexible poly (vinyl alcohol)/MXene nanofiber-based humidity sensor self-powered by monolayer molybdenum diselenide piezoelectric nanogenerator, *Nano–Micro Lett.*, 2021, **13**, 1–13.

294 W. Zheng, T. Li, F. Jin, L. Qian, J. Ma, Z. Wei, X. Ma, F. Wang, J. Sun and T. Yuan, Interfacial Polarization Locked Flexible β-Phase Glycine/Nb2CTx Piezoelectric Nanofibers, *Small*, 2024, 2308715.

295 J. Kim, M. Jang, G. Jeong, S. Yu, J. Park, Y. Lee, S. Cho, J. Yeom, Y. Lee and A. Choe, MXene-enhanced β-phase crystallization in ferroelectric porous composites for highly-sensitive dynamic force sensors, *Nano Energy*, 2021, **89**, 106409.

296 R. Z. Auliya, P. C. Ooi, R. Sadri, N. A. Talik, Z. Y. Yau, M. A. S. Mohammad Haniff, B. T. Goh, C. F. Dee, N. Aslfattahi and S. Al-Bati, Exploration of 2D Ti3C2 MXene for all solution processed piezoelectric nanogenerator applications, *Sci. Rep.*, 2021, **11**(1), 17432.

297 T. Bhatta, P. Maharjan, H. Cho, C. Park, S. H. Yoon, S. Sharma, M. Salauddin, M. T. Rahman, S. S. Rana and J. Y. Park, High-performance triboelectric nanogenerator based on MXene functionalized polyvinylidene fluoride composite nanofibers, *Nano Energy*, 2021, **81**, 105670.

298 X. Li, W. Wang, W. Cai, H. Liu, H. Liu, N. Han and X. Zhang, Mxene/multiwalled carbon nanotube/polymer hybrids for tribopiezoelectric nanogenerators, *ACS Appl. Nano Mater.*, 2022, **5**(9), 12836–12847.

299 N. A. Shepelin, P. C. Sherrell, E. N. Skountzos, E. Goudeli, J. Zhang, V. C. Lussini, B. Imtiaz, K. A. S. Usman, G. W. Dicinoski and J. G. Shapter, Interfacial piezoelectric polarization locking in printable Ti3C2Tx MXene-fluoropolymer composites, *Nat. Commun.*, 2021, **12**(1), 3171.

300 W. Wu, W. Zhao, Q. Sun, B. Yu, X. Yin, X. Cao, Y. Feng, R. K. Li and J. Qu, Surface treatment of two dimensional MXene for poly (vinylidene fluoride) nanocomposites with tunable dielectric permittivity, *Compos. Commun.*, 2021, **23**, 100562.

301 S. Tu, L. Qiu, C. Liu, F. Zeng, Y.-Y. Yuan, M. N. Hedhili, V. Musteata, Y. Ma, K. Liang and N. Jiang, Suppressing Dielectric Loss in MXene/Polymer Nanocomposites through Interfacial Interactions, *ACS Nano*, 2024, **18**(14), 10196–10205.

302 Y. Li, X. Bai, J. Liu and B. Yang, Stretchable MXene/PVDF Piezoelectric Sensor for Finger Motion Detection and Tactile Recognition, in *2024 IEEE 37th International Conference on Micro Electro Mechanical Systems (MEMS)*, IEEE, 2024, pp 113–116.

303 X. Ji, L. Ge, C. Liu, Z. Tang, Y. Xiao, W. Chen, Z. Lei, W. Gao, S. Blake and D. De, Capturing functional two-dimensional nanosheets from sandwich-structure vermiculite for cancer theranostics, *Nat. Commun.*, 2021, **12**(1), 1124.

304 W. Feng, R. Wang, Y. Zhou, L. Ding, X. Gao, B. Zhou, P. Hu and Y. Chen, Ultrathin molybdenum carbide MXene with fast biodegradability for highly efficient theory-oriented photonic tumor hyperthermia, *Adv. Funct. Mater.*, 2019, **29**(22), 1901942.

305 Y. Fu, C. Li, Y. Cheng, Y. He, W. Zhang, Q. Wei and D. Li, Biomass aerogel composite containing BaTiO3 nanoparticles and MXene for highly sensitive self-powered sensor and photothermal antibacterial applications, *Composites, Part A*, 2023, **173**, 107663.

306 K. McLellan, T. R. Li, Y. C. Sun, M. B. Jakubinek and H. E. Naguib, 4D Printing of MXene Composites for Deployable Actuating Structures, *ACS Appl. Polym. Mater.*, 2022, **4**(12), 8774–8785, DOI: **10.1021/acsapm.2c01192**.

307 K. McLellan, T. R. Li, Y. C. Sun, M. B. Jakubinek and H. E. Naguib, 4D Printing of MXene Composites for Deployable Actuating Structures, *ACS Appl. Polym. Mater.*, 2022, **4**(12), 8774–8785, DOI: **10.1021/acsapm.2c01192**.

308 W. T. Cao, C. Ma, D. S. Mao, J. Zhang, M. G. Ma and F. Chen, MXene-Reinforced Cellulose Nanofibril Inks for 3D-Printed Smart Fibres and Textiles, *Adv. Funct. Mater.*, 2019, **29**(51), 1905898, DOI: **10.1002/adfm.201905898**.

309 K. Li, J. Zhao, A. Zhussupbekova, C. E. Shuck, L. Hughes, Y. Y. Dong, S. Barwich, S. Vaesen, I. V. Shvets, M. Mobius, *et al.*, 4D printing of MXene hydrogels for high-efficiency pseudocapacitive energy storage, *Nat. Commun.*, 2022, **13**(1), 6884, DOI: **10.1038/s41467-022-34583-0**.

310 Y. W. Li, S. Q. Peng, R. K. Kankala, L. X. Wu, A. Z. Chen and S. B. Wang, 3D printing of mechanically robust MXene-encapsulated polyurethane elastomer, *Composites, Part A*, 2022, **163**, 107182, DOI: **10.1016/j.compositesa.2022.107182**.

311 (*a*) H. B. Liu, Z. Y. Huang, T. Chen, X. Q. Su, Y. N. Liu and R. L. Fu, Construction of 3D MXene/Silver nanowires aerogels reinforced polymer composites for extraordinary electromagnetic interference shielding and thermal conductivity, *Chem. Eng. J.*, 2022, **427**, 131540, DOI: **10.1016/j.cej.2021.131540**; (*b*) X. Chu, Y. H. Wang, L. C. Cai, H. C. Huang, Z. Xu, Y. T. Xie, C. Yan, Q. Wang, H. T. Zhang, H. Li, *et al.*, Boosting the energy density of aqueous MXene-based supercapacitor by integrating 3D conducting polymer hydrogel cathode, *Susmat*, 2022, **2**(3), 379–390, DOI: **10.1002/sus2.61**.

312 (*a*) P. J. Bora, A. G. Anil, P. C. Ramamurthy and D. Q. Tan, MXene interlayered crosslinked conducting polymer film for highly specific absorption and electromagnetic interference shielding, *Mater. Adv.*, 2020, **1**(2), 177–183, DOI: **10.1039/d0ma00005a**; (*b*) R. H. Sun, H. B. Zhang, J. Liu, X. Xie, R. Yang, Y. Li, S. Hong and Z. Z. Yu, Highly Conductive Transition Metal Carbide/Carbonitride(MXene)@polystyrene Nanocomposites Fabricated by Electrostatic Assembly for Highly Efficient Electromagnetic Interference Shielding, *Adv. Funct. Mater.*, 2017, **27**(45), 1702807, DOI: **10.1002/adfm.201702807**.

313 R. S. Li, L. Ding, Q. Gao, H. M. Zhang, D. Zeng, B. A. Zhao, B. B. Fan and R. Zhang, Tuning of anisotropic electrical conductivity and enhancement of EMI shielding of polymer composite foam *via* CO2-assisted delamination and orientation of MXene, *Chem. Eng. J.*, 2021, **415**, 128930, DOI: **10.1016/j.cej.2021.128930**.

314 (*a*) J. Liu, H. B. Zhang, R. H. Sun, Y. F. Liu, Z. S. Liu, A. G. Zhou and Z. Z. Yu, Hydrophobic, Flexible, and Lightweight MXene Foams for High-Performance Electromagnetic-Interference Shielding, *Adv. Mater.*, 2017, **29**(38), 1702367, DOI: **10.1002/adma.201702367**; (*b*) Y. Sun, R. Ding, S. Y. Hong, J. Lee, Y. K. Seo, J. D. Nam and J. Suhr, MXene-xanthan nanocomposite films with layered microstructure for electromagnetic interference shielding and Joule heating, *Chem. Eng. J.*, 2021, **410**, 128348, DOI: **10.1016/j.cej.2020.128348**.

315 Q. M. Zhang, Q. Wang, J. Cui, S. Zhao, G. F. Zhang, A. L. Gao and Y. H. Yan, Structural design and preparation of Ti3C2Tx MXene/polymer composites for absorption-dominated electromagnetic interference shielding, *Nanoscale Adv.*, 2023, **5**(14), 3549–3574, DOI: **10.1039/d3na00130j**.

316 G. Chang, L. Zeng, L. Xie, B. Xue and Q. Zheng, Ultrathin multifunctional electromagnetic interference shielding MXene/AgNWs/PEDOT:PSS coatings with superior electro/photo-thermal transition ability and water repellency, *Chem. Eng. J.*, 2023, **470**, 144033, DOI: **10.1016/j.cej.2023.144033**.

317 Z. H. Zeng, N. Wu, J. J. Wei, Y. F. Yang, T. T. Wu, B. Li, S. B. Hauser, W. D. Yang, J. R. Liu and S. Y. Zhao, Porous and Ultra-Flexible Crosslinked MXene/Polyimide Composites for Multifunctional Electromagnetic Interference Shielding, *Nano–Micro Lett.*, 2022, **14**(1), 59, DOI: **10.1007/s40820-022-00800-0**.

318 K. Hussain, S. Mehboob, I. Ahmad, M. Mumtaz, A. R. Khan, S. Mujtaba-ul-Hassan, M. T. Mehran, Z. Iqbal, J. Ahmad, M. Mehmood, *et al.*, Terahertz time-domain spectroscopy of thin and flexible CNT-modified MXene/polymer composites, *Appl. Phys. A*, 2021, **127**(5), 382, DOI: **10.1007/s00339-021-04525-6**.

319 G. Monastyreckis, L. Mishnaevsky, C. B. Hatter, A. Aniskevich, Y. Gogotsi and D. Zeleniakiene, Micromechanical modeling of MXene–polymer composites, *Carbon*, 2020, **162**, 402–409, DOI: 10.1016/j.carbon.2020.02.070.

320 R. T. Liu, M. Miao, Y. H. Li, J. F. Zhang, S. M. Cao and X. Feng, Ultrathin Biomimetic Polymeric Ti3C2Tx MXene Composite Films for Electromagnetic Interference Shielding, *ACS Appl. Mater. Interfaces*, 2018, **10**(51), 44787–44795, DOI: 10.1021/acsami.8b18347.

321 Y. Nie, J. K. Huang, S. Y. Ma, Z. C. Li, Y. K. Shi, X. F. Yang, X. Fang, J. B. Zeng, P. Y. Bi, J. T. Qi, *et al.*, MXene-hybridized silane films for metal anticorrosion and antibacterial applications, *Appl. Surf. Sci.*, 2020, **527**, 146915, DOI: 10.1016/j.apsusc.2020.146915.

322 F. Y. Zhang, W. Q. Liu, S. Wang, C. H. Liu, H. Y. Shi, L. Y. Liang and K. Pi, Surface functionalization of Ti3C2Tx and its application in aqueous polymer nanocomposites for reinforcing corrosion protection, *Composites, Part B*, 2021, **217**, 108900, DOI: 10.1016/j.compositesb.2021.108900.

323 D. M. He, M. Cai, H. Yan, Q. L. Lin, X. Q. Fan, L. Zhang and M. H. Zhu, Tribological properties of Ti3C2Tx MXene reinforced interpenetrating polymers network coating, *Tribol. Int.*, 2021, **163**, 107196, DOI: 10.1016/j.triboint.2021.107196.

324 Y. Zou, X. Jin, X. P. Zhang, X. L. Kong, Q. Zhang, X. H. Xie, C. J. Liu, L. N. Ke, W. G. Liu and W. Wang, A multifunctional biomedical patch based on hyperbranched epoxy polymer and MXene, *Sci. China: Technol. Sci.*, 2021, **64**(12), 2744–2754, DOI: 10.1007/s11431-021-1843-3.

325 K. Chen, Y. H. Chen, Q. H. Deng, S. H. Jeong, T. S. Jang, S. Y. Du, H. E. Kim, Q. Huang and C. M. Han, Strong and biocompatible poly(lactic acid) membrane enhanced by Ti3C2Tz (MXene) nanosheets for Guided bone regeneration, *Mater. Lett.*, 2018, **229**, 114–117, DOI: 10.1016/j.matlet.2018.06.063.

326 (*a*) Z. L. Li, H. Zhang, J. Han, Y. Chen, H. Lin and T. Yang, Surface Nanopore Engineering of 2D MXenes for Targeted and Synergistic Multitherapies of Hepatocellular Carcinoma (vol 30, 1706981, 2018), *Adv. Mater.*, 2019, **31**(27), 1902282, DOI: 10.1002/adma.201902282; (*b*) C. Murugan, V. Sharma, R. K. Murugan, G. Malaimegu and A. Sundaramurthy, Two-dimensional cancer theranostic nanomaterials: Synthesis, surface functionalization and applications in photothermal therapy, *J. Contr. Release*, 2019, **299**, 1–20, DOI: 10.1016/j.jconrel.2019.02.015; (*c*) H. Lin, S. S. Gao, C. Dai, Y. Chen and J. L. Shi, A Two-Dimensional Biodegradable Niobium Carbide (MXene) for Photothermal Tumor Eradication in NIR-I and NIR-II Biowindows (vol 139, pg 16235, 2017), *J. Am. Chem. Soc.*, 2020, **142**(23), 10567, DOI: 10.1021/jacs.0c04999.

327 C. Y. Xing, S. Y. Chen, X. Liang, Q. Liu, M. M. Qu, Q. S. Zou, J. H. Li, H. Tan, L. P. Liu, D. Y. Fan, *et al.*, Two-Dimensional MXene (Ti3C2)-Integrated Cellulose Hydrogels: Toward Smart Three-Dimensional Network Nanoplatforms Exhibiting Light-Induced Swelling and Bimodal Photothermal/Chemotherapy Anticancer Activity, *ACS Appl. Mater. Interfaces*, 2018, **10**(33), 27631–27643, DOI: 10.1021/acsami.8b08314.

328 C. Dai, Y. Chen, X. X. Jing, L. H. Xiang, D. Y. Yang, H. Lin, Z. Liu, X. X. Han and R. Wu, Two-Dimensional Tantalum Carbide (MXenes) Composite Nanosheets for Multiple Imaging-Guided Photothermal Tumor Ablation, *ACS Nano*, 2017, **11**(12), 12696–12712, DOI: 10.1021/acsnano.7b07241.

329 A. P. Liu, Y. Liu, G. J. Liu, A. T. Zhang, Y. J. Cheng, Y. Li, L. Zhang, L. S. Wang, H. Zhou, J. Q. Liu, *et al.*, Engineering of surface modified Ti3C2Tx MXene based dually controlled drug release system for synergistic multitherapies of cancer, *Chem. Eng. J.*, 2022, **448**, 137691, DOI: 10.1016/j.cej.2022.137691.

330 (*a*) B. Yao, J. Zhang, Z. Q. Fan, Y. D. Ding, B. Zhou, R. L. Yang, J. F. Zhao and K. Zhang, Rational Engineering of the DNA Walker Amplification Strategy by Using a Au@Ti3C2@PEI-Ru(dcbpy)(3)(2+) Nanocomposite Biosensor for Detection of the SARS-CoV-2 RdRp Gene, *ACS Appl. Mater. Interfaces*, 2021, **13**(17), 19816–19824, DOI: 10.1021/acsami.1c04453; (*b*) Y. J. Lei, E. N. Zhao, Y. Z. Zhang, Q. Jiang, J. H. He, A. Baeumner, O. S. Wolfbeis, Z. L. Wang, K. N. Salama and H. N. Aishareef, A MXene-Based Wearable Biosensor System for High-Performance *In Vitro* Perspiration Analysis, *Small*, 2019, **15**(19), 1901190, DOI: 10.1002/smll.201901190.

331 B. Lin, A. C. Y. Yuen, S. Oliver, J. J. Liu, B. Yu, W. Yang, S. Y. Wu, G. H. Yeoh and C. H. Wang, Dual functionalisation of polyurethane foam for unprecedented flame retardancy and antibacterial properties using layer-by-layer assembly of MXene chitosan with antibacterial metal particles, *Composites, Part B*, 2022, **244**, 110147, DOI: 10.1016/j.compositesb.2022.110147.

332 L. Liu, M. H. Zhu, Z. W. Ma, X. D. Xu, S. M. Seraji, B. Yu, Z. Q. Sun, H. Wang and P. G. Song, A reactive copper-organophosphate-MXene heterostructure enabled antibacterial, self-extinguishing and mechanically robust polymer nanocomposites, *Chem. Eng. J.*, 2022, **430**, 132712, DOI: 10.1016/j.cej.2021.132712.

333 K. Rasool, K. A. Mahmoud, D. J. Johnson, M. Helal, G. R. Berdiyorov and Y. Gogotsi, Efficient Antibacterial Membrane based on Two-Dimensional Ti3C2Tx (MXene) Nanosheets, *Sci. Rep.*, 2017, **7**, 1598, DOI: 10.1038/s41598-017-01714-3.

334 H. G. Yang, Q. Zheng, P. Zhang, G. C. Nie, T. Ali and S. Raza, Fabrication of MXene (Ti2C3Tx) based conducting polymer materials and their applications as anticancer and metal ions removal from wastewater, *Surf. Interfaces*, 2023, **36**, 102493, DOI: 10.1016/j.surfin.2022.102493.

335 N. Rabiee, M. Bagherzadeh, M. Jouyandeh, P. Zarrintaj, M. R. Saeb, M. Mozafari, M. Shokouhimehr and R. S. Varma, Natural Polymers Decorated MOF-MXene

Nanocarriers for Co-delivery of Doxorubicin/pCRISPR, *ACS Appl. Bio Mater.*, 2021, **4**(6), 5106–5121, DOI: **10.1021/acsabm.1c00332**.

336 C. Yang, Y. Luo, H. Lin, M. Ge, J. L. Shi and X. L. Zhang, Niobium Carbide MXene Augmented Medical Implant Elicits Bacterial Infection Elimination and Tissue Regeneration, *ACS Nano*, 2021, **15**(1), 1086–1099, DOI: **10.1021/acsnano.0c08045**.

337 N. Tao, Y. D. Liu, Y. J. Wu, X. L. Li, J. Li, X. Y. Sun, S. Chen and Y. N. Liu, Minimally Invasive Antitumor Therapy Using Biodegradable Nanocomposite Micellar Hydrogel with Functionalities of NIR-II Photothermal Ablation and Vascular Disruption, *ACS Appl. Bio Mater.*, 2020, **3**(7), 4531–4542, DOI: **10.1021/acsabm.0c00465**.

338 X. Wu, M. M. Ding, H. Xu, W. Yang, K. S. Zhang, H. L. Tian, H. T. Wang and Z. L. Xie, Scalable Ti3C2Tx MXene Interlayered Forward Osmosis Membranes for Enhanced Water Purification and Organic Solvent Recovery, *ACS Nano*, 2020, **14**(7), 9125–9135, DOI: **10.1021/acsnano.0c04471**.

339 I. Ihsanullah, MXenes (two-dimensional metal carbides) as emerging nanomaterials for water puri fication: Progress, challenges and prospects, *Chem. Eng. J.*, 2020, **388**, 124340, DOI: **10.1016/j.cej.2020.124340**.

340 (*a*) J. Abraham, K. S. Vasu, C. D. Williams, K. Gopinadhan, Y. Su, C. T. Cherian, J. Dix, E. Prestat, S. J. Haigh, I. V. Grigorieva, *et al.*, Tunable sieving of ions using graphene oxide membranes, *Nat. Nanotechnol.*, 2017, **12**(6), 546, DOI: **10.1038/Nnano.2017.21**; (*b*) M. Thomas, B. Corry and T. A. Hilder, What Have We Learnt About the Mechanisms of Rapid Water Transport, Ion Rejection and Selectivity in Nanopores from Molecular Simulation?, *Small*, 2014, **10**(8), 1453–1465, DOI: **10.1002/smll.201302968**; (*c*) L. A. Richards, A. I. Schafer, B. S. Richards and B. Corry, The Importance of Dehydration in Determining Ion Transport in Narrow Pores, *Small*, 2012, **8**(11), 1701–1709, DOI: **10.1002/smll.201102056**.

341 J. Wang, Z. J. Zhang, J. N. Zhu, M. T. Tian, S. C. Zheng, F. D. Wang, X. D. Wang and L. Wang, Ion sieving by a two-dimensional Ti3C2Tx alginate lamellar membrane with stable interlayer spacing, *Nat. Commun.*, 2020, **11**(1), 3540, DOI: **10.1038/s41467-020-17373-4**.

342 Y. X. Zeng, P. Wang, B. L. He, S. J. Liu, Q. Ye and F. Zhou, Fabrication of zwitterionic polymer-functionalized MXene nanosheets for anti-bacterial and anti-biofouling applications, *Prog. Org. Coat.*, 2023, **183**, 107727, DOI: **10.1016/j.porgcoat.2023.107727**.

343 A. Khosla, Sonu, H. T. A. Awan, K. Singh, Gaurav, R. Walvekar, Z. H. Zhao, A. Kaushik, M. Khalid and V. Chaudhary, Emergence of MXene and MXene–polymer Hybrid Membranes as Future- Environmental Remediation Strategies, *Adv. Sci.*, 2022, **9**(36), 2203527, DOI: **10.1002/advs.202203527**.

344 (*a*) C. Hou, C. Huang, H. Yu and S. Shi, Surface-Engineered Ti3C2T with Tunable Work Functions for Highly Efficient Polymer Solar Cells, *Small*, 2022, **18**(21), 2201046, DOI: **10.1002/smll.202201046**; (*b*) J. Wen, Z. Sun, Y. Qiao, Y. Zhou, Y. Liu, Q. Zhang, Y. Liu and S. Jiao, Ti3C2 MXene-Reduced Graphene Oxide Composite Polymer-Based Printable Electrolyte for Quasi-Solid-State Dye-Sensitized Solar Cells, *ACS Appl. Energy Mater.*, 2022, **5**(3), 3329–3338, DOI: **10.1021/acsaem.1c03928**.

345 (*a*) Y. Liu, H. Xiao and W. A. Goddard III, Schottky-barrier-free contacts with two-dimensional semiconductors by surface-engineered MXenes, *J. Am. Chem. Soc.*, 2016, **138**(49), 15853–15856; (*b*) G. Li, N. Li, S. Peng, B. He, J. Wang, Y. Du, W. Zhang, K. Han and F. Dang, Highly efficient Nb2C MXene cathode catalyst with uniform O-terminated surface for lithium–oxygen batteries, *Adv. Energy Mater.*, 2021, **11**(1), 2002721.

346 B. Deng, H. Lian, B. Xue, R. Song, S. Chen, Z. Wang, T. Xu, H. Dong and S. Wang, Niobium-Carbide MXene Modified Hybrid Hole Transport Layer Enabling High-Performance Organic Solar Cells Over 19, *Small*, 2023, **19**(23), 2207505.

347 T. Yang, M. Wang, C. Duan, X. Hu, L. Huang, J. Peng, F. Huang and X. Gong, Inverted polymer solar cells with 8.4% efficiency by conjugated polyelectrolyte, *Energy Environ. Sci.*, 2012, **5**(8), 8208–8214.

348 C. Huang, S. Shi and H. Yu, Work function adjustment of Nb2CTx nanoflakes as hole and electron transport layers in organic solar cells by controlling surface functional groups, *ACS Energy Lett.*, 2021, **6**(10), 3464–3472.